INFORMATION TO USERS

This manuscript has been reproduced from the microfilm master. UMI films the text directly from the original or copy submitted. Thus, some thesis and dissertation copies are in typewriter face, while others may be from any type of computer printer.

The quality of this reproduction is dependent upon the quality of the copy submitted. Broken or indistinct print, colored or poor quality illustrations and photographs, print bleedthrough, substandard margins, and improper alignment can adversely affect reproduction.

In the unlikely event that the author did not send UMI a complete manuscript and there are missing pages, these will be noted. Also, if unauthorized copyright material had to be removed, a note will indicate the deletion.

Oversize materials (e.g., maps, drawings, charts) are reproduced by sectioning the original, beginning at the upper left-hand corner and continuing from left to right in equal sections with small overlaps.

Photographs included in the original manuscript have been reproduced xerographically in this copy. Higher quality 6" x 9" black and white photographic prints are available for any photographs or illustrations appearing in this copy for an additional charge. Contact UMI directly to order.

ProQuest Information and Learning
300 North Zeeb Road, Ann Arbor, MI 48106-1346 USA
800-521-0600

UMI®

Université d'Ottawa • University of Ottawa

Uncoupling Protein 2 and Mitochondrial Bioenergetics in Drug Sensitive and Drug Resistant Leukemic Cells

Andreas Antoniou

Thesis submitted to the Department of Biochemistry, Microbiology and Immunology in partial fulfilment of the requirements for the degree of Master of Science

Faculty of Medicine
University of Ottawa
Ottawa, Ontario, Canada
August 8, 2001

ABSTRACT

The overall objective of this research was to characterize the differences in the metabolic control of oxidative phosphorylation in drug sensitive and drug resistant leukemic cells. Anti-cancer agents may function to promote tumor cell death in a number of ways, however acquired or inherent drug resistance is a major problem in successful cancer treatment. The role of mitochondria in apoptosis has received a great deal of attention from a variety of biochemical perspectives in the past few years. Based on evidence that mitochondrial metabolism is altered during apoptotic processes, this research built on the hypothesis that an alteration in mitochondrial energy metabolism which decreases the production of reactive oxygen species plays a significant role in the protection of tumor cells from cytotoxic therapies. Two pairs of sensitive and resistant leukemic cell lines were studied: the mouse L1210 cell line and its drug resistant L1210/DDP subline, as well as the human HL60 cell line and the HL60/MDR resistant cell line. Oxygen consumption was higher, and mitochondrial membrane potential was lower in the resistant sublines of cells under both resting and non-phosphorylating conditions. An analysis of the kinetics of mitochondrial proton leak reactions revealed that a higher amount of oxygen consumption was used to balance the leak in the resistant cells compared to the sensitive cells. Uncoupling proteins in the mitochondrial inner membrane may cause mitochondrial proton leak and thereby reversibly uncouple oxidation from phosphorylation. Levels of uncoupling protein 2 (UCP2) were found to be higher in the mitochondria of resistant cells.

Northern blot analysis confirmed the expression of uncoupling protein 2 mRNA in the L1210 and L1210/DDP cell lines, with a higher amount present in the sensitive cells. Based on evidence of the presence of certain mitochondrial proteins in the plasma membrane, immunoblots of plasma membrane proteins were conducted. Results revealed the presence of UCP2, with higher amounts observed in the sensitive leukemic cells. The plasma membrane potential of the sensitive cells was significantly lower than in the resistant cells, and in the case of the L1210 cells, was sensitive to GDP, a proposed inhibitor of UCP2. Other mitochondrial differences were revealed through the analysis of cellular ATP content and the activity of cytochrome oxidase in both cell types. The findings from this research suggest that drug resistant leukemic cells use a metabolic strategy in which mitochondrial oxidative phosphorylation is uncoupled. Uncoupling proteins, in particular UCP2, have been proposed to regulate reactive oxygen species production through modulation of mitochondrial membrane potential. As reactive oxygen species have been implicated in various aspects of apoptosis, uncoupling proteins may provide a mechanism for resistance to chemotherapeutic agents and radiation by minimizing the production of reactive oxygen species.

Dedication

"We are what we repeatedly do. Excellence then, is not an act, but a habit."
- Aristotle (384 BC - 322 BC)

This thesis is dedicated to my family and friends who have
provided me with a better understanding of happiness.
Their encouragement and support is only matched
by their ability in helping me improve as a
person with every passing day.

ACKNOWLEDGMENTS

I would like to offer my thanks and appreciation to those who contributed to the successful completion of this thesis and who made these past few years in the laboratory so enjoyable and unforgettable.

First and foremost, to my supervisor Dr. Mary-Ellen Harper for her support, encouragement, guidance, and caring nature. I cannot imagine being a graduate student in another laboratory. Mary-Ellen has had a tremendous influence on my life, and I am grateful to have her as a friend.

To the members of my advisory committee, Dr. Jean Himms-Hagen and Dr. Steffany Bennett, for their helpful insights, advice, and suggestions throughout my research.

To Shadi Monemdjou, whose friendship I cannot describe in this limited space. No other person has impacted my life in the past few years the way she has. Shadi has made me a better person. All the memories and laughs shared until this point are merely a stepping stone for the future, and I am thankful for this.

To Dr. Anna Melnyk, whose friendship is especially important to me. She is a terrific, thoughtful, and beautiful person who makes me realize how fortunate I am to know somebody like her.

To Jennifer Roundell, an incredible person whose amazing energy made the laboratory a better place each and every week. I also thank Jennifer for performing the RNA work described in this thesis, including the isolation of total RNA and Northern blot analysis.

To all the members of the laboratory who helped me throughout the years and who helped create a work environment that often failed to resemble a scientific setting, which I appreciated . Thank you to Azhar Shaikh for performing the analysis of ATP content as well as obtaining the confocal images presented in this thesis.

To Dr. Alvin Chan for his advice, encouragement, and never ending support of my educational goals. He has taught me to stay positive, focused, and undeterred in the face of obstacles that I have no control over.

To Dr. M. Karen Newell for her collaboration in this research and her assistance in a number of areas of this thesis.

To Dr. Cathy Chan, Dr. Min De Leo, and Dr. Mike Wheeler for providing the UCP2-pIRES2-EGFP construct and all the help associated with its use.

To my family and friends, in particular Preetham Natarajan, who serve as a constant reminder that the results of an experiment are not nearly as important as the events, thoughts, and occurrences that make up the rest of the day.

Finally, I would like to thank my father Costas, my mother Vasilia, and my brother George for their life-long support and encouragement in the path that I have decided to follow.

Table of Contents

METHODS AND MATERIALS

RESULTS

List of Figures

List of Tables

List of Abbreviations

Symbols

$\Delta\Psi_m$	mitochondrial inner membrane potential
$\Delta\Psi_p$	plasma membrane potential
Δp	mitochondrial protonmotive force
ΔpH	pH gradient
ϵ	elasticity
°C	degrees Celsius
μCi	microcurie
μg	microgram
μl	microlitre
μm	micrometre
μM	micromole/litre

A

a_c	cytoplasmic and nuclear $TPMP^+$ activity coefficient
a_e	extracellular $TPMP^+$ activity coefficient
a_m	mitochondrial $TPMP^+$ activity coefficient
ADP	adenosine 5'-diphosphate
AIF	apoptosis inducing factor
ALL	acute lymphocytic leukemia
AML	acute myeloid leukemia
ANOVA	analysis of variance

ANT	adenine nucleotide translocator
Apaf-1	apoptotic protease activating factor-1
ATP	adenosine 5'-triphosphate

B

BAT	brown adipose tissue
BMCP1	brain mitochondrial carrier protein 1
BMR	basal metabolic rate
bp	base pairs
BSA	bovine serum albumin

C

$CaCl_2$	calcium chloride
CH_3COOK	potassium acetate
CH_3COONa	sodium acetate
$C_3H_3O_2COOH$	maleic acid
CLL	chronic lymphocytic leukemia
cm	centimetre
CML	chronic myeloid leukemia
CO_2	carbon dioxide
COX	cytochrome oxidase
$CuSO_4 \cdot 5H_2O$	cupric sulfate
CyP-D	cyclophilin d

D

ddH_2O	deionized distilled water
DDP	cis-diammine dichloroplatinum (II)
DEPC	diethylpyrocarbonate
DMSO	dimethyl sulphoxide
DNA	deoxyribonucleic acid
dpm	disintegrations per minute

E

ECL	enhanced chemiluminescence
E. Coli	*Escherichia coli*
EDTA	ethylene diamine tetraactetic acid
EDTA-$Na_2 \cdot 2H_2O$	EDTA, disodium salt, dihydrate
EGTA	ethylene glycol-bis(β-aminoethylether)N,N,N',N'-tetraacetic acid

F

f.c.	final concentration
FCCP	carbonyl cyanide p-trifluoromethoxyphenlylhydrazone
FCS	fetal calf serum

G

g	centrifugal force
g	gram
GDP	guanosine 5'-diphosphate

GFP	green fluorescence protein
GTP	guanosine 5'-triphosphate

H

H_3BO_3	boric acid
HCHO	formaldehyde
$HCONH_2$	formamide
HEPES	N-(2-hydroxyethyl)piperazine-N'-(2-ethanesulfonic acid)
H_2O	water
H_2O_2	hydrogen peroxide

K

$K_2C_4H_4O_6 \cdot ½H_2O$	potassium tartrate
KCl	potassium chloride
kDa	kilodalton
K_2HPO_4	di-potassium hydrogen orthophosphate
KH_2PO_4	potassium dihydrogen orthophosphate

M

M	mole/litre
MCA	metabolic control analysis
MDR	multidrug resistance
mg	milligram
$MgCl_2$	magnesium chloride
$MgSO_4$	magnesium sulfate

MIM	mitochondrial inner membrane
min	minute
ml	millilitre
mM	millimole/litre
$MnCl_2 \cdot 4H_2O$	manganese chloride
mol	mole
MOPS	3-(N-Morpholino) propanesulfonic acid
MPT	mitochondrial permeability transition
mRNA	messenger ribonucleic acid
mtDNA	mitochondrial deoxyribonucleic acid
MTF	mitochondrially transmitted factors
mV	millivolt
MV	mitochondrial matrix volume

N

$Na_3C_6H_5O_7 \cdot 2H_2O$	sodium citrate
NaCl	sodium chloride
Na_2CO_3	sodium carbonate
$NaHCO_3$	sodium hydrogen carbonate
Na_2HPO_4	di-sodium hydrogen orthophosphate
$NaH_2PO_4 \cdot H_2O$	sodium dihydrogen orthophosphate
NaN_3	sodium azide
NaOH	sodium hydroxide
NCM	nitrocellulose membrane
ng	nanogram
nm	nanometre

NO·	nitric oxide

O

O_2	molecular oxygen
$O_2^{\cdot-}$	superoxide radical anion
OH·	hydroxyl radical
ONNO·	peroxynitrite

P

PAGE	polyacrylamide gel electrophoresis
PBS	phosphate buffered saline
PES	polyethersulfone
P-gp	P-glycoprotein
P_i	inorganic phosphate
PMSF	phenylmethyl sulfonylfluoride

R

RbCl	rubidium chloride
RNA	ribonucleic acid
ROS	reactive oxygen species
rpm	revolutions per minute

S

SDS	sodium dodecyl sulfate
SEM	standard error of the mean

SLB	sample loading buffer
SMR	standard metabolic rate
State 3	maximal phosphorylating respiration
State 4	maximal non-phosphorylating (leak-dependent) respiration

T

TEMED	N,N,N',N'-tetramethylethylenediamine
TNF	tumor necrosis factor
$TPMP^+$	methyltriphenylphosphonium cation
TPMP-Br	methyltriphenylphosphonium-bromide
Tris-HCl	tris (hydroxymethyl)aminomethane hydrochloride
Tween-20	polyoxyethylene sorbitan monolaurate

U

UCP	uncoupling protein

V

V_c	cytoplasmic volume
V_m	mitochondrial matrix volume
VDAC	voltage-dependent anion channel
v/v	volume per volume

W

WAT	white adipose tissue
w/v	weight per volume

INTRODUCTION

1. LEUKEMIA

Leukemia is a form of cancer that results in the uncontrolled production of abnormal white blood cells that can no longer protect against disease (Castoldi, et al., 1992). It also inhibits the growth of red blood cells, causing anemia in virtually every patient. All blood cells pass through many stages of development, beginning in the bone marrow as blasts. Leukemia can occur at any of these stages affecting one of the two major categories of white blood cells: lymphoid cells or myeloid cells. Lymphoid leukemia and myeloid leukemia have different symptoms as well as different treatments (Beutler, 2001). Leukemia is also classified according to the course and duration of the disease. Acute leukemia involves a sudden onset and involves immature cells that cannot perform their proper function. The symptoms of acute leukemia are more severe than that of chronic leukemia, which progresses more slowly. Chronic leukemia typically involves more mature cells that can partially perform their function. There are about sixteen specific types identified to date (Castoldi, et al., 1992), however the four broad types are named based on the categories discussed. They are: acute lymphocytic leukemia (ALL), acute myeloid leukemia (AML), chronic lymphocytic leukemia (CLL), and chronic myeloid leukemia (CML).

The primary feature of leukemia is the failure of the bone marrow to produce enough healthy white blood cells, red blood cells, and platelets to carry on regular

bodily functions. Marrow failure is characterized by increasing vulnerability to infection, fatigue, bone pain, and bleeding/bruising (Estey, 2001). Leukemia affects 13.2 per 100,000 men and 7.7 per 100,000 women in the United States (The Leukemia and Lymphoma Society℠; http://www.leukemia.org). Seventy percent of leukemia occurs in adults (mostly CLL and AML). ALL is the predominant form of leukemia in children.

The three major categories of possible and established causes of leukemia are genetic factors, diseases, and physical and chemical agents. Risk factors include genetic and chromosomal abnormalities, radiation exposure, chemical and drug exposure, and smoking.

Main treatments of leukemia are chemotherapy, radiation therapy, and bone marrow transplantation.

2. Tumor Cell Division and Metabolism

Cancer cells are distinguished by cell division in defiance of normal growth control mechanisms and by the ability to invade other tissues. Rapid cell division, characteristic of most tumor cells, is also a feature of developing tissues and of adult tissues that must regenerate such as hematopoietic cells, skin cells, and regenerating liver cells. Paradoxically when cells rapidly divide, there is a pronounced metabolic shift away from the more energy efficient mitochondrial adenosine triphosphate (ATP) production (oxidative phosphorylation) towards an increased rate of cytoplasmic, glucose dependent ATP synthesis (glycolysis). Compared to oxidative phosphorylation, glycolysis results in far fewer molecules of ATP per molecule of glucose. The reasons

underlying this metabolic shift during cell division are not well understood. It is well documented that fast growing tumor cells have elevated rates of glycolysis (Biswas, et al., 1997) facilitated by increased activities of key processes in glycolytic regulation. These include glucose transporter expression, glucose uptake, glucose-6-phosphatase, tissue hexokinase activity, and increased lactate production (Halicka, et al., 1995, Oudard, et al., 1997). These changes positively correlate with malignant transformation and with the progression of malignancy (Weber, 1977). A major consequence of the high rate of glycolysis is that glucose carbons are no longer an important carbon source for mitochondrial oxidation in tumor cells.

3. Drug Resistance

Resistance to anticancer drugs is a major problem in successful cancer treatment. A patient may initially present with resistant tumors, develop resistance during treatment, or develop resistance at the time of relapse (Bradshaw and Arceci, 1998). A major goal in cancer research is to understand the mechanisms by which cells become resistant to chemotherapeutic drugs, and then find ways to prevent or bypass the cellular resistance. Factors proposed to explain this phenomenon include decreased drug uptake, increased deoxyribonucleic acid (DNA) damage repair, enhanced drug detoxification, altered expression of molecule(s) targeted by the drugs, and loss of cell surface death inducing receptors such as CD95 (Fas) (Arceci, 1995). Tumor cells develop an enhanced ability to survive by altering the cellular pathways that function to overcome the cytotoxic effects of drugs at one or more of these levels.

The exact mechanism may depend on the drug of interest as well as the tumor type treated. However, the mechanisms of pleiotropic drug resistance remain obscure. Many cancers that initially respond to treatment later become resistant, often to a wide range of unrelated drugs. This has been termed 'multidrug resistance' (MDR).

A major cause of MDR seems to be the activation of the MDR1 gene which encodes the efflux pump P-glycoprotein (P-gp). This protein is thought to confer resistance by removing the cytotoxic drug from the cell (Marks, et al., 1996). There is a significant amount of evidence that increased expression of P-gp is associated with decreased responsiveness to chemotherapy and poor outcome in a variety of solid tumors and also in leukemia (Chan, et al., 1997, Leith, 1998, Leith, et al., 1999). To date the largest amount of work on MDR has focused on transport-mediated drug resistance mechanisms and, in particular, drug efflux systems (Arceci, 2000).

4. APOPTOSIS

Physiological cell death occurs through the processes of apoptosis and necrosis. The boundaries between these processes, once thought to be distinct, have recently blurred. However, it is widely accepted that necrotic cell death typically results in the osmotic rupture of a cell leading to inflammation of surrounding tissue, while apoptosis involves cell shrinkage, membrane blebbing, nuclear DNA degradation, cell fragmentation, and phagocytosis of the fragments by surrounding cells. The development of certain types of cancers involves the loss of apoptosis that is needed to remove damaging cells. As well, resistance to chemotherapeutic agents is related

to expression of proteins that act to inhibit apoptosis.

Apoptosis, also referred to as programmed cell death or cell suicide, describes a cascade of cellular pathways leading to a series of well-defined biochemical and morphological changes (Hannun, 1997). Apoptosis is essential for normal development and maintenance of tissue homeostasis. A number of regulatory switches exist in most cells to induce apoptosis or prevent it from occurring (Hannun, 1997). Defects in the machinery of programmed cell death contribute to many prevalent diseases. An excess of unwanted apoptosis is linked to nerve cell loss in Alzheimer's disease, whereas not enough apoptosis is a cause of many cancers and autoimmune diseases (Finkel, 2001).

To date, two main mechanisms of apoptosis have been identified: death-receptor-induced apoptosis and apoptosis induced by chemicals and stress. On the plasma membrane of many cells there exist death receptors which, when triggered by their corresponding ligands, result in an activation of caspases and induction of apoptosis (Ashkenazi and Dixit, 1998). Death receptors are members of the tumor necrosis factor (TNF)-receptor family; the best known are CD95 (also known as Fas) and TNF Receptor-1. Apoptosis induced by other stimuli such as stress, DNA-damaging agents, and cancer chemotherapeutic agents involves a disruption of mitochondria and subsequent release of pro-apoptotic molecules into the cytosol.

A) Mitochondria and Apoptosis

Over the past few years apoptosis research has experienced a shift in thinking from a theory that had the nucleus ultimately determining the cell's fate to a paradigm

that has mitochondria playing a major regulatory role. Mitochondria undergo significant changes in membrane integrity before the morphological changes associated with apoptosis present themselves. There is a loss of mitochondrial membrane potential leading to the release of cytochrome c and apoptosis inducing factor (AIF) from the intermembrane space into the cytosol. Cytochrome c can interact with apoptotic protease activating factor-1 (Apaf-1) to activate caspase 9 which in turn activates other caspases and a nuclease activating factor (Alnemri, 1999). Caspases are a family of cysteine proteases that play a critical role in the execution phase of apoptosis (Cohen, 1997). AIF can directly activate nuclear endonucleases, causing the characteristic oligonucleosomal DNA fragmentation pattern observed during apoptosis.

Opening of the mitochondrial permeability transition (MPT) pore within the mitochondrial inner membrane occurs during apoptosis and is thought to be the primary cause of loss of mitochondrial function (Figure 1). MPT is known to be induced by exposure to high calcium concentrations as well as oxidative stress (Kowaltowski, et al., 2001). The latter may represent a mechanism of induction of reactive oxygen species (ROS)-linked apoptosis. Studies have shown that a wide variety of antioxidants can protect against MPT (Kowaltowski, et al., 2001). The main souce of ROS leading to MPT is the mitochondrial electron transport chain (described below). There is general agreement that the adenine nucleotide translocator (ANT) and cyclophilin d (CyP-D) are components of the pore (Kowaltowski, et al., 2001). Some suggest that other proteins may be involved, such as the outer membrane voltage-dependent anion channel (VDAC), also known as porin.

Figure 1 The mitochondrial permeability transition. Reactive oxygen species (ROS), high calcium concentrations, and possibly other triggers lead to pore opening. Water and solutes up to 1500 Daltons in size enter the matrix, leading to dissipation of the mitochondrial inner membrane potential ($\Delta\Psi_m$), matrix swelling, and outer membrane disruption and the release of cytochrome c into the cytosol. (Figure modified from Green and Reed, 1998)

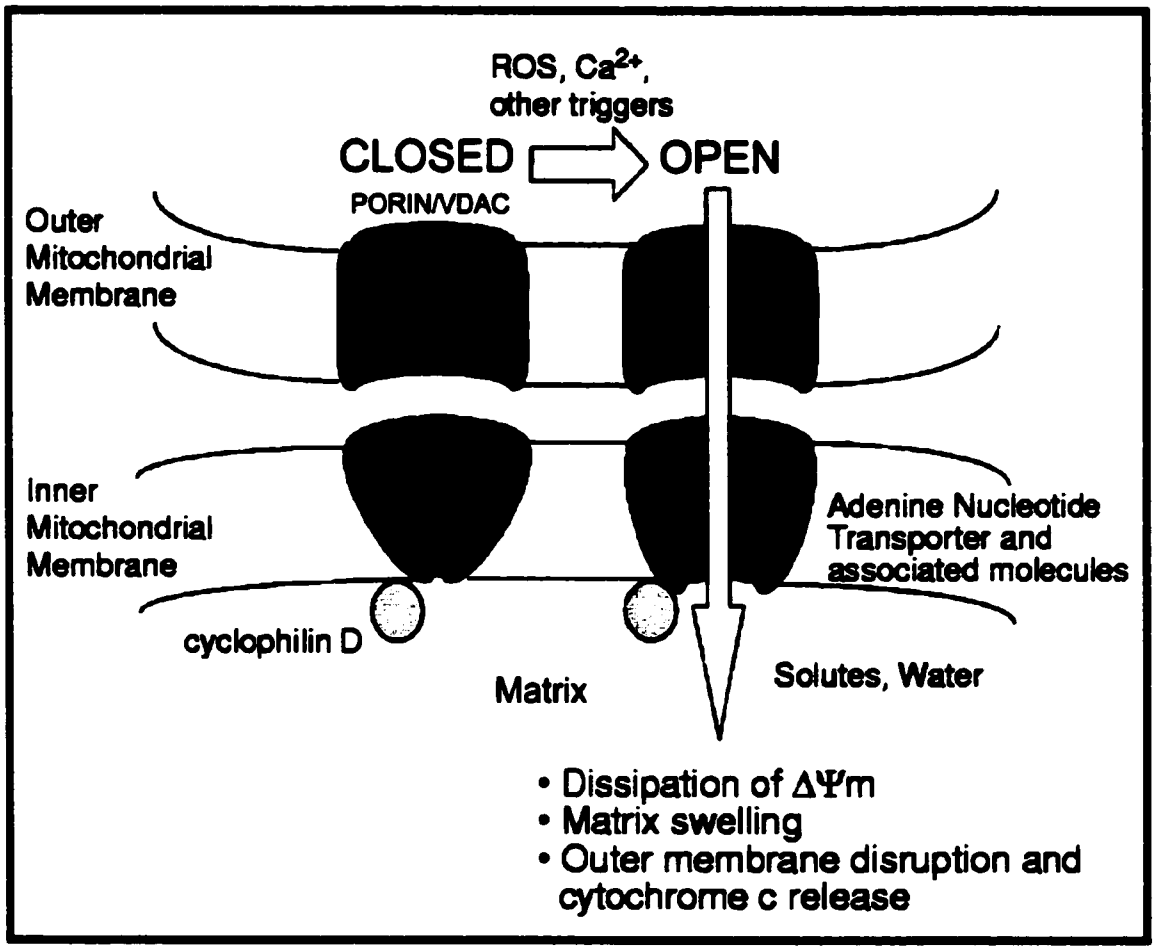
ROS, Ca^{2+},
other triggers
CLOSED
OPEN
PORIN/VDAC
Outer
Mitochondrial
Membrane
Inner
Mitochondrial
Membrane
Adenine Nucleotide
Transporter and
associated molecules
cyclophilin D
Matrix
Solutes, Water
• Dissipation of $\Delta\Psi m$
• Matrix swelling
• Outer membrane disruption and
cytochrome c release

In addition to proteins that are released from the mitochondria during apoptosis, the other group of mitochondrial proteins involved in programmed cell death are the pro- and anti-apoptotic members of the Bcl-2 family that largely localize to the outer mitochondrial membrane (Bernardi, et al., 1999). Bax is an example of a pro-apoptotic member of the family that can serve as a docking protein for other proteins involved in the apoptotic cascade. Bcl-2 is an anti-apoptotic member that appears to affect MPT and/or the release of cytochrome c and AIF. Increased expression of Bcl-2 or of its apoptosis-inhibitory homologues is involved in the pathogenesis of a number of human cancers (Susin, et al., 1998).

B) Reactive Oxygen Species and Apoptosis

It is well documented that apoptosis can be induced by oxidative stress (Lenaz, 1998, Skulachev, 1997, Skulachev, 1996). Apoptosis can be divided into two phases: an activation phase that consists of the signaling pathways that initiate apoptosis, and an execution phase that involves the molecular machinery required for cell death to occur. ROS do not seem to be required in the execution phase, but can be involved in the activation phase, for example, as activators of MPT (Jacobson, 1996). Mitochondria are the major cellular source of ROS (discussed in Section 7).

5. Mitochondria

A) Oxidative Phosphorylation

Mitochondria are the main source of ATP, the major energy 'currency' of cells

(Figure 2). In non-dividing cells of the body, mitochondria normally provide over 90% of cellular ATP (Rolfe and Brown, 1997). The synthesis of ATP from adenosine diphosphate (ADP) and inorganic phosphate (P_i) by mitochondria is driven by electron flow from a reduced substrate to oxygen. The transfer of electrons through the electron transport chain is carried out by four inner membrane-associated complexes, along with cytochrome c and ubiquinone (Nishikawa, et al., 2000). Complex I (NADH:ubiquinone oxidoreductase) accepts electrons from NADH + H^+, derived from glucose oxidation and mitochondrial tricarboxylic acid (TCA) cycle activity. Complex II (succinate:ubiquinone oxidoreductase) receives electrons from $FADH_2$. Regardless of the initial source of electrons, both complex I and complex II transfer their electrons to ubiquinone, which in turn transfers them to complex III (ubiquinol:cytochrome c oxidoreductase). The electrons then proceed through cytochrome c, complex IV (cytochrome c oxidase), and then to molecular oxygen which combine with protons to form water. As electrons pass through complexes I, III, and IV, a protonmotive force (Δp) is generated by the pumping of protons from the mitochondrial matrix into the intermembrane space (Brand, et al., 1994). The Δp consists of two components: a transmembrane electrical potential ($\Delta\Psi_m$) and a pH gradient (ΔpH). Δp fuels proton movement back into the matrix through ATP synthase and the combined action of the adenine nucleotide translocator and phosphate carrier, resulting in the formation of ATP.

B) Proton Leak

If the flow of protons back into the matrix is always through ATP synthase, then

Figure 2 The mitochondrion. Mitochondria are the main source of cellular ATP. The mitochondrion contains an outer and an inner membrane that divides the organelle into two distict compartments: the intermembrane space which is located between the two membranes, and the matrix which is enclosed by the inner membrane. (Figure adapted from Kleinsmith and Kish, 1995; electron micrograph provided to our laboratory by Dr. L.P. Kozak)

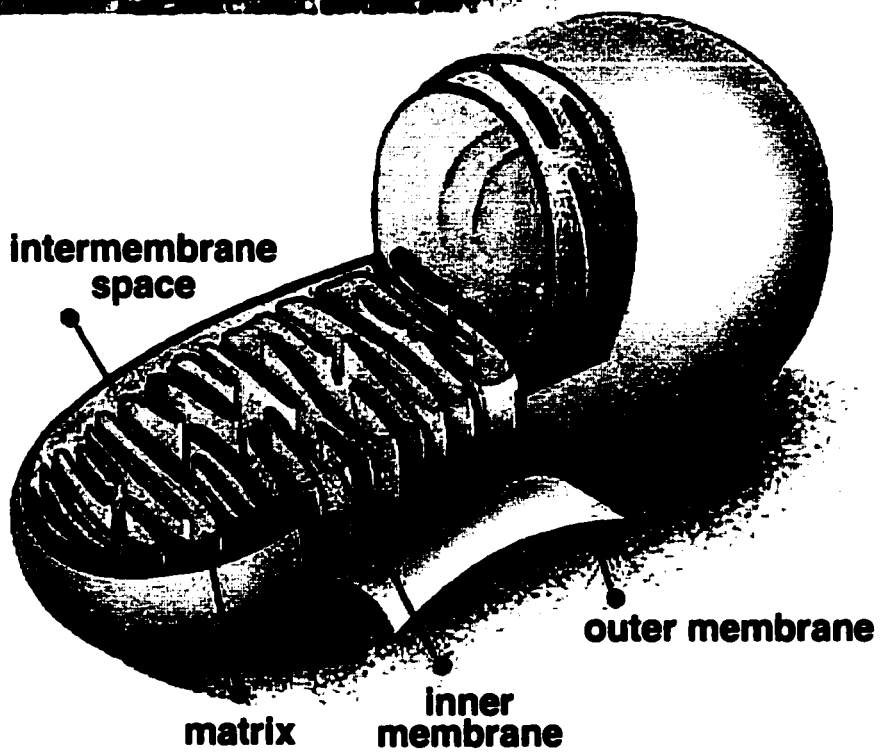
intermembrane
space
outer membrane
matrix
inner
membrane

the processes of substrate oxidation and ADP phosphorylation are said to be completely coupled. Research in the last decade, however, has shown convincingly that oxidative phosphorylation is never fully coupled, in isolated mitochondria as well as mitochondria in intact cells (Brand, et al., 1994). There exists a passive leak of protons across the mitochondrial inner membrane such that a significant proportion return to the matrix without being coupled to ATP synthesis or any other energy conserving reaction (Brown, 1992, Brown and Brand, 1986). This nonproductive proton conductance pathway has been termed "proton leak". The energy of the protonmotive force is released as heat.

At first the question arose whether the proton leak is an artefact of mitochondrial isolation or whether proton leak is a real physiological phenomenon. It was thought that the forces used to disrupt cellular membranes and thus free the mitochondria for subsequent analyses were responsible for disrupting the physical properties of the mitochondrial inner memebrane, thus allowing a form of proton movement that could not occur in normal, intact mitochondria. This was answered by numerous studies in which mitochondrial proton leak has been shown to exist in intact cells and tissues, including hepatocytes (Harper and Brand, 1993, Nobes, et al., 1990), thymocytes (Buttgereit, et al., 1992), and lymphocytes (Buttgereit, et al., 1991). It is now generally accepted that mitochondrial proton leak is a substantial contributor to basal metabolism (Porter, 2001).

The existence of a proton leak was first measured by Mitchell and Moyle (Mitchell and Moyle, 1967). They added a pulse of oxygen to anaerobic mitochondria and bacteria and detected the pumping out of protons with a pH electrode. When

the supply of oxygen was consumed, the protons leaked back across the membrane as evidenced by an increase in pH. Measurements of proton leak were later conducted by first inhibiting all known proton transport processes and then inducing an artificial Δp with potassium gradients (Brown and Brand, 1986, Krishnamoorthy and Hinkle, 1984). Results showed that the rate of leak was larger at high Δp values and had a roughly exponential dependence on Δp. The dependence of leak on Δp reflected earlier findings by Nicholls (Nicholls, 1974). In these experiments an approach was used whereby the substrate oxidation reactions of mitochondria in the absence of ATP synthesis (state 4) could be progressively slowed by the addition of electron transport chain inhibitors such as malonate. Results showed that only small reductions in Δp were required to substantially reduce the respiration rate of mitochondria.

c) Physiological Significance of the Proton Leak

Regardless of the efficiency of mitochondrial ATP synthesis, mitochondrial energy expenditure is proportional to oxygen consumption, as oxygen is the final electron acceptor in the electron transport chain. The amount of energy consumed through leaks is carefully controlled by cells and leak is low when ATP needs are high (Hafner, et al., 1990). Leak thus has a tonic effect on overall oxygen consumption, and it has been proposed as an important contributor to standard metabolic rate (SMR) (Brand, 1990).

The energy consumed by proton leak in isolated rat hepatocytes has been shown to account for 26 ± 7% of the total oxygen consumption rate or 33 ± 7% of the mitochondrial respiration rate (Nobes, et al., 1990). In resting perfused rat skeletal

muscle, Rolfe and Brand (Rolfe and Brand, 1996) determined that up to 52% of the resting respiration rate was dedicated to countering the leak of protons into the mitochondrial matrix. However, the proton leak and mitochondrial ATP synthesis compete for the same driving force, and while proton leak accounted for a large proportion of energy expenditure in these resting systems, the question arose as to whether the contribution of proton leak is still significant at higher metabolic rates. Under this condition, flux through ATP synthase must increase to accommodate greater workloads. Rolfe *et al.* (Rolfe, et al., 1999) increased the respiration rate twofold, by stimulating the ornithine-urea cycle and gluconeogenesis in hepatocytes, and by inducing vigorous contraction in perfused rat hindquarters. The results of these experiments indicated that proton leak decreased with increased workload, but only slightly. Proton leak was measured as 22% of the overall available energy in hepatocytes, and 34% in skeletal muscle. Taken together, these studies show that proton leak is very important to the overall energy expenditure of the rat and, by inference, of mammals. It is estimated that proton leak in a rat accounts for 20-25% of the SMR, making it the largest single contributor to energy metabolism.

D) Postulated Functions of the Mitochondrial Proton Leak

What is the purpose of a seemingly wasteful process that makes such a substantial contribution to cellular respiration? A number of different functions have been proposed, including (i) maintenance of normal body temperature through heat production, (ii) control over energy metabolism, and (iii) reduction of reactive oxygen species (ROS) production.

(I) Maintenance of Normal Body Temperature Through Heat Production

It has been suggested that the proton leak in mammals serves to maintain a constant body temperature by balancing the heat lost by the body with heat produced by leak mechanisms. Smaller mammals have a larger surface area to volume ratio relative to larger mammals, which leads to a larger amount of heat lost that needs to be balanced by an increased metabolic rate (Brand, 1990). Relative to body size, both the mass and metabolic rate of heat-producing organs is larger in smaller mammals (Krebs, 1950). In 1993 Porter and Brand (Porter and Brand, 1993) established that the rate of mitochondrial proton leak as well as the metabolic rate of mammals are inversely proportional to body size. Experiments using an ectotherm (cold-blooded) model, the bearded dragon lizard, showed that the state 4 rate of isolated hepatocytes is only about 20% of that of hepatocytes isolated from a rat of similar body mass and housed at the same environmental temperature (Brand, et al., 1991). However, the lizard hepatocytes utilize oxygen at only 25% the rate of rat hepatocytes. Therefore, even though the rate of proton leak is reduced in the bearded dragon relative to the rat, the cost of the proton leak as a proportion of metabolic rate is similar in both models. Extending these findings, there is evidence that the proportional contribution that proton leak makes to SMR in mitochondria isolated from ectothermic and endothermic vertebrates with a range of whole body standard metabolic rates is similar (Brookes, et al., 1998). This suggests that heat production to maintain body temperature is not the only function of the leak.

(ii) Control Over Energy Metabolism

Since the oxygen that is used to drive the futile cycle of proton pumping and leak across the mitochondrial inner membrane cannot be used to drive ATP synthesis, the occurrence of the leak effectively lowers the P/O ratio (ATP produced per mole oxygen consumed) below its maximum possible values (Brand, et al., 1994). Increased ATP demand causes an increase in the rate of phosphorylation reactions at any Δp, thereby lowering Δp and proton leak and increasing the coupling ratio. Conversely, increased proton leak will divert more of the energy flux to proton cycling, lowering the effective P/O ratio. This allows oxidative phosphorylation to vary its coupling efficiency depending on demand without the need to make large changes in the rate of oxygen consumption. This rapid, short-term response may provide a mechanism for increasing the sensitivity and responsiveness to effectors in the cell that ultimately affect ATP requirements.

(iii) Reduction of Reactive Oxygen Species Production

An increased mitochondrial membrane potential (as when coupling of respiration is increased) is associated with components of the electron transport chain being reduced as well as a slower respiratory rate. This can stimulate ROS production by increasing the life span of highly reactive intermediates of the electron transfer chain such as semiquinone radicals (Korshunov, et al., 1997). It has been proposed that a reduction in $\Delta\Psi_m$ through proton leak could provide protection against ROS production at the mitochondrial level (Skulachev, 1996). An increase in proton leak would stimulate oxygen consumption and decrease the formation of ROS. In this

respect, the accompanying loss of energy in the form of ATP would be a 'price worth paying' to increase metabolic flexibility or to avoid the damaging effects of ROS (Bouillaud, et al., 2001). A more detailed explanation of mitochondria and ROS is provided below.

6. Proton Leak and the Uncoupling Proteins

The proton permeability of the mitochondrial inner membrane is particularly high compared to other ions. Aspects of the phospholipid composition of the mitochondrial inner membrane strongly correlate with the proton conductance of the membrane. But experiments by Brookes and colleagues (Brookes, et al., 1997) demonstrated that proton leak through the lipid bilayer can only account for approximately 5% of total proton leak. Another possibility is proton leak occurring through protein-lipid interactions. The other major feature of the inner membrane determining bilayer proton permeability is the existence of specific proteins catalysing some or most of the proton leak.

Uncoupling proteins (UCPs) present in the mitochondrial inner membrane have been proposed to cause mitochondrial proton leak and thereby reversibly uncouple oxidation from phosphorylation (Figure 3) (Boss, et al., 1998). Uncoupling causes a decrease in $\Delta\Psi_m$, an increase in the rate of substrate oxidation, and the release of energy as heat. A number of proteins belong to the uncoupling protein family, and they in turn belong to the much larger mitochondrial carrier protein family that also

Figure 3 Schematic representation of the mitochondrial inner membrane illustrating the components of the oxidative phosphorylation system and the proposed function of uncoupling proteins in proton leak. As electrons from reduced substrates are transferred through the components of the electron transport chain (shown in blue), protons are translocated from the matrix to the intermembrane space. The protonmotive force produced fuels proton movement back into the matrix through ATP synthase (purple) and the combined action of the adenine nucleotide (red) and phosphate (green) carriers, resulting in the synthesis of ATP. Uncoupling proteins (UCPs) present in the mitochondrial inner membrane have been proposed to cause proton leak and thereby reversible uncouple oxidation from phosphorylation.

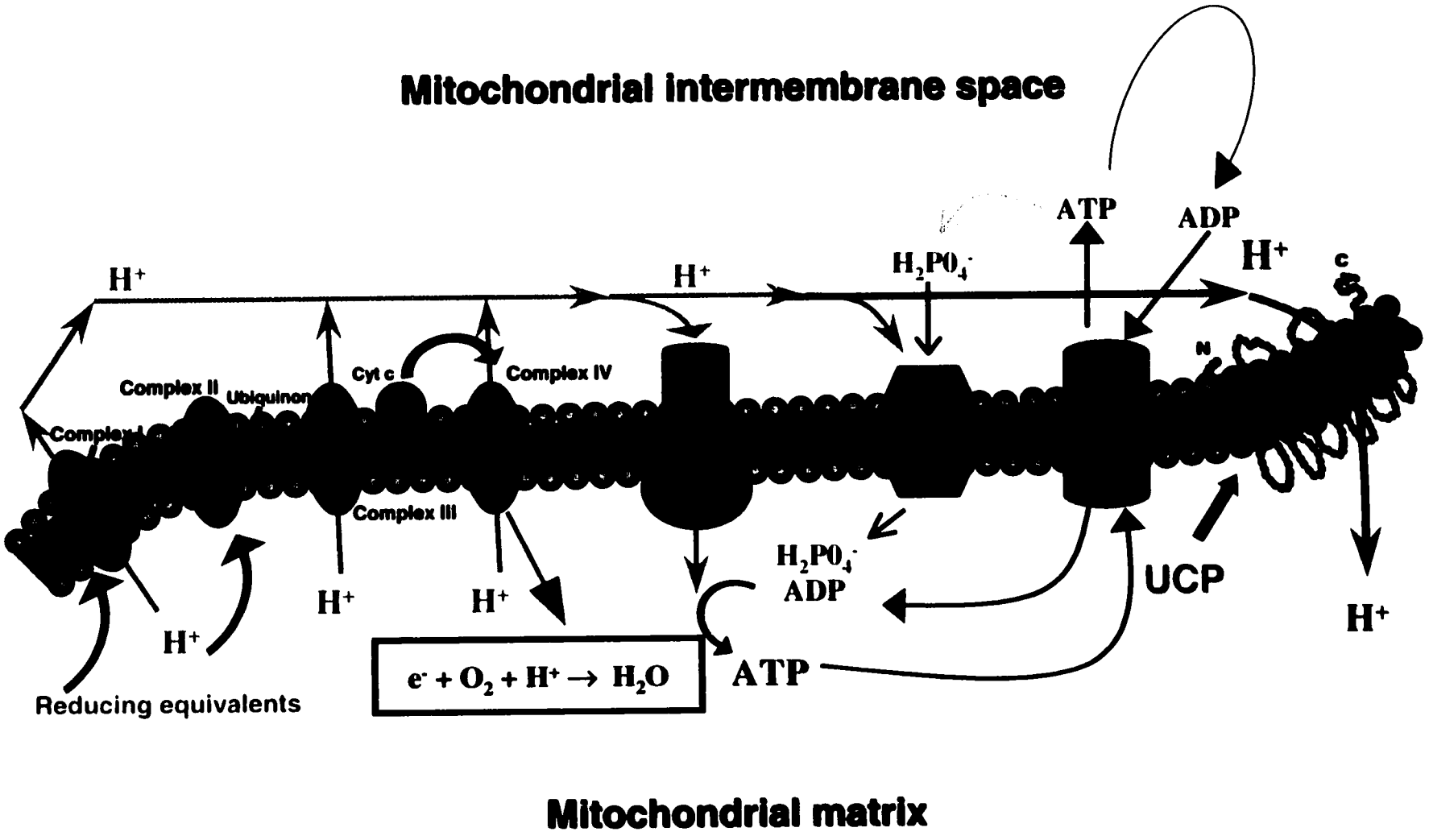
Mitochondrial intermembrane space
ATP
ADP
H+
H+
H+
H2P04-
C
N
Complex II
Ubiquinon
Cyt c
Complex IV
Complex III
H+
H+
H+
H2P04-
ADP
UCP
H+
e- + O2 + H+ → H2O
ATP
Reducing equivalents
Mitochondrial matrix

includes the ATP/ADP translocator and the phosphate translocator.

A) UCP1

The first UCP was found in mitochondria from brown adipose tissue (BAT). The mitochondria of mature brown adipocytes contain UCP1 (originally called thermogenin or uncoupling protein), a 32 kDa protein that dissipates the proton gradient generated by the electron transport chain, producing heat instead of ATP (Figure 4). UCP1 was cloned in 1985 by Bouillaud and colleagues (Bouillaud, et al., 1985), nearly a decade after its identification. The features of UCP1 and its regulation were first uncovered by David Nicholls (Nicholls, 1979). The physiological function of UCP1, and of BAT in general, is thermogenesis (heat production) (Himms-Hagen, 1990). It is of major importance for thermoregulation in newborn humans. As well, small mammals adapt to cold by increasing the amount of UCP1 in their BAT mitochondria, allowing heat to be produced at a greater rate. A number of other features may be important in response to an animal's need to produce heat. Fatty acids are required to achieve maximum UCP1 activity. The mechanism of action of fatty acids is currently a matter of discussion, with two models being proposed: the fatty acid flip-flop model and the model where the fatty acid acts as a prosthetic group to UCP1 (Klingenberg and Huang, 1999, Nicholls and Rial, 1999). Conversely, activity is inhibited by purine nucleoside di- and tri-phosphates (ADP, ATP, GDP, GTP). The binding site is located on the cytosolic side towards the C-terminus of the protein. The relative physiological importance of UCP1 to adult humans is limited, however, because adults possess very little active BAT. As well, because UCP1 is exclusive to BAT, this protein cannot account

Figure 4 Membrane-spanning model of uncoupling protein 1 (UCP1). UCP1 is a member of the mitochondrial carrier family. It contains six transmembrane α-helices with both the N- and C- terminals facing the intermembrane space. The protein is organized as a triplicated structure, with each domain containing approximately 100 residues with two transmembrane helices. The transmembrane structure and amino acid composition of the other members of the UCP family are similar.

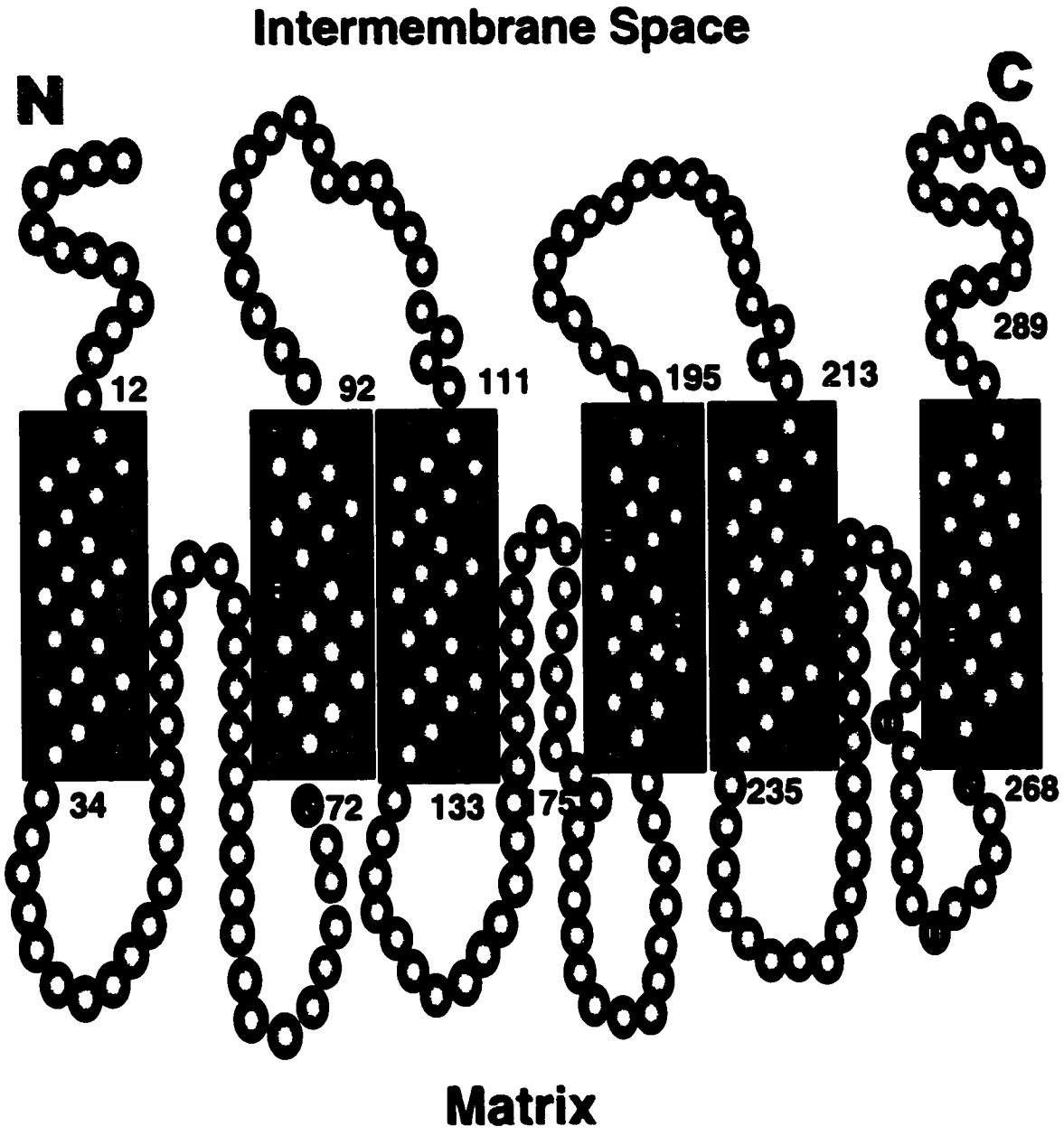
Intermembrane Space
N
C
12
92
111
195
213
289
34
72
133
175
235
268
Matrix

for proton leak observed in other tissues. It did, however, provide the crucial foundation for the identification of other candidate uncoupling proteins.

B) UCP2

In 1997, Fleury and colleagues (Fleury, et al., 1997) cloned the first UCP1 isoform, UCP2. Human UCP2 is 59% identical to human UCP1, and is also able to uncouple mitochondrial respiration as demonstrated by transfection into *Saccharomyces cerevisiae* (Fleury, et al., 1997). The amino acid sequence of mouse UCP2 is 95% identical to human UCP2. Mitochondrial carrier protein motifs exhibited in UCP1 are conserved in UCP2, as are the amino acids essential for purine nucleotide binding. Unlike UCP1, UCP2 is ubiquitously expressed with the highest levels found in white adipose tissue (WAT), BAT, heart, kidney, spleen, thymus, leukocytes, macrophages, Kupffer cells (liver), bone marrow and stomach in both mice and humans (Fleury, et al., 1997). Its expression throughout the immune system suggested a role for UCP2 in immunity and/or thermoregulatory responses to infection (Fleury, et al., 1997). In BAT of transgenic mice deficient in UCP1, UCP2 messenger RNA (mRNA) was found to be increased 5-fold (Enerback, et al., 1997). In these mice UCP2 was thought to provide the compensatory mechanism by which these mice remained lean even when fed a high fat diet. At the chromosomal level, UCP2 was mapped to regions of human chromosome 11 and mouse chromosome 7 that had been previously linked to hyperinsulinemia and obesity (DeBry and Seldin, 1996, Warden, et al., 1995).

c) UCP3

Soon after the cloning of UCP2, a third uncoupling protein was discovered (Boss, et al., 1997, Vidal-Puig, et al., 1997). UCP3 is expressed in skeletal muscle of humans; in rodents it is also expressed in BAT. This selective expression in tissues where energy expenditure can be very high makes it a potential mediator of adaptive thermogenesis. Human UCP3 is 58% identical to human UCP1 and 73% identical to human UCP2. The gene is found adjacent to that for UCP2 on chromosome 7 in mice and on chromosome 11 in humans (Solanes, et al., 1997). Two isoforms of UCP3 have been found: a long form ($UCP3_L$) and a short form (UCP_S) (Boss, et al., 1997). The short form does not have the 37 residues of the C-terminus that the long form contains. These residues form part of the sixth transmembrane domain as well as the putative nucleotide binding domain.

d) BMCP1 AND UCP4

The discovery of UCP2 and UCP3 in 1997 was closely followed by the cloning of two more related proteins. Brain mitochondrial carrier protein 1 (BMCP1) is expressed mainly in the brain, but is also present in other tissues to a small extent (Sanchis, et al., 1998). The fifth member of the uncoupling protein family, characterized in January 1999, is UCP4. It is expressed exclusively in the brain (Mao, et al., 1999). The sequence homology of BMCP1 and UCP4 to UCP1 are about 34%. Both BMCP1 and UCP4 genes have been expressed in yeast and have been shown to lower $\Delta\Psi_m$, interpreted as an increase in proton leak.

E) Function(s) of the Uncoupling Protein Homologues

Most of what is known about uncoupling proteins has been acquired from studies of UCP1 (Nicholls and Rial, 1999). The thermogenic function of UCP1 seems to have influenced many of the hypotheses as to the physiological roles of the UCP homologues (Stuart, et al., 2001). UCP2, for instance, is most highly expressed in tissues that do not play an important role in heat production. The mRNA levels of BAT UCP2 increase in UCP1 knockout mice, yet these mice are cold intolerant. This suggests that UCP2 has not replaced the thermogenic function of UCP1 in this tissue (Stuart, et al., 2001). Their function does not seem to be thermogenesis, but nevertheless studies have shown that they catalyze a proton conductance (Echtay, et al., 2001). Many studies have been conducted on the uncoupling protein homologues over the past four years, yet their true physiological function is still a matter of debate. Other potential roles proposed for these proteins include involvement in obesity, diabetes, and fatty acid metabolism. Another postulated role that provides a basis for this research project is the regulation of ROS production (described below).

7. Mitochondria and Reactive Oxygen Species

It is well established that mitochondria are the main source of ROS in the cell (Vidal-Puig, 2000), produced under normal conditions as inevitable by-products of aerobic metabolism. Reactive oxygen species include the superoxide radical anion ($O_2^{\cdot -}$), hydroxyl radical ($OH^{\cdot}$), hydrogen peroxide (H_2O_2), nitric oxide ($NO^{\cdot}$) and peroxynitrite ($ONNO^{-}$) (Lenaz, 1998). The two main sites of superoxide generation in the

mitochondrial inner membrane are NADH dehydrogenase at complex I and the interface between ubiquinone and complex III (Nishikawa, et al., 2000). It is calculated that 1-4% of oxygen reacting with the electron transport chain is incompletely reduced and results in ROS production (Richter, 1988). During respiration, the primary reactive product is $O_2^{\cdot-}$, which is subsequently converted to H_2O_2 by superoxide dismutase. As H_2O_2 molecules are potentially involved in various cellular regulatory processes including signal transduction, gene transcription, oxidative damage, and apoptosis (Halliwell, 1987, Kroemer, et al., 1995, Sen and Packer, 1996), their levels must be tightly regulated. Cells are equipped with extensive antioxidant defense mechanisms to counteract the damaging effects of ROS. Survival can be considered to depend on a balance between ROS production and antioxidant activity. The production of H_2O_2 is higher when respiration rates are slow than when respiration rates are high, and low when proton return to the matrix is almost exclusively through ATP synthase (Chance, et al., 1979). In state 4 (no ATP production) the reduced electron transport chain and the high $\Delta\Psi_m$ would increase $O_2^{\cdot-}$ production. By being major producers of ROS, mitochondria are exposed to high concentrations and are therefore particularly susceptible to their attack. Damage to mitochondrial components includes lipid peroxidation, protein oxidation and mitochondrial DNA (mtDNA) mutations. Cardiolipin is a lipid found in the mitochondrial inner membrane and is required for cytochrome oxidase activity (Lenaz, 1998). ROS decrease cardiolipin to a larger extent than other lipids due to its high degree of unsaturation. Protein oxidation has been described to affect the enzymes of the electron transport chain, ATP synthase, the adenine nucleotide translocator (ANT), and other proteins found in mitochondria (Lenaz, 1998).

Mitochondrial DNA is also very susceptible to oxidative damage. Since it is located in the matrix, it is very close to the source of ROS. Also, mtDNA does not have introns and lacks histones and other DNA-associated proteins which makes the probability of damaging a coding region of mtDNA very high. Studies involving human brain regions showed that damage to mtDNA is approximately ten times greater than damage to nuclear DNA (Richter, et al., 1988). Since mtDNA encodes for a number of polypeptide chains that belong to complexes of the electron transport chain, one of the consequences as a result of damage caused by ROS would be defective electron transfer and oxidative phosphorylation (Johns, 1995). It has been established that defects in the electron transport chain lead to enhanced production of ROS (Richter, et al., 1995, Sohal and Sohal, 1991). This would therefore establish an unstoppable feedback of mtDNA alterations and oxidative stress.

A) Uncoupling Proteins and ROS

A high $\Delta\Psi_m$ is accompanied by a slower respiratory rate which stimulates ROS production by increasing O_2 tension and favoring longer life spans of highly reactive intermediates of the electron transfer chain. It has been proposed that mild mitochondrial uncoupling could provide a mechanism to reduce $\Delta\Psi_m$ and therefore ROS production at the mitochondrial level. Nègre-Salvayre *et al.* (Negre-Salvayre, et al., 1997) showed that inhibition of UCP1 by GDP (a known inhibitor of UCP1) increased $\Delta\Psi_m$ and H_2O_2 production. An uncoupling agent reversed this effect. GDP was also able to increase $\Delta\Psi_m$ and H_2O_2 production of the mitochondria from UCP2-expressing cells of the liver (Kupffer cells), spleen, and thymus. Altogether these results strongly

suggest that UCP2 is sensitive to GDP and is able to modulate H_2O_2 generation. This role for UCP2 as a regulator of oxidative stress would be consistent with the importance of ROS in tissues of the immune system which express this protein. Arsenijevic *et al.* (Arsenijevic, et al., 2000) showed that macrophages from UCP2 knockout mice generated 80% more ROS than wild-type mice.

Studies have demonstrated an increased production of ROS in skeletal muscle mitochondria of UCP3 knockout mice as determined by measurement of superoxide production and aconitase activity(Vidal-Puig, et al., 2000). Activation of UCP1 *in vitro* was shown to decrease ROS production (Vidal-Puig, et al., 2000). Diabetic hyperglycemia causes a number of biochemical changes, including an increase in the production of ROS. Nishikawa *et al.* showed that this increase was produced by the proton electrochemical gradient generated by the electron transport chain, and could be prevented by overexpression of UCP1 as well as an uncoupler of oxidative phosphorylation. In pancreatic β-cells, overexpression of UCP2 is accompanied by protection against H_2O_2-induced toxicity (Li, et al., 2001).

8. OBJECTIVE

The possibility that uncoupling proteins may act to protect cells from apoptosis through regulation of ROS production provided the rationale for investigating the involvement of uncoupling proteins in tumor cell mitochondrial bioenergetics. The aim of this research was to characterize the differences in the metabolic control of oxidative phosphorylation in drug sensitive leukemic cells, which die apoptotically, and

drug resistant leukemic cells, which withstand apoptosis-induced cell death. This was based on the hypothesis that an alteration in mitochondrial energy metabolism which decreases production of ROS plays an important role in the protection of tumor cells from cytotoxic therapies. Specifically, the proposal put forward is that mitochondrial UCP2 is actively involved in this protection. The significance of this research comes from the potential to understand the metabolic pathways which regulate susceptibility of tumor cells to cell death and the potential to reverse drug resistance in tumor cells that are difficult to kill during chemo- and radiotherapy.

A) Cell Lines

This research began by using a leukemic cell line called L1210. The L1210 cells, derived from a DBA/2 mouse in 1949, are lymphocytic cells and are sensitive to cisplatin and methotrexate (Richon, et al., 1987). The cisplatin-derived L1210/DDP subline is cross resistant to methotrexate. The L1210 cell line and its subline have been used for many years to study the mechanism of drug resistance. The L1210 cells are non-adherent, morphologically round, and rapidly dividing whereas the L1210/DDP cells are adherent, morphologically large and amorphous, and slowly dividing (Bhushan, et al., 1998). The L1210/DDP cells are also cell surface Fas negative, rendering them insensitive to Fas-induced cellular signals (Bhushan, et al., 1998).

Cisplatin (cis-diammine dichloroplatinum (II)) (DDP) is a common chemotherapeutic agent used in the treatment of patients with ovarian, testicular, bladder, neck, and lung cancers (Bhushan, et al., 1999). Although it has been used extensively, its effectiveness had been limited, due to the development of resistant

cancer cells. Accompanying the resistance to DDP is the acquisition of cross resistance to a number of unrelated drugs. A great deal of research has been devoted to overcoming this resistance by understanding the interactions between DDP and DNA.

DDP enters the cell by diffusion, and hydrolysis of its chloride ions produces an active platinum compound (Rosenberg, 1979). These compounds react with DNA forming crosslinks which alter the tertiary structure of DNA and inhibit DNA functions (Erickson, et al., 1981). Resistance to DDP has been proposed to occur by a number of mechanisms including increased repair of DDP-DNA lesions, altered DDP uptake by the cell, and altered intracellular localization of DDP by compounds such as glutathione and metallothionein.

DDP resistance is often associated with cross resistance to methotrexate (MTX), a folate antagonist (Schabel, et al., 1983, Teicher, et al., 1986). MTX exerts its cytotoxic effects through competitive inhibition of dihydrofolate reductase (DHFR), preventing it from maintaining an adequate cellular supply of tetrahydrofolate. Tetrahydrofolates are required as cofactors in the synthesis of purine nucleotides and thymidylate (Taylor and Tattersall, 1981). Therfore, despite the dissimilarity in action of these two anti-cancer agents, cross resistance is commonly found.

L1210 mouse leukemia cells employ a high-affinity transport system for MTX and reduced folate compounds. Transport is mediated by a 48 kDa integral plasma membrane protein and a 38 kDa peripheral protein (Price, et al., 1988).

The research continued by examining another pair of sensitive and resistant leukemic cells. The HL60 cells are a promyelocytic cell line of human origin. The HL60/MDR resistant subline expresses the P-gp membrane protein (described above).

The HL60/MDR cells exhibit low level extended cross resistance to a wide range of chemotherapeutic drugs (Su, et al., 1994).

B) Top-Down Metabolic Control Analysis

Metabolic Control Analysis (MCA), used extensively in this research, is a method for analysing the control of metabolic systems. MCA attempts to describe the relative control each component in a metabolic system exerts on the pathway fluxes (rates) and metabolite concentrations. In this scenario the metabolic system is the independent variable while the fluxes and metabolite concentrations are the dependent variables. The amount of control that any individual component of a metabolic system has is measured by changing the level of that component and monitoring its effect on the system variable (flux or metabolite concentration) of concern. MCA can simplify the study of complex metabolic systems.

MCA was first developed by Kacser and Burns (Kacser and Burns, 1973) and Heinrich and Rapoport (Heinrich and Rapoport, 1974). Flux control coefficients were described which provided a quantification of control of each individual enzyme in a metabolic pathway. The first application of MCA to oxidative phosphorylation was the measurement of the flux control coefficients of the various components of the system in isolated rat liver mitochondria (Groen, et al., 1982). This was performed by titration experiments with irreversible inhibitors of mitochondrial enzymes and transporters. The decreases seen in their activity were related to changes in respiration. This approach is now referred to as the bottom-up approach because the description of control is generated from analysing individual enzymatic components (Murphy, 2001). This

approach is limited, however, in that all system components must be known, and the measurement of flux control coefficients is difficult in intact cells. Another disadvantage lies in the difficulty of determining flux control coefficients for every enzyme in a pathway since specific inhibitors with known kinetic properties are often not available (Kunz, 2001). This led to the development of the top-down approach to metabolic control analysis.

In the top-down approach, a metabolic system is grouped into a number of blocks of reactions that either feed into or consume a common intermediate (Brown, et al., 1990). In contrast to the bottom-up approach, the top-down approach provides flux control coefficients for blocks of enzymatic reactions in a metabolic pathway rather than for individual reactions. The kinetic response of each block of the system to the concentration of the intermediate is measured in the presence and absence of an effector (Buttgereit, et al., 1994). Only those blocks that have a changed kinetic response to the intermediate contain sites of action that are important in changing the flux through the intermediate (Harper and Brand, 1993, Harper and Brand, 1995). A requirement for this approach is that the blocks of reactions must affect each other solely through the concentration of the intermediate. In other words, the blocks must not be able to influence each other without involving the intermediate of the system. The overall kinetics of a block of reactions is described in terms of elasticity. Elasticity describes the responsiveness of a branch of a metabolic pathway to changes in the amount of the intermediate in that pathway (Harper, et al., 1998). If the elasticity of a branch differs between two cell types being studied, for example, then one site of difference is located within the reactions encompassed by that branch.

The metabolic system that was investigated in this research is the oxidative phosphorylation system. In applying the top-down approach to oxidative phosphorylation, the system is divided into three blocks of reactions and the common intermediate is mitochondrial membrane potential ($\Delta\Psi_m$) (Figure 5). $\Delta\Psi_m$ is produced by the substrate oxidation block of the system, which includes cellular catabolic reactions, the citric acid cycle, and ultimately the electron transport chain. The $\Delta\Psi_m$ is consumed by the remaining two blocks. The phosphorylation branch of the system includes ATP synthesis and all cellular ATP-consuming reactions. The proton leak branch consists of the leak of protons and any cation cycles across the mitochondrial inner membrane. To manipulate the concentration of the intermediate, the blocks of reactions are titrated with various inhibitors or activators. Sites of regulation within the system are determined by simultaneously measuring the oxygen consumption (ie., flux) through the pathway.

For the purposes of this research, the top-down approach was used to examine the kinetics of proton leak reactions and look for differences between that in drug sensitive and drug resistant leukemic cells. This branch of reactions was made to be the only consumer of $\Delta\Psi_m$ by adding oligomycin, a specific inhibitor of ATP synthase that prevents any protons from returning to the mitochondrial matrix through this route. Any oxygen consumption that remains is that which is used to drive proton leak. This is referred to as state 4 respiration or maximal non-phosphorylating respiration. The kinetic response of the leak to $\Delta\Psi_m$ was assessed by titrating with antimycin, an inhibitor of complex III of the electron transport chain, in the presence of saturating amounts of oligomycin. Also, for one pair of sensitive and resistant leukemia cells the kinetics of

Figure 5 Schematic representation of the oxidative phosphorylation system. The intermediate within the system, mitochondrial membrane potential ($\Delta\Psi_m$), is produced by the substrate oxidation reactions and consumed by both the phosphorylation reactions and the proton leak reactions. The substrate oxidation reactions consist of glucose and endogenous substrate oxidations, the tricarboxylic acid (TCA) cycle, and the electron transport chain. The phosphorylation branch of the system includes $\Delta\Psi_m$-dependent ATP synthesis and cellular ATP-consuming reactions. Proton leak reactions consists of the leak of protons and any cation cycles across the mitochondrial inner membrane.

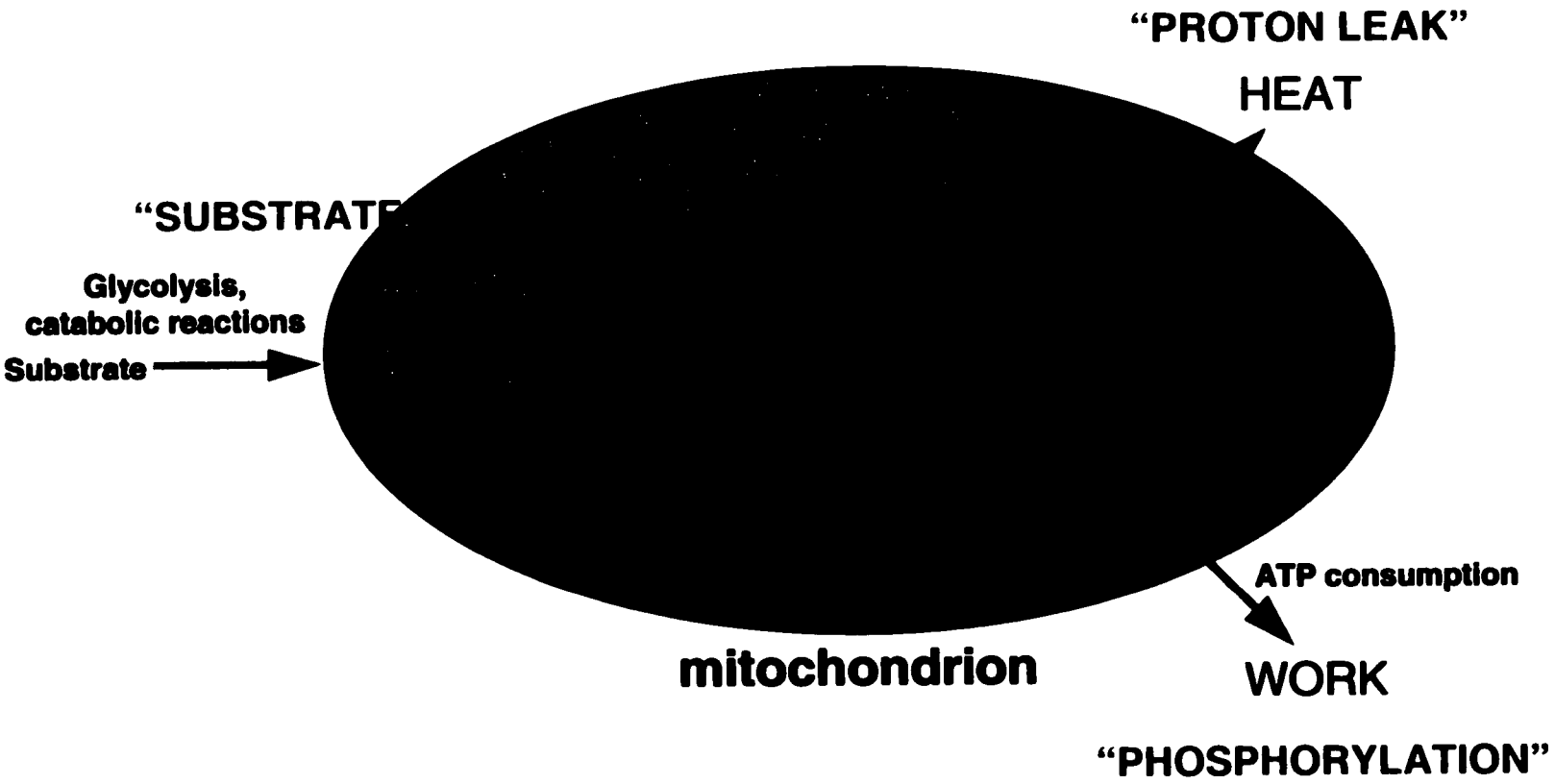
"PROTON LEAK"
HEAT
"SUBSTRATE"
Glycolysis,
catabolic reactions
Substrate
ATP consumption
mitochondrion
WORK
"PHOSPHORYLATION"

substate oxidation reactions was measured by titrating the $\Delta\Psi_m$ consumers with oligomycin. As well, the elasticity of the phosphorylation block to $\Delta\Psi_m$ was measured from titrations with antimycin alone.

METHODS AND MATERIALS

1. GENERAL METHODS

A) CELL CULTURE

(i) Cell Lines

L1210, L1210/DDP, HL60, and HL60/MDR cells were obtained from Dr. M. Karen Newell of the Department of Biology, University of Colorado at Colorado Springs. Cells were stored prior to use in liquid nitrogen containers in 2.0 ml cryovial microtubes (Sarstedt). The cells were stored at a concentration of 2.5×10^6 cells/ml in 1 ml of complete RPMI 1640 medium containing 10% dimethyl sulphoxide (DMSO). Cells were thawed at 37°C and added to 15 ml conical tubes (Sarstedt) containing 10 ml of medium and spun at 1000 rpm (200g) for 10 minutes at room temperature using a Beckman J-6B centrifuge. The medium was removed by suction and the cells were respuspended in 2 ml of medium and placed in a 8.8 cm^2 Nunclon® cell culture dish (Nalge Nunc International). The medium was replaced after 24 hours.

(ii) Incubation of Cells

All cell lines were cultured in complete RPMI 1640 medium. Cells were kept in 175 cm^2 tissue culture flasks (Falcon) at 37°C in a 5% CO_2/ 95% air Queue Systems incubator.

(iii) Preparation of Complete RPMI 1640 Medium

To a 500 ml bottle of RPMI 1640 medium (Wisent Inc.) containing 2 mM glutamine, the following were added under sterile conditions: 50000 units penicillin, 50 mg streptomycin, 1 mM sodium pyruvate, 50 μM 2-mercaptoethanol, and 4 mg gentamycin. Approximately 400 ml of this solution was poured into a sterile 500 ml media bottle (Gibco) through a 500 ml capacity bottle top filter (Nalgene). The filter is a polyethersulfone (PES) membrane with a 0.2 μm pore size. The contents were transferred to the bottle by suction, and when 100 ml was remaining in the filter 25 ml of heat-inactivated Fetal Calf Serum (5% final concentration; see section (iv) below) and the remaining volume of RPMI solution was added. The bottle of complete RPMI 1640 medium was stored at 4°C.

(iv) Heat Inactivation of Fetal Calf Serum

Fetal Calf Serum (FCS, Wisent Inc.) was removed from -20°C, heated to 56°C and held at this temperature for 45 minutes. 25 ml aliquots were transferred to sterile 50 ml conical tubes (Sarstedt) and the tubes were wrapped in Fisher® All-Purpose laboratory wrap. The tubes were stored at -20°C prior to use.

B) LOWRY ASSAY OF PROTEIN CONCENTRATION

The protein concentration of samples was measured using the Lowry assay adapted from Lowry et al. (Lowry, et al., 1951). Bovine serum albumin (BSA) at a concentration of 300 μg/ml in 0.5 N NaOH was used in the preparation of the reference standards. A six point calibration curve was constructed consisting of 0, 15, 30, 60, 90, and 120 μg of protein. The standards and samples were prepared simultaneously,

according to the following table:

	Standard/ Sample (µl)	Isolation medium (µl)	0.5 N NaOH (µl)	Copper Reagent (ml)	Phenol Reagent (ml)	Mass of Protein (µg)
standards	0	10	990	1	4	0
	50	10	940	1	4	15
	100	10	890	1	4	30
	200	10	790	1	4	60
	300	10	690	1	4	90
	400	10	590	1	4	120
sample	5	5	990	1	4	

Solutions were prepared in 16 x 100 mm borosilicate glass disposable culture tubes. Samples were assayed in triplicate to improve accuracy. The standard or the sample was added to the tubes followed by isolation medium (specific to that in which the sample was originally suspended) and 0.5 N NaOH. The tubes were mixed well by vortexing and then the copper reagent (10% Na_2CO_3, 0.1% $K_2C_4H_4O_6 \cdot \frac{1}{2}H_2O$, 0.05% $CuSO_4 \cdot 5H_2O$) was added and the tubes were mixed again and left for 10 minutes at room temperature. A commercially available 2N phenol reagent (Folin & Ciocalteu; BDH) was diluted 1:16 with H_2O just before use. The phenol reagent was added and the tubes were mixed immediately and incubated at 55°C for 5 minutes. To stop the reaction the tubes were placed on ice for 5-10 minutes and the solutions were transferred to polystyrene semi-micro disposable cuvettes. The absorbance was read at 550 nm using a Beckman DU®-65 spectrophotometer. The absorbance of the

standards was plotted as a function of protein content to produce a standard curve. The protein concentrations of the samples were calculated based on the equation for the standard curve.

2. Mitochondrial Bioenergetics in Intact Cells

A) Isolation and Incubation of Cells

Cells were transferred from the culture flasks to several 50 ml Falcon conical tubes and spun at 1000 rpm (200g) for 10 minutes at 4°C using a Beckman J-6B centrifuge. The culture medium was removed from the tubes by suction and the cell pellet in each tube was resuspended in isolation medium (100 mM sucrose, 10 mM EDTA, 100 mM Tris-HCl, and 46 mM KCl; pH 7.4). The volume of isolation medium added to each pellet was approximately twice that of the volume of the pellet. For each cell type, the cell suspensions were combined into one 50 ml conical tube. Cell concentration and cell viability were determined using a hemocytometer at 160x magnification and trypan blue dye (Sigma®). Two drops of cells, five drops of isolation medium, and three drops of 0.6% trypan blue were mixed in a minitube. The trypan blue dye exclusion method relies on a breakdown in membrane integrity determined by the uptake of the dye to which the cell is normally impermeable. A Pasteur pipette was used to transfer approximately 20 μl of the cell mixture from the minitube to the hemocytometer by ejecting the mixture at the edge of the chamber and allowing it to be drawn underneath the coverslip by capillary action until the surface was

uniformly covered. A grid made up of 25 squares, each containing 16 smaller squares, was used to count the cells. After determining the number of cells contained in the larger 25 square pattern, the concentration of cells was calculated as follows:

$$c = n \times 10^4 \times \text{dilution factor}, \quad \text{where } c = \text{concentration (cells/ml)}, \; n = \text{number of cells counted}$$

All cell suspensions had a viability of at least 90%. Prior to the incubations, the cell suspensions were stored on ice.

To study the kinetics of oxidative phosphorylation reactions (Figure 5), cell suspensions were diluted to a concentration of 1.0×10^7 cells/ml in a total volume of 2.5 ml with incubation medium (106 mM NaCl, 0.41 mM $MgSO_4$, 25 mM $NaHCO_3$, 10 mM Na_2HPO_4, 10 mM glucose, 2.5 mM $CaCl_2$, 5 mM KCl, 0.1 mg/ml inulin, and 0.1 mM methyltriphenylphosphonium bromide (TPMP-Br); pH 7.4). This cell suspension was placed in a 20 ml screw cap glass scintillation vial and the gas phase above the suspension was 95% air and 5% CO_2 to allow the medium to equilibrate to a pH of 7.4. Duplicate glass vials were prepared for the simultaneous determinations of oxygen consumption and mitochondrial membrane potential. The cells were preincubated at 37°C in a shaking water bath (50 cycles/second) for 10 minutes to allow the cells to reestablish steady state ion gradients after being stored on ice. Various inhibitors, uncouplers, and/or isotopes were then added to the cells and the incubation period continued for an additional 20 minutes. After a total of 30 minutes in the water bath, aliquots were taken for the measurements of oxygen consumption and mitochondrial membrane potential.

The resting state values for oxygen consumption and membrane potential were measured in the absence of inhibitors or uncouplers. Saturating concentrations of oligomycin (100 nM) were added to produce state 4 (non-phosphorylating) respiration conditions. Then to characterize the responsiveness of mitochondrial proton leak reactions to decreases in mitochondrial membrane potential, incremental amounts of the electron transport chain inhibitor, antimycin, were added (50 nM, 250 nM, and 5 μM). To characterize the responsiveness of the ATP synthesis and turnover reactions in cells incubated in the absence of oligomycin, increasing amounts of antimycin were added (100 nM, and 200 nM).

B) Determination of Oxygen Consumption

The respiration rate of the cells was determined using a Hansatech (Norfolk, U.K.) Clark-type oxygen electrode contained within a magnetically stirred incubation chamber kept at 37°C through the use of a water bath circulator. Assessments were performed in duplicate, each using 1.0 ml of cell suspension (1.0×10^7 cells). Respiration rates were measured approximately 2-3 minutes after the cell suspension was added to the chamber in order to allow a linear rate to be established. To determine the maximum respiratory capacity of the cells, 10 μM carbonyl cyanide p-trifluoromethoxyphenlyihydrazone (FCCP) was added to cells in the resting state and measured for approximately 5 minutes. Rates were monitored using the Duo 18™ data acquisition program (World Precision Instruments, FL) which provided real-time recording on a personal computer.

C) Determination of Mitochondrial Membrane Potential

(i) Measurement of Cellular Volume

After the 10 minute preincubation period, 2.5 μCi ^3H_2O/ml and 0.1 μCi (^{14}C)methoxyinulin/ml were added to the glass vial. After the cells were incubated for an additional 20 minutes at 37°C, triplicate aliquots of cell suspension (700 μl) were removed from the glass vial and transferred into 1.5 ml minitubes containing 300 μl of silicone oil (42% (v/v) dinonylphthalate and 58% silicone fluid D.C. 550) layered over 100 μl of Triton X-100 (2% (v/v) in 250 mM sucrose). The minitubes were spun at 13000g for 2 minutes at room temperature using a Hermle Z230M minicentrifuge. 200 μl aliquots of the supernatant were removed from the minitubes and transferred to 20 ml polyethylene scintillation vials and mixed with 5 ml of scintillation cocktail (Formula-989; Packard Bioscience B.V.). The residual supernatant and most of the oil layer were aspirated, and the walls of the minitubes were wiped with a twisted tissue. The pellet was resuspended by vortex mixing, and each minitube was placed into a scintillation vial and mixed with 5 ml of scintillation cocktail. The radioactivity of the supernatant and pellet were determined by dual-channel scintillation counting for ^{3}H and ^{14}C using a Beckman LS 1701 Liquid Scintillation Counter, with quench and cross-over accounted for. The volume of cell pellet available to each isotope, measured as its space in μl, was calculated as pellet dpm divided by the dpm/μl of the supernatant. Cellular volume was calculated as (^3H_2O space - (^{14}C)methoxyinulin space). The ^3H_2O provided a measure of total pellet volume while the (^{14}C)methoxyinulin, an impermeable probe, provided a measure of the extracellular volume of the pellet. Cellular volume was

measured each day in parallel with mitochondrial membrane potential ($\Delta\Psi_m$) to ensure accurate results.

(ii) Measurement of Plasma Membrane Potential

After the 10 minute preincubation period, 0.1 μCi $^{36}Cl^-$/ml and 2.5 μCi ^3H_2O/ml were added to the glass vial. To examine the effects of GDP on plasma membrane potential, 10 μl of 250 mM GDP was added at this time. After the cells were incubated for an additional 20 minutes at 37°C, triplicate aliquots of cell suspension (700 μl) were removed from the glass vial and processed as described above for the measurement of cellular volume. The radioactivity of the supernatant and pellet were determined by dual-channel scintillation counting for ^3H and ^{36}Cl, with quench and cross-over accounted for. The volume of cell pellet available to each isotope, measured as its space in μl, was calculated as pellet dpm divided by the dpm/μl of the supernatant. The chloride accumulation ratio ($([Cl^-]_e/[Cl^-]_{tot}$) was calculated as ((^3H_2O space - (^{14}C)methoxyinulin space) - (^3H_2O space - $^{36}Cl^-$ space)/(^3H_2O space - (^{14}C)methoxyinulin space)). Cellular volume was measured in parallel to obtain values for ^3H_2O space and (^{14}C)methoxyinulin space. $\Delta\Psi_p$ was calculated using the Nernst equation as follows:

$$\Delta\Psi_p = -61.5 \times \log([Cl^-]_e/[Cl^-]_{tot})$$

(iii) Measurement of Mitochondrial Membrane Potential

The $\Delta\Psi_m$ was calculated based on the cellular distribution of the lipophilic cation, methyltriphenylphosphonium (TPMP$^+$) as described by Nobes et al. (Nobes, et al., 1990) and Harper and Brand (Harper and Brand, 1993). The relationship between

$\Delta\Psi_m$ and distribution of $TPMP^+$ at 37°C is:

$$\Delta\Psi_m = -61.5 \log \left| \frac{V_c \cdot a_m}{V_m \cdot a_c} \left[\frac{[Cl^-]_{tot}[TPMP]_{tot}\, a_c\, (V_c + V_m)}{[Cl^-]_e[TPMP]_e\, a_e\, V_c} - 1 \right] \right|$$

After the 10 minute preincubation period, 0.1 μCi (^{3}H)$TPMP^+$/ml was added to the glass vial prepared for the determination of $\Delta\Psi_m$. After the cells were incubated for an additional 20 minutes at 37°C, triplicate aliquots of cell suspension (700 μl) were removed from the glass vial and processed as described above for the measurement of cellular volume. The radioactivity of the supernatant and pellet were determined by dual-channel scintillation counting for ^{3}H and ^{14}C, with quench and cross-over accounted for. The volume of cell pellet available to each isotope, measured as its space in μl, was calculated as pellet dpm divided by the dpm/μl of the supernatant.

$\Delta\Psi_m$ is calculated by knowing the proportion of cytoplasmic volume that is occupied by the mitochondrial matrix ((V_m/V_c) or mitochondrial volume/cell volume), the apparent activity coefficient of $TPMP^+$ in the extracellular, cytoplasmic plus nuclear, and mitochondrial compartments (a_e, a_c, and a_m, respectively), and the extent of $TPMP^+$ accumulation into the whole cell ($([TPMP^+]_t/[TPMP^+]_e$) and within the cytoplasm in relation to the external medium ($([Cl^-]_e/[Cl^-]_t$), where t = total and e = extracellular. The volume of pellet available to each isotope, measured as its space in μl, was calculated as pellet dpm divided by the dpm/μl of the supernatant. The (^{3}H)$TPMP^+$ accumulation ratio ($([TPMP^+]_t/[TPMP^+]_e$) was calculated as ((^{3}H)$TPMP^+$ space - (^{14}C)methoxyinulin space)/(^3H_2O space - (^{14}C)methoxyinulin space). The values for V_m,

$(Cl^-)_e/(Cl^-)_v$ and the activity coefficients were adopted from Buttgereit et al. (Buttgereit, et al., 1994).

3. Expression of Uncoupling Protein 2

A) Isolation of Mitochondria

Mitochondria were isolated using differential centrifugation as adapted from the protocol described by Reinhart et al. (Reinhart, et al., 1982). Cells were transferred from the culture flasks to several 50 ml Falcon conical tubes and spun at 1000 rpm (200g) for 10 minutes at 4°C using a Beckman J-6B centrifuge. The culture medium was removed from the tubes by suction and the pellet in each tube was resuspended in isolation medium (100 mM sucrose, 10 mM EDTA, 100 mM Tris-HCl, and 46 mM KCl; pH 7.4). The volume of isolation medium added to each pellet was approximately twice that of the pellet. The cell suspensions were combined into one 50 ml conical tube and spun at 1000 rpm (200g) for 10 minutes at room temperature. The cell pellet was resuspended in 12 ml of isolation medium and 3.8 ml of 60% glycerol/40% isolation medium (2 M final glycerol concentration) was added. The solution was gently mixed and left at room temperature for 10 minutes. The cell suspension was spun at 1800 rpm (700g) for 10 minutes at room temperature. The cell pellet was resuspended in 10 ml of isolation medium and a sample of cells in the presence of trypan blue (as described above) was examined using a hemocytometer to ensure that the cells had been broken open. The resulting cell homogenate was spun at 2000 rpm (480g) for 10

minutes at 4°C using a Sorvall Superspeed RC2-B Automatic Refrigerated Centrifuge equipped with a SS-34 rotor. The supernatant was then poured through a 250 μm filter (Nitex) into a clean centrifuge tube and spun at 10000 rpm (12000g) for 10 minutes at 4°C. The resulting supernatant was discarded and the pellet was resuspended, using a blunt ended glass stirring rod, with 5 ml of isolation medium. The suspension was spun at 10000 rpm (12000g) for 10 minutes at 4°C. The final mitochondrial pellet was resuspended in suspension medium (120 mM KCl, 20 mM sucrose, 20 mM glucose, 10 mM KH_2PO_4, 5 mM HEPES, 2 mM $MgCl_2$, and 1 mM EGTA; pH 7.4). The protein concentration of the mitochondrial suspension was determined by the Lowry method described above.

B) Isolation of Plasma Membrane Fractions

To isolate plasma membranes of cells, the method described by Caldwell *et al.* (Caldwell, et al., 1988) was employed. Using this method, the authors (including our collaborator) demonstrated plasma membrane separation using adenylate cyclase as an enzymatic marker, and also measured GTP in the isolated fractions as a indicator of contamination. Cells were transferred from the culture flasks to several 50 ml Falcon conical tubes and spun at 1000 rpm (200g) for 10 minutes at 4°C using a Beckman J-6B centrifuge. The culture medium was removed from the tubes by suction and the pellet in each tube was resuspended in PB-PI buffer (86 mM glucose, 96 mM NaCl, 0.1 mM EGTA, 5 mM EDTA, 20 mM HEPES; pH 7.4 containing 30 μg/ml soybean trypsin inhibitor, 6 μg/ml leupeptin, 6 μg/ml antipain, 15 units/ml aprotinin, and 3 μg/ml pepstatin). The cell suspensions were combined into one 50 ml conical tube and PB-PI buffer was

added to a total volume of 50 ml. The cell suspension was spun at 1000 rpm (200g) for 5 minutes at 4°C. The cell pellet was resuspended in 12 ml of PB-PI and 3.8 ml of 60% glycerol/40% PB-PI buffer (2 M final glycerol concentration) was added. The solution was gently mixed and left at room temperature for 10 minutes. The cell suspension was spun at 1800 rpm (700g) for 10 minutes at room temperature. The cell pellet was resuspended in 10 ml of hypotonic lysis buffer (20 mM HEPES, 25 mM sucrose, 0.1 mM EGTA; pH 7.4) and a sample of cells in the presence of trypan blue (as described above) was examined using a hemocytometer to ensure that the cells had been lysed. The 10 ml of cell homogenate was mixed with 10 ml of a 60% sucrose solution. 10 ml of the resulting 30% sucrose solution was layered onto 20 ml of a 50% sucrose solution in a polyethylene ultracentrifuge tube and balanced with an identical tube to within +/- 0.01 g. The tubes were spun at 23000 rpm (96500g) for 1 hour at 4°C using a Beckman L8-55M ultracentrifuge equipped with a SW-28 rotor. The material that collected at the interface of the two sucrose solutions was collected and diluted with 10 ml of lysis buffer, and spun at 17000 rpm (35000g) for 20 minutes at 4°C using a Sorvall Superspeed RC2-B Automatic Refrigerated Centrifuge equipped with a SS-34 rotor. The final plasma membrane pellet was resuspended in PB-PI buffer, and the protein concentration was determined by the Lowry method described above.

C) Polyacrylamide Gel Electrophoresis and Western Blotting

(i) Sample Preparation

Detection of uncoupling protein 2 in samples was performed using polyacrylamide gel electrophoresis and Western blotting. Samples were prepared by

diluting them with an appropriate amount of phosphate buffered saline (PBS; 5.2 mM K_2HPO_4, 1.5 mM KH_2PO_4, 140 mM NaCl, 3 mM KCl; pH 7.4) followed by the addition of an equal volume of sample loading buffer (2% sodium dodecyl sulfate (SDS), 100 mM Tris-HCl, 4 mM PMSF in isopropanol, 2 mM EDTA with bromophenol, 25% glycerol (w/v), 10% 2-mercaptoethanol (v/v)) to achieve a final concentration of 2 μg protein/μl. Molecular weight markers (Santa Cruz Biotechnology, Inc.) were used undiluted as recommended by the supplier, and Rainbow molecular weight markers (Amersham Pharmacia Biotech) were prepared by addition of PBS and sample loading buffer in a 2:3:5 ratio, respectively. Recombinant mouse UCP2 (Stratagene®) was prepared with PBS and sample loading buffer in a 1:49:50 ratio, respectively, to a concentration of 1 ng/μl.

(ii) Electrophoresis

For the casting and running of gels, the Mini-PROTEAN® II Electrophoresis Cell (Bio-Rad) was used. Glass plate sandwiches were assembled on a casting stand and checked for leaks using 100% ethanol. The separation gel (16% acrylamide, 1% bisacrylamide, 9% Tris base, 120 mM HCl, 0.06% TEMED, 0.1% SDS, 0.1% ammonium persulfate) was poured into the assembled gel sandwiches using a 1 ml pipette to a level approximately 1 cm below the point at which the comb would be placed. The separation gel was immediately overlaid with distilled water and left to polymerize for 45 minutes. Following polymerization, the distilled water was removed by inversion of the casting stand and the area above the separation gel was dried. The stacking gel (4% acrylamide, 0.3% bisacrylamide, 0.8% Tris base, 60 mM HCl, 0.06% TEMED, 0.1% SDS,

0.1% ammonium persulfate) was poured above the separation gel and a comb was placed in the solution. The gel was left to polymerize for 30 minutes. Following polymerization, the comb was removed gently and the gel cassettes were removed from the casting stand and attached to the inner cooling core. The inner cooling core was lowered into the electrophoresis cell and running buffer (0.3% Tris base, 1.4% glycine, 0.1% SDS) was added to the inner chamber until it overflowed and reached approximately 2 cm above the bottom of the gels. Prior to loading the samples, Rainbow molecular weight markers were boiled for 1 minute and recombinant UCP2 and molecular weight markers were boiled for 3 minutes. The samples were loaded with a Hamilton syringe inserted approximately 1-2 mm from the well bottom before delivery. Runner buffer was added to completely fill the chamber and the lid was placed on top of the electrophoresis cell. The electrical leads were attached to a power supply and the gels were run for 170 minutes at 180 V.

(iii) Transfer

After electrophoresis was complete, the gels were removed from the glass plates and placed in transfer buffer (0.7% glycine, 0.15% Tris base, 20% methanol (v/v)) to equilibrate for 30 minutes at room temperature with moderate shaking. For the transfer procedure, a Mini Trans-Blot® Electrophoretic Transfer Cell (Bio-Rad) was used. The 0.45 μm nitrocellulose membrane (NCM; Bio-Rad) and the filter paper (Whatman® Grade No. 1) were cut to the dimensions of the gel and were soaked in transfer buffer along with the fiber pads for 30 minutes prior to assembling the gel sandwich. The sandwich was assembled in the gel holder cassette in the following order: fiber pad,

2 pieces of filter paper, gel, NCM, 2 pieces of filter paper, fiber pad. The cassette was placed into the electrode module situated in the buffer tank. A frozen Bio-Ice cooling unit (used to absorb heat during the transfer) was placed in the tank which was then filled with transfer buffer. A stir bar was added to help maintain even buffer temperature and ion distribution in the tank. The lid was placed on top of the transfer cell, the leads were attached to a power supply, and the transfer proceeded for one hour at 120 V.

After the transfer was complete, the NCM was removed, wrapped in Fisher® All-Purpose laboratory wrap and stored at 4°C until immunoblotting took place. Storage of NCM following protein transfer never exceeded 2 days.

(iv) Immunoblotting

For immunoblotting, all incubations and washes were performed at room temperature with shaking on a Belly Dancer® shaker (Stovall Life Science Inc.). To block non-specific binding sites the membrane was incubated in blocking solution (5% skim milk powder, 0.1% Tween® 20 in PBS) for 45 minutes with gentle shaking. The membrane was rinsed using two changes of washing solution (0.1% Tween® 20 in PBS) followed by two washes for 5 minutes and one wash for 10 minutes with vigorous shaking. Incubation of the membrane with primary antibody (goat anti-human UCP2; Santa Cruz Biotechnology, Inc.) diluted in antibody keeping solution (3% BSA, 0.2% NaN_3 in H_2O) to a concentration of 1.5 μg/ml was performed for one hour with gentle shaking. The membrane was rinsed with washing solution followed by two washes for 5 minutes and two washes for 10 minutes with vigorous shaking. Incubation of the

membrane with secondary antibody (donkey anti-goat IgG horseradish peroxidase conjugate; Santa Cruz Biotechnology, Inc.) diluted 1:5000 in PBS containing 5% skim milk powder was performed for one hour with gentle shaking. The membrane was rinsed with washing solution followed by two washes for 5 minutes and three washes for 15 minutes with vigorous shaking. A final two washes were performed for 5 minutes each in PBS alone.

(v) Detection

Detection of the immobilized specific antigens conjugated indirectly with the horseradish peroxidase labelled secondary antibody was performed using an Enhanced chemiluminescence (ECL™) Western Blotting Detection System (Amersham Pharmacia Biotech). The blot was placed in the detection boat of an ECL™ Mini-Camera (Amersham Pharmacia Biotech), protein side down. The lid was closed and the blot was exposed to the film (Polaroid Polapan) for various exposure times.

4. Enzymatic Assays

A) Measurement of Cytochrome Oxidase Activity

Cytochrome oxidase (COX) was determined in cellular homogenates as an indicator of mitochondrial content based on the method of Yonetani and Ray (Yonetani and Ray, 1965). A spectrophotometric assay was used to measure the rate at which COX can oxidize its substrate, cytochrome c. This was done be measuring the rate of disappearance of the reduced cytochrome c, which absorbs light at 550 nm.

Cellular homogenates were solubilized with a 0.3% Lubrol WX solution. For each 10 μg of cellular protein, 1 μl of the Lubrol solution was added and the sample was then diluted to a final protein concentration of 1.0 mg/ml with 0.1M phosphate buffer (K_2HPO_4, pH 7.0). The Lubrol solubilized homogenate was mixed well and kept on ice for 1.5 hours, with occasional mixing. During this period, a fresh solution of 202 μM cytochrome c, pH 7.0 (horse heart, type III; Sigma®) was prepared containing 0.025% ascorbic acid to keep the cytochrome c in its reduced form. For each determination an aliquot of Lubrol solubilized homogenate (100 μg) was added to a polystyrene semi-micro disposable cuvette containing phosphate buffer and mixed well. Cytochrome c was then added to the cuvette, mixed well by inversion, and immediately placed in a Beckman DU®-65 spectrophotometer and the absorbance was read continuously for 1 minute at 550 nm. The Beckman Kinetic Soft-Pac module (program 6: kindata) was used to compile the data and obtain reaction rates. For each assay, six different concentrations of cytochrome c (13.4, 20.1, 26.8, 33.5, 40.2, and 46.9 μM) were used. A Lineweaver-Burk plot was constructed by plotting the reciprocal of the initial velocity against the reciprocal of the cytochrome c concentration in order to obtain a V_{max} for each sample, calculated as the reciprocal of the y-intercept.

B) Quantitation of Intracellular ATP Levels

For each determination, 50000 cells were aliquoted into 1.5 ml minitubes and six minitubes were prepared for each cell line. The minitubes were spun at 13000g for 2 minutes at room temperature using a Hermle Z230M minicentrifuge. The supernatant was removed with a pipette and the cells were resuspended in 200 μl PBS with gentle

mixing. The cells were washed once more and resuspended in 300 µl glycine buffer (20 mM glycine, 50 mM $MgSO_4$, 4 mM EDTA; pH 7.4). The samples were heated at 100°C for 1 minute to extract the ATP. Samples were cooled at room temperature and stored at -20°C until ready for use. To determine cellular protein content, samples were resuspended in 300 µl glycine buffer containing 0.5% Triton X-100 and assayed using the Lowry determination of protein concentration as described above.

Samples were thawed at room temperature and 100 µl from each sample was transferred into two 20 ml screw cap glass scintillation vials for duplicate determinations. A Luciferase-luciferin (Sigma®) working solution was prepared at a concentration of 0.5 mg/ml and kept on ice. A fresh working solution was prepared for each cell line to optimize enzyme activity. To the 100 µl of sample, 75 µl of Luciferase-luciferin working solution was added and the vial was mixed quickly yet gently and placed in a Beckman LS 1701 Liquid Scintillation Counter for immediate counting. A standard curve for ATP was constructed from 50 nM to 700 nM in 50 nM increments and processed as above.

5. RNA Analysis

Precautions taken to prevent RNase contamination included the use of powder-free disposable gloves at all times, use of glassware that had been previously heated at 200°C for at least 4 hours, and treatment of solutions (where possible) with diethylpyrocarbonate (DEPC). DEPC binds to RNase, irreversibly inactivating it.

A) Isolation of Total RNA

Isolation of total RNA was performed according to the insert provided with the TRIzol® Reagent (Gibco BRL™) and is adapted from the method developed by Chomczynski and Sacchi (Chomczynski and Sacchi, 1987). Cells were transferred from the culture flask to a 50 ml Falcon conical tube and spun at 1000 rpm (200g) for 10 minutes at 4°C using a Beckman J-6B centrifuge. The culture medium was removed from the tube by suction and the cells were lysed in TRIzol® Reagent by repetitive pipetting. Approximately 1 ml of the reagent was used for every 5×10^6 cells. The cell lysate was transferred to a 1.5 ml minitube and incubated for 5 minutes at room temperature to allow the complete dissociation of nucleoprotein complexes. For every 1 ml of TRIzol® Reagent, 200 µl of chloroform was added and the tube was shaken vigorously by hand for 25 seconds followed by incubation for 3 minutes at room temperature. The tube was spun at 11300 rpm (12000g) for 15 minutes at 4°C using a Micromax mini centrifuge (International Equipment Co.). Following centrifugation, the RNA remained in the upper aqueous phase, separated from the interphase and a lower phenol-chloroform phase. The aqueous phase was transferred to another 1.5 ml minitube and the RNA was precipitated by adding 500 µl of isopropyl alcohol for every 1 ml of TRIzol® Reagent used to lyse the cells. The sample was incubated for 10 minutes at room temperature and spun at 11300 rpm (12000g) for 10 minutes at 4°C. The supernatant was removed and the RNA pellet was washed once with 1 ml of 75% ethanol for every 1 ml of TRIzol® Reagent initially used. The sample was mixed by vortexing and spun at 9000 rpm (7500g) for 5 minutes at 4°C. The supernatant was removed and the pellet was air dried for 10 minutes. The RNA was dissolved in DEPC-

treated sterile distilled water by repetitive pipetting and incubated at 55°C for 10 minutes to release any remaining ethanol vapour.

The concentration of the RNA was determined by measuring the absorbance at 260 nm and using the following equation:

$$\text{RNA concentration (in } \mu g/\mu l) = \frac{\text{absorbance} \times 40 \times \text{dilution factor}}{1000}$$

Absorbance was also measured at 270 nm and 280 nm to determine the purity of the isolated sample. The ratio of A_{260}/A_{280} equals 1.8 for pure nucleotides and the ratio of A_{260}/A_{270} equals 1.28 for pure RNA. The RNA was stored at -20°C.

B) Northern Blot Analysis

(i) Electrophoresis

A 1.2% agarose gel was prepared by adding 1.2 g of agarose to 87 ml of DEPC-treated sterile distilled water. The solution was boiled until the agarose melted and allowed to cool for approximately 20 minutes. 10 ml of 10X 3-(N-Morpholino) propanesulfonic acid (MOPS) buffer (200 mM Mops, 50 mM CH_3COONa, 20 mM ethylene diamine tetraacetic acid (EDTA); pH 7.0) and 5.1 ml of 37% formaldehyde were added to the solution and the gel was immediately poured onto the casting plate containing a comb. Any air bubbles on the surface of the gel were removed by touching with a sterile pipette tip. The gel was left to set for 1 hour.

RNA samples were prepared in 1.5 ml minitubes with 20 μg of RNA added to 20 μl of loading buffer (12.4 M formamide, 2.2 M formaldehyde, 1X MOPS, 7% glycerol, 0.25% bromophenol blue). The RNA sample was heat-denatured at 65°C for 10 minutes

in a water bath, and cooled on ice for 2 minutes. Ethidium bromide was added to give a final concentration of 2 μg/ml.

The comb was removed and the wells of the gel were rinsed with running buffer (1X MOPS). The electrophoresis tank was filled with running buffer and the samples were loaded. The gel was run for 4 hours at 68V.

(ii) Transfer

The gel was soaked in denaturation buffer (50 mM NaOH, 100 mM NaCl in DEPC-treated sterile distilled water) for 20 minutes with gentle shaking on the Belly Dancer® shaker. This partially cleaves the RNA molecules and aids in the transfer of larger molecules. The gel was placed in neutralization buffer (100 mM Tris-HCl pH 7.6 in DEPC-treated sterile distilled water) for 20 minutes with gentle shaking and then washed twice for 20 minutes each in 2X SSC buffer (300 mM NaCl, 30 mM $Na_3C_6H_5O_7 \cdot 2H_2O$; pH 7.0). A piece of nylon membrane (Roche Molecular Biochemicals) was cut to the size of the gel and soaked for 5 minutes in DEPC-treated sterile distilled water followed by a 10 minute soak in 20X SSC buffer.

The blotting apparatus was set up by placing several sheets of Whatman® Grade No. 1 filter paper soaked in 20X SSC buffer on a glass plate contained in a dish filled with 20X SSC buffer to just below the glass plate level. The ends of the filter paper are immersed in the 20X SSC buffer to act as a wick for the buffer. The gel is placed on the filter paper and surrounded with a layer of Parafilm® "M" Laboratory Film (American National Can™) on the exposed areas of the filter paper. This ensures that the only route for the 20X SSC buffer from the dish is through the gel. The surface of the gel was

kept wet with buffer, and the nylon membrane was placed on top of the gel, avoiding air bubbles being trapped in between. Three layers of pre-soaked filter paper were cut to the exact size of the gel and placed on top of the membrane. Several inches of paper towels were placed on the filter papers, and covered with a glass plate and a lead weight. The transfer proceeded overnight with the paper towels being replaced as they became completely wet. Following transfer, the paper towels were removed and the gel orientation on the membrane was marked. The membrane was removed from the gel and washed twice in 2X SSC for 5 minutes, then baked at 80°C for 2 hours. At this stage the membrane could be stored dry at 4°C until ready for hybridization.

(iii) Hybridization

The membrane was placed in a plastic dish containing DIG Easy Hyb (Roche Molecular Biochemicals) hybridization buffer. The dish was closed and placed in a 65°C water bath for 30 minutes with gentle shaking. The digoxigenin-labeled UCP2 probe (previously prepared in our laboratory) was boiled for 5 minutes and cooled on ice for 1 minute. The probe was added to hybridization buffer to give a final concentration of 100 ng/ml and the membrane was placed in this solution. The membrane was hybridized at 65°C overnight. Following hybridization, the membrane was washed twice for 5 minutes in post-hybridization solution 1 (2X SSC, 0.1% SDS in DEPC treated water) at room temperature with vigorous shaking. The membrane was then washed twice for 15 minutes in post-hybridization solution 2 (0.1X SSC, 0.1% SDS in DEPC treated water) at 65°C with vigorous shaking.

(iv) Immunological Detection

The membrane was removed from the washing solution and incubated for 30 minutes at room temperature in 100 ml blocking solution consisting of 1% blocking reagent (Roche Molecular Biochemicals) in maleic acid buffer (100 mM $C_3H_3O_2COOH$, 150 mM NaCl; pH 7.5). Anti-Digoxigenin-AP (Roche Molecular Biochemicals) was diluted 1:10000 in 10 ml of blocking solution and the membrane was incubated for 30 minutes in this solution. The membrane was rinsed briefly in the remaining 90 ml of blocking solution and washed twice for 10 minutes in washing buffer (0.3% Tween® 20 in maleic acid buffer) at room temperature. The membrane was removed from the washing buffer and equilibrated for 5 minutes in 20 ml of detection buffer (100 mM Tris-HCl, 100 mM NaCl; pH 9.5). Following equilibration the membrane was placed on a sheet of plastic laboratory wrap and approximately 1 ml of CDP-Star (Roche Molecular Biochemicals) was added per 100 cm^2 of membrane. A second sheet of plastic laboratory wrap was used to cover the membrane. After a 5 minute incubation, the membrane was photographed under ultraviolet light in a MultiImage™ Light Cabinet using Alpha Ease™ imaging software (AlphaInnotech Corporation).

6. Molecular Biology Techniques in the Visualization of Uncoupling Protein 2 Cellular Localization

A) Preparation of Competent Bacterial Cells

All manipulations were made in sterile conditions and all solutions were

autoclaved prior to use. An overnight culture of *Escherichia coli* (*E. coli*) DH5α bacteria was grown on Lenox broth (LB) medium plates (1% tryptone, 0.5% yeast extract, 0.5% NaCl, 1 mM NaOH, 1.5% agar; pH 7.4) at 37°C. The following day an average size colony was selected from the plate by touching a sterile pipette tip to the colony. The tip was placed in an Erlenmeyer flask containing 25 ml of LB medium (1% tryptone, 0.5% yeast extract, 0.5% NaCl, 0.5% NaCl; pH 7.4 with 1N NaOH) and the flask was covered with plastic laboratory wrap and placed into a controlled environment incubator shaker (New Brunswick Scientific Co.) at 250 rpm and 37°C in a darkroom and left overnight. The next morning, the overnight culture was diluted 1:100 in LB medium to obtain a final volume of 60 ml in a sterile Erlenmeyer flask. The diluted bacteria were grown in the incubator shaker (250 rpm, 37°C) until the absorbance of the solution measured at 600 nm was between 0.30 and 0.60. The absorbance was measured as 1 ml of culture against 1 ml of LB medium. The culture was transferred into two 50 ml conical tubes and spun at 2000 rpm (900g) for 15 minutes at 4°C using a Beckman J-6B centrifuge. The supernatant was discarded and the cells were resuspended in a total volume of 20 ml of cold RF1 solution (100 mM RbCl, 50 mM $MnCl_2 \cdot 4H_2O$, 30 mM CH_3COOK, 10 mM $CaCl_2 \cdot 2H_2O$, 15% (w/v) glycerol; pH 5.8). The cells were incubated on ice for 30 minutes and spun at 2000 rpm (800g) for 15 minutes at 4°C. The supernatant was discarded and the cells were resuspended in 5 ml cold RF2 solution (10 mM MOPS, 10 mM RbCl, 75 mM $CaCl_2 \cdot 2H_2O$, 15% (w/v) glycerol; pH 6.8). The cells were incubated on ice for 15 minutes, and 250 μl aliquots were transferred to 2.0 ml cryovial microtubes and flash frozen in a liquid nitrogen bath for 3 minutes. The cells were stored at -80°C.

B) Transformation of *E. Coli* with UCP2-pIRES2-EGFP Construct

All manipulations were made in sterile conditions and all solutions were autoclaved prior to use. In a 15 ml conical tube, 1 ng of UCP2-pIRES2-EGFP DNA construct (obtained from Dr. Mike Wheeler) was added to 10 μl sterile distilled H_2O and the tube was placed on ice. Competent E. Coli cells were thawed on ice and 200 μl of cells were transferred to the conical tube. The tube was swirled gently to mix the DNA evenly with the cells and was incubated on ice for 45 minutes. The cells were heat shocked by placing the tube in a 42°C water bath for 90 seconds and then immediately on ice. 800 μl of SOC medium (2% tryptone, 0.5% yeast extract, 10 mM NaCl, 2.5 mM KCl, 10 mM $MgCl_2$, 10 mM $MgSO_4$, 20 mM glucose; pH 7.0) was added to the tube followed by incubation at 37°C for 45 minutes with moderate agitation. The solution was spread on LB medium plates containing 50 μg/ml kanamycin A (Sigma®) and left overnight at 37°C.

C) Mini-Prep Procedure to Isolate Plasmid from Transformed Cells

All manipulations were made in sterile conditions and all solutions were autoclaved prior to use. The following day an average sized colony was selected from the plate by touching a sterile pipette tip to the colony. The tip was placed in an Erlenmeyer flask containing 25 ml of LB medium and the flask was covered with plastic laboratory wrap and placed into the incubator shaker (250 rpm, 37°C) in a darkroom and left overnight. The next day 2.0 ml of culture was transferred to a 2.0 ml minitube and spun at 14000 rpm (18300g) for 2 minutes at room temperature using a Micromax mini centrifuge. The supernatant was removed by suction and the cells were

resuspended in 150 µl of cold P1 buffer (50 mM Tris-HCl, 10 mM EDTA, 400 µg/ml RNAse) and mixed by vortexing. An equal volume of P2 buffer (200 mM NaOH, 1% SDS) was added and the minitube was mixed by inversion several times until the contents became very viscous, then incubated for 5 minutes at room temperature. An equal volume of P3 buffer (3 M CH_3COOK, 12% (v/v) glacial acetic acid) was added and the minitube was mixed gently by hand until a white precipitate formed. The minitube was spun at 14000 rpm (18300g) for 10 minutes at 4°C to pellet the white precipitate. The supernatant was transferred to a new minitube containing 1 ml of 100% ethanol and was mixed by vortexing. The minitube was spun at 14000 rpm (18300g) for 10 minutes at 4°C to pellet the plasmid DNA. The ethanol was removed using a pipette and the pellet was air dried for 10 minutes at room temperature. Depending on the size of the pellet, 30-50 µl of TE buffer (10mM Tris-HCl, 1 mM EDTA; pH 8.0) was added and the pellet was resuspended by vortexing. The minitube was placed in a 65°C incubator for 15 minutes (cap closed) to remove any remaining ethanol from the minitube. The tube was opened to release any pressure that had built up.

The concentration of the DNA was determined by measuring the absorbance at 260 nm and using the following equation:

$$\text{DNA concentration (in } \mu g/\mu l) = \frac{\text{absorbance} \times 50 \times \text{dilution factor}}{1000}$$

The DNA was stored at -20°C.

D) Restriction Endonuclease Digestion of DNA

All components of the solution to be prepared were thawed, with the exception

of the restriction enzyme, and placed on ice. The final volume of the digest was 25 μl and consisted of 5 μg DNA, 2 μl of 10X REact 3 buffer (50 mM Tris-HCl, 10 mM $MgCl_2$, 100 mM NaCl; Gibco BRL™), 10 units EcoRI (2 units/μg DNA; Gibco BRL™), and sterile distilled water. The components were added into a sterile 1.5 ml minitube with the restriciton enzyme stock being added last, directly from -20°C. In a separate minitube, 40 μl of λ DNA (Gibco BRL™) was mixed with 5 μl of 10X reaction buffer and 50 units EcoRI. The minitubes were mixed gently and incubated at 37°C for 1 hour. A 1% agarose gel was prepared by mixing 0.8g agarose in 80 ml of 1X TBE buffer (50 mM Tris base, 50 mM H_3BO_3, 1 mM EDTA-$Na_2 \cdot 2H_2O$). The solution was boiled until the agarose melted and allowed to cool for approximately 20 minutes. Ethidium bromide was added to give a final concentration of 2 μg/ml and the gel was poured onto the casting plate containing a comb and left 20 minutes to polymerize. Samples were prepared for loading by combining 5 μl of the digest with 2 μl of DNA loading buffer (50%(v/v) glycerol, 50 mM EDTA, 0.125% (w/v) bromophenol blue, 0.125% (w/v) xylene cyanol, pH 8.0) and 5 μl of sterile distilled water. For the λ DNA sample to be loaded, 3 μl of the digest was combined with 2 μl of DNA loading buffer and 7 μl of sterile distilled water. Following polymerization, the comb was removed and the samples were loaded into the gel. The electrophoresis tank was filled with 1X TBE and the gel was run for approximately 1 hour at 68V. Image analysis of the gel was performed under ultraviolet light in a MultiImage™ Light Cabinet using Alpha Ease™ imaging software. Restriction endonuclease digestion confirmed the successful isolation of the UCP2-pIRES2-EGFP construct from the transformed cells.

E) Transfection of Leukemic Cells with UCP2-pIRES2-EGFP Construct

Transfection of cells was performed according to the insert provided with the LipofectAMINE™ Reagent (Gibco BRL™). In a Nunclon® 9.6 cm^2 6 well cell culture plate (Naige Nunc International), 3×10^5 cells were seeded out per well in 2 ml of complete RPMI 1640 medium. The wells contained sterile glass cover slips coated with 0.1% gelatin that had been dried in a laminar flow hood the previous day. The cells were incubated for 20 hours at 37°C in a 5% CO_2/ 95% air incubator, until they were approximately 80% confluent. Solution A consisted of 2 μg of the construct in 100 μl of serum-free Opti-MEM® Reduced Serum Medium (Gibco BRL™). Solution B consisted of 15 μl of LipofectAMINE™ Reagent in 100 μl of serum-free medium. Solutions A and B were combined into one 1.5 ml minitube, mixed gently, and incubated at room temperature for 45 minutes to allow the DNA-liposome complexes to form. During this incubation, the cells were rinsed with 2 ml of serum-free medium. Following the incubation, 0.8 ml of serum-free medium was added to the minitube containing the complexes and the solution was mixed gently and overlayed onto the rinsed cells. The cells were incubated with the complexes for 10 hours at 37°C after which 1 ml of complete RPMI 1640 medium containing twice the normal concentration of serum (10%) was added without removing the transfection mixture. The medium was replaced with 3 ml fresh complete medium 24 hours following the beginning of the transfection. The transfection proceeded for a total of 48 hours, after which cells were treated with the fluorescent probe Mitotracker® Red (Molecular Probes Inc.) followed by cell fixation and confocal microscopy analysis.

F) Treatment of Cells with Mitotracker® Red

Mitotracker® Red is a mitochondrion-selective dye that stains mitochondria with an intensity that is proportional to $\Delta\Psi_m$. Following the transfection period, the medium was removed from the cells and 2 ml of complete medium containing 100 nM of Mitotracker® Red was added. The cells were incubated for 45 minutes at 37°C followed by replacement of the dye-containing medium with fresh medium.

G) Cell Fixation

The medium was removed from the well and the cells were washed twice with 10 mM tissue culture PBS (10 mM Na_2HPO_4, 1 mM $NaH_2PO_4 \cdot H_2O$, 3 mM KCl, 140 mM NaCl, pH 7.4) for 5 minutes at room temperature. Cells were fixed with methanol for 10 minutes at 4°C followed by three washes each of 5 minutes with tissue culture PBS at room temperature. The fixed coverslip was removed from the well using needle-nosed forceps. One drop of VECTASHIELD® Mounting Medium (Vector Laboratories Inc.) was placed on a glass microscope slide and the coverslip was placed on the slide with the cells facing down. The coverslip was anchored to the slide with nailpolish and allowed to dry. Tissue culture PBS was added on top of the slide to assist in the removal of any excess nailpolish, then removed.

H) Confocal Microscopy Analysis

Cells were visualized for green fluorescence protein (GFP) and Mitotracker® Red by confocal microscopy using a Zeiss® LSM 410 invert scan laser microscope. The fluorescence excitation maximum and emission maximum for GFP were 488 nm and 507 nm, respectively. The fluorescence excitation maximum and emission maximum

for Mitotracker® Red were 579 nm and 599 nm, respectively. Data were analyzed using Carl Zeiss LSM software (Zeiss®).

7. Materials

RPMI 1640 medium, penicillin/streptomycin, sodium pyruvate, and gentamycin were from Wisent Inc. Oligomycin, antimycin, FCCP, trypan blue, BSA, 2-mercaptoethanol, inulin, TPMP-Br, ATP, GDP, cytochrome c, tryptone, yeast extract, soybean trypsin inhibitor, leupeptin, antipain, aprotinin, and pepstatin were from Sigma®. Dinonylphthalate was from ICN Biomedicals Inc.. Silicone fluid D.C. 550 was from Aldrich Chemical Company, Inc.. All radioisotopes were from DuPont-NEN® and Mandel Scientific Co. Limited. (^{3}H)TPMP$^+$ was also purchased from American Radiolabeled Chemicals, Inc.. DEPC was from Amersham Pharmacia Biotech. RNAse was from Roche Molecular Biochemicals. UCP2-pIRES2-EGFP construct was obtained from Dr. Mike Wheeler at the University of Toronto, Toronto, Canada.

8. Statistical Analysis

Data were analysed by unpaired t-tests or one way ANOVA followed by Tukey's post hoc tests using Prism® 3.00 (GraphPad Software Inc.) for Windows. A p value less than 0.05 was considered statistically significant. Data are expressed as means and standard error of the mean (SEM).

RESULTS

Based on evidence showing that mitochondrial metabolism is altered during apoptotic processes (Garland and Halestrap, 1997), the aim of this research was to characterize the differences in the metabolic control of oxidative phosphorylation in drug sensitive leukemic cells, which die apoptotically, and drug resistant leukemic cells, which die non-apoptotically. The research began by investigating the L1210 mouse leukemic cell line and the L1210/DDP resistant subline. This was followed by further analyses with the HL60 human leukemic cells and the resistant HL60/MDR cells.

1. ANALYSIS OF L1210 AND L1210/DDP CELLS

A) RESTING AND STATE 4 CONDITIONS

Resting and State 4 conditions were compared between the two cell types. Resting respiration was measured in the absence of any inhibitors or uncouplers, and was found to be significantly higher ($p < 0.005$) in the drug resistant L1210/DDP cells (Figure 6A). Values were 13.32 ± 0.61 (n=7) and 9.47 ± 0.66 (n=7) nmol $O_2 \times 10^7$ cells^{-1} $\times$ min^{-1} for the L1210/DDP cells and L1210 cells, respectively. State 4 respiration was determined by adding a saturating concentration of oligomycin, a specific inhibitor of ATP synthase. During state 4 respiration the route of proton return to the matrix is through mitochondrial proton leak. Again the L1210/DDP cells exhibited a higher rate

Figure 6 Oxygen consumption and mitochondrial membrane potential of L1210 and L1210/DDP cells. Cells were incubated at 37 °C in a shaking water bath at a concentration of 10 million cells per ml of incubation medium in glass vials. The gas phase above each suspension was 95% air and 5% CO_2 to allow the medium to equilibrate to a pH of 7.4. The cells were preincubated in the water bath for 10 minutes to allow the cells to reestablish steady state ion gradients after being stored on ice. Cells were then incubated a further 20 minutes in the presence of any inhibitors and isotopes before aliquots were taken for the measurement of oxygen consumption and mitochondrial membrane potential. Panel A: Oxygen consumption of L1210 and L1210/DDP cells under 'resting' (absence of inhibitors) and 'state 4' (100 nM saturating concentration of the specific inhibitor of ATP synthase oligomycin) conditions. Values are presented as the mean ± SEM of 7 determinations (assessments performed in duplicate for each determination). Panel B: Mitochondrial membrane potential under 'resting' and 'state 4' conditions. Values are presented as the mean ± SEM of 7 determinations (assessments performed in triplicate for each determination).

Oxygen Consumption

A

Mitochondrial Membrane Potential

B

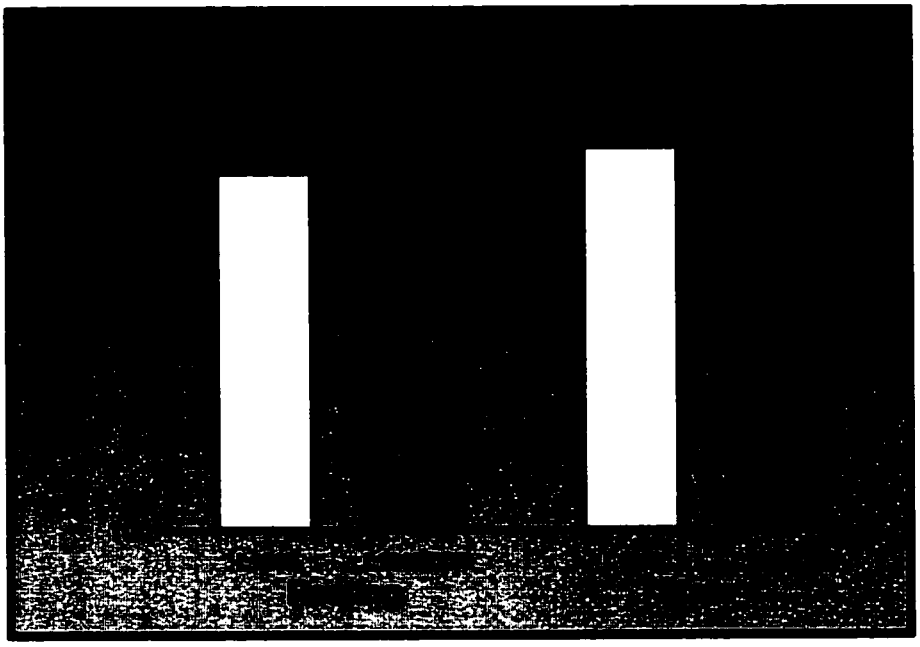

of oxygen consumption (Figure 6A) with a value of 9.61 ± 0.76 nmol $O_2 \times 10^7$ cells^{-1} × min^{-1} (n=7), compared to 7.45 ± 0.83 nmol $O_2 \times 10^7$ cells^{-1} × min^{-1} (n=7) for the L1210 cells. Although the difference is not statistically significant, the trend is towards increased oxygen consumption in the resistant subline.

Concurrent with measurements of oxygen consumption, mitochondrial membrane potential was also determined (Figure 6B). Under both resting and state 4 conditions, $\Delta\Psi_m$ was significantly lower ($p < 0.0001$) in the L1210/DDP cells than in the L1210 cells. Resting $\Delta\Psi_m$ values were 159.8 ± 1.7 mV (n=7) and 139.5 ± 7.2 mV (n=7) for L1210 and L1210/DDP cells, respectively. State 4 $\Delta\Psi_m$ values were 164.2 ± 0.9 mV (n=7) and 148.8 ± 2.0 mV (n=7) for L1210 and L1210/DDP cells, respectively. Within each cell line, there is also a significant increase in $\Delta\Psi_m$ ($p < 0.05$) as respiration is taken from a resting state to non-phosphorylating conditions.

Higher oxygen consumption and lower $\Delta\Psi_m$ in the drug resistant cells suggests that mitochondrial proton leak is increased in these cells.

B) Overall Metabolic Kinetics

With these results the research was extended to a full analysis of the overall metabolic kinetics of oxidative phosphorylation in the two cells lines, focusing primarily on the overall kinetics of mitochondrial proton leak reactions. These analyses require simultaneous determinations of oxygen consumption and $\Delta\Psi_m$, and the use of specific mitochondrial inhibitors. The overall kinetics of mitochondrial proton leak reactions are shown in Figure 7. In the presence of a saturating amount of oligomycin (state 4), $\Delta\Psi_m$ is gradually inhibited with the addition of increasing amounts of antimycin, an inhibitor

Figure 7 Relationship between mitochondrial membrane potential ($\Delta\Psi_m$) and leak-dependent respiration (per cell) in L1210 and L1210/DDP cells. The kinetic response of the proton leak subsystem to $\Delta\Psi_m$ was determined by titrating the substrate oxidation reactions with increasing amounts of antimycin (50 nM, 250 nM, 5 μM) in the presence of a saturating concentration of oligomycin (100 nM). State 4 respiration is defined as maximal non-phosphorylating respiration and is achieved with the saturating concentration of oligomycin. Oxygen consumption is expressed in this figure on a per cell basis. Values are presented as the mean ± SEM of 6 determinations for both cell lines. Assessments were performed in duplicate for oxygen consumption and triplicate for mitochondrial membrane potential.

Proton Leak Kinetic Curves

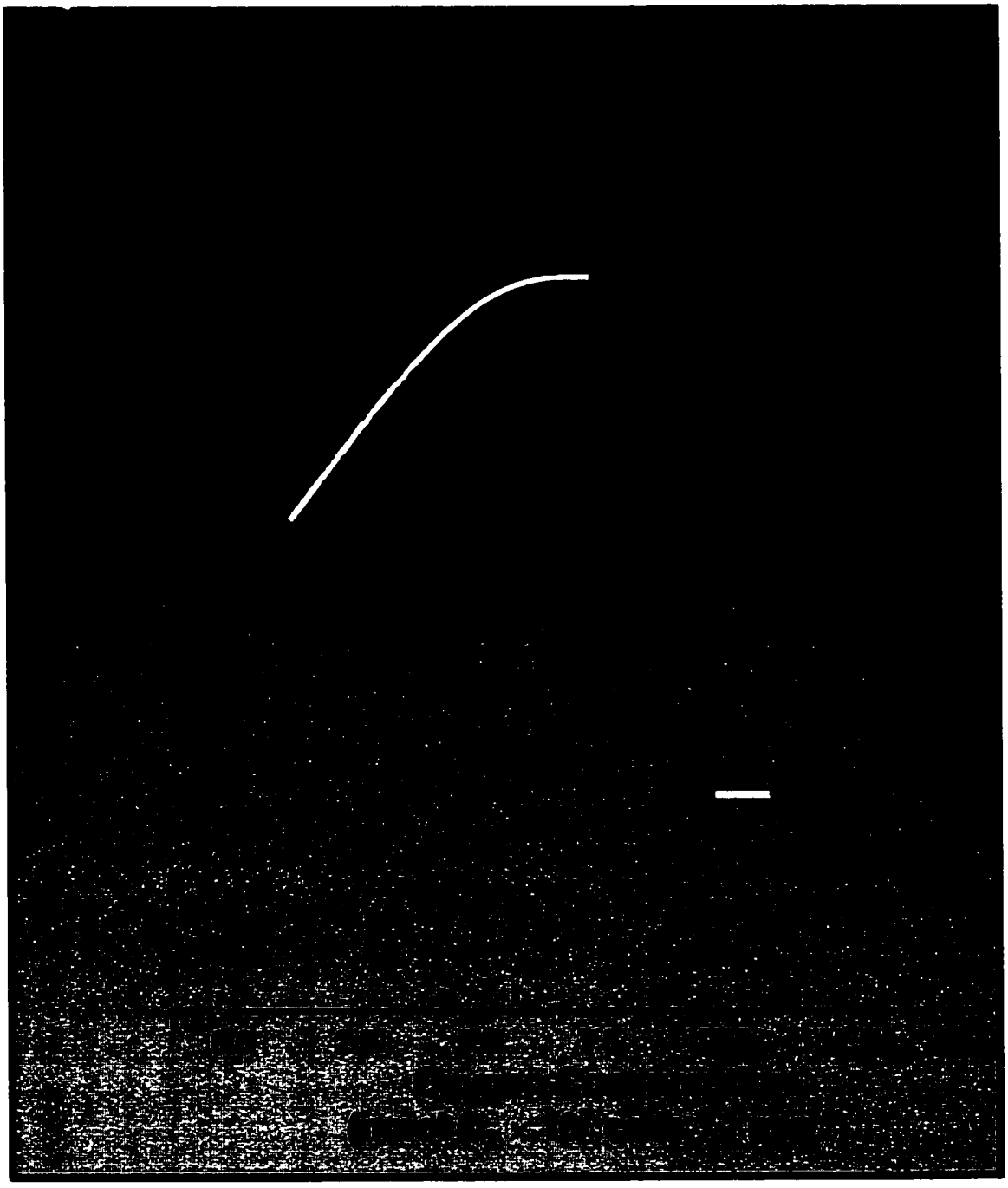

of complex III of the electron transport chain. Leak dependent oxygen consumption for any given value of $\Delta\Psi_m$ (e.g., between 145 and 150 mV) is markedly higher in the L1210/DDP cells. In other words, more oxygen is required by the resistant cells in order to maintain the same level of $\Delta\Psi_m$ as in the sensitive cells. Thus leak is increased in the resistant cell type.

It is also clear from Figure 8 that the overall kinetics of substrate oxidation (Figure 8A) and of phosphorylation (Figure 8B) are quite different between the two cell types. Taken together, these results show that there exists significant difference in the metabolic kinetics of L1210 and L1210/DDP cells.

C) Cellular Respiratory Capacity

To investigate the maximum respiratory capacity of the two cell lines, 10 μM of the artificial uncoupler carbonyl cyanide p-trifluoromethoxyphenylhydrazone (FCCP) was added to cells in the resting state. FCCP increases the proton conductance of the mitochondrial inner membrane. Figure 9 reveals a significant increase ($p < 0.05$) in oxygen consumption in the presence of FCCP for both cell lines. Values for L1210 cells were 9.05 ± 0.77 (n=7) and 12.01 ± 0.68 (n=7) nmol $O_2 \times 10^7$ cells^{-1} × min^{-1} for resting and FCCP-stimulated, respectively. For the L1210/DDP cells, values were 11.90 ± 0.99 (n=7) and 15.80 ± 0.91 (n=7) nmol $O_2 \times 10^7$ cells^{-1} × min^{-1} for resting and FCCP-stimulated, respectively. Thus the resistant cells have a higher maximum respiratory capacity than the sensitive cells ($p < 0.01$).

D) Uncoupling Protein 2 Expression

Because the results demonstrate lower $\Delta\Psi_m$ in the drug resistant L1210/DDP cells,

Figure 8 Relationship between mitochondrial membrane potential ($\Delta\Psi_m$) and respiration rate of (A) substrate oxidation reactions and (B) phosphorylation reactions in L1210 and L1210/DDP cells. (A) The kinetic response of the substrate oxidation subsystem was determined by the addition of a saturating amount of oligomycin (100 nM) to achieve state 4 (maximal non-phosphorylating) respiration. (B) The kinetic response of the phosphorylating subsystem was determined by titration of resting respiration with increasing amounts of antimycin (100, 200 nM) and correcting for leak-dependent respiration at that value of $\Delta\Psi_m$. For both graphs, values are presented as the mean ± SEM of 5 determinations. Assessments were performed in duplicate for oxygen consumption and triplicate for mitochondrial membrane potential.

A

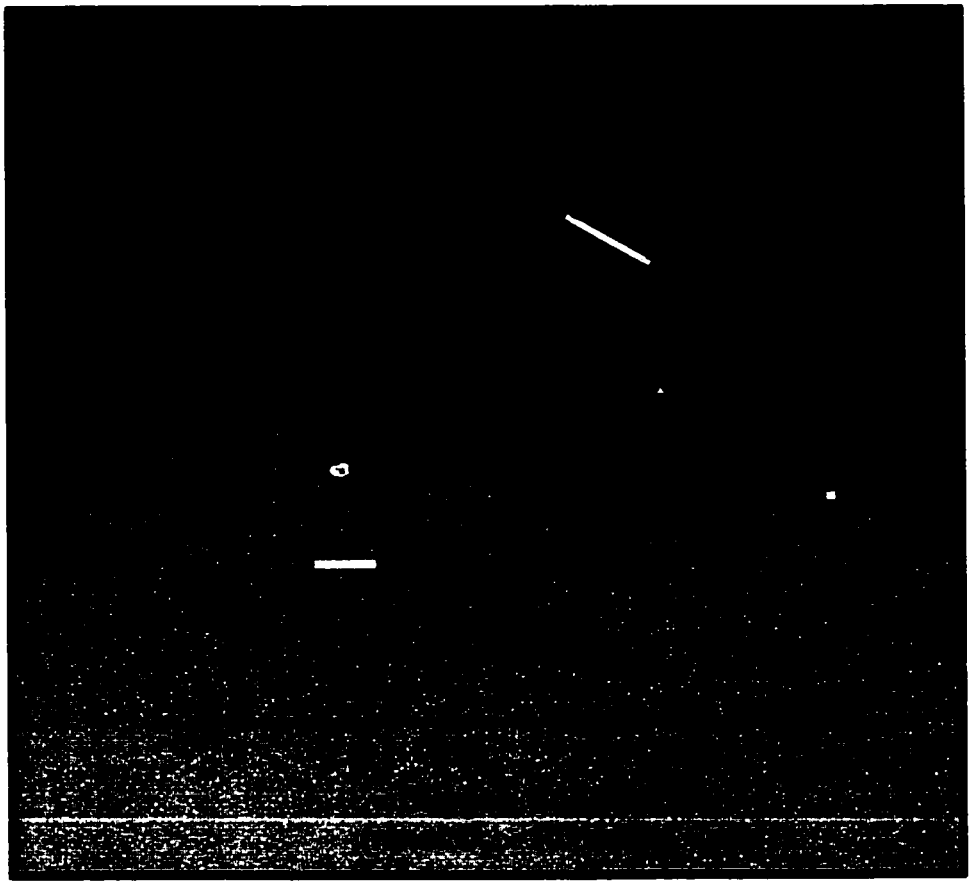

B

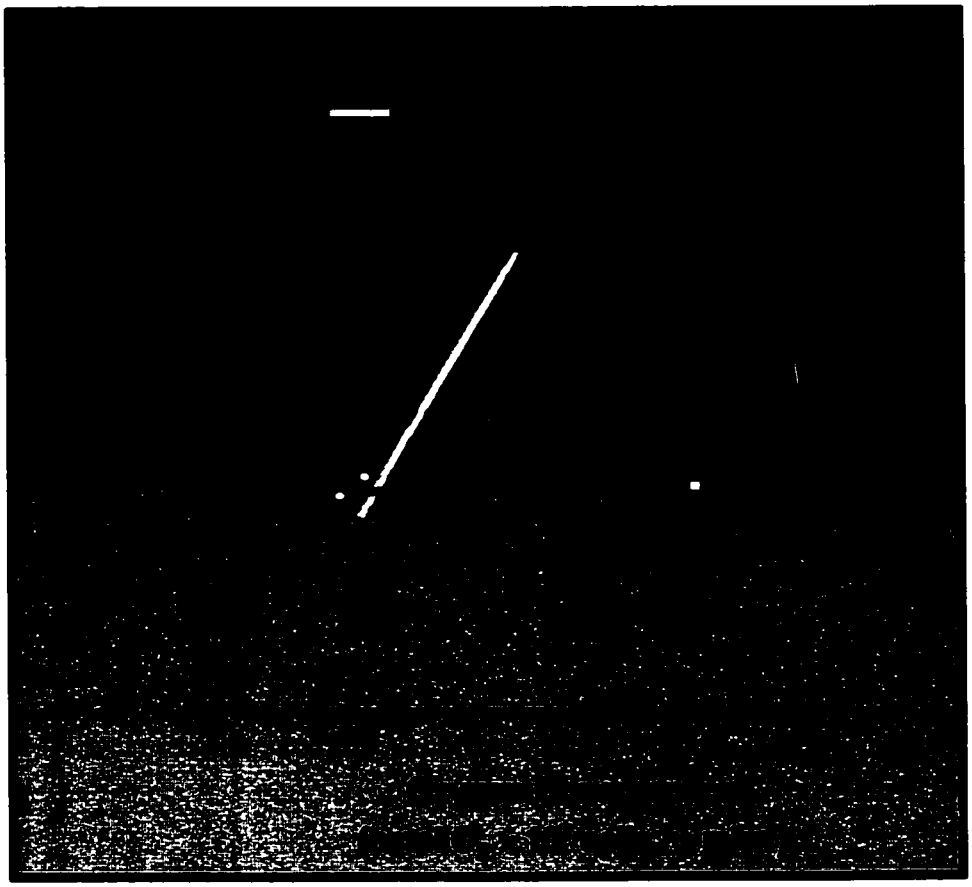

Figure 9 Acute effect of FCCP on the resting respiration rates in (A) L1210 and (B) L1210/DDP cells. To determine the maximum respiratory capacity of the cells, 10 μM of the artificial uncoupler carbonyl cyanide p-trifluoromethoxyphenylhydrazone (FCCP) was added to cells in the resting state and measured for approximately 5 minutes. FCCP is a protonphore that catalyzes the net electrical uniport of protons and increases the proton conductance of the mitochondrial inner membrane. For both graphs, values are presented as the mean ± SEM of 7 determinations (assessments performed in duplicate for each determination).

L1210

A

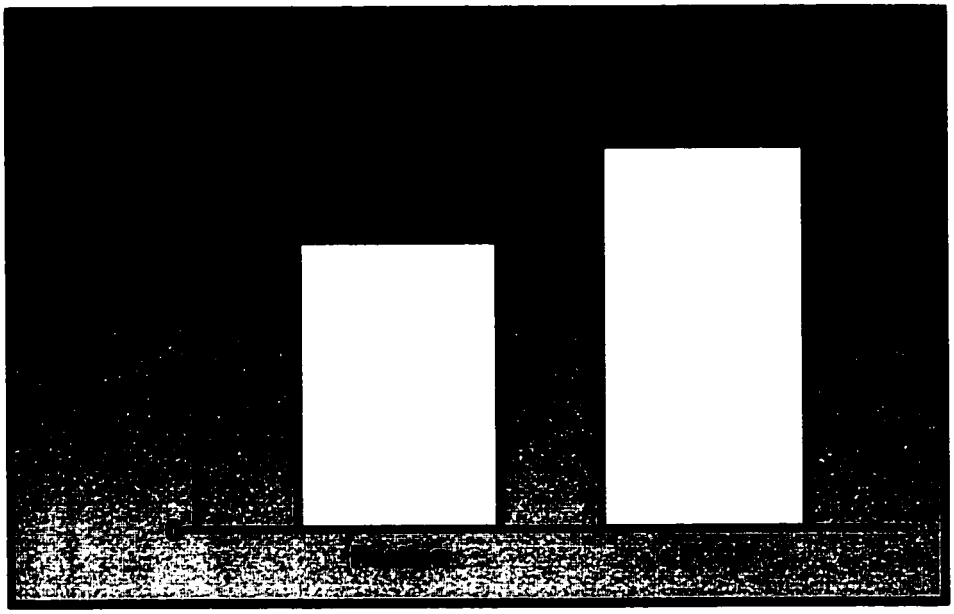

L1210/DDP

B

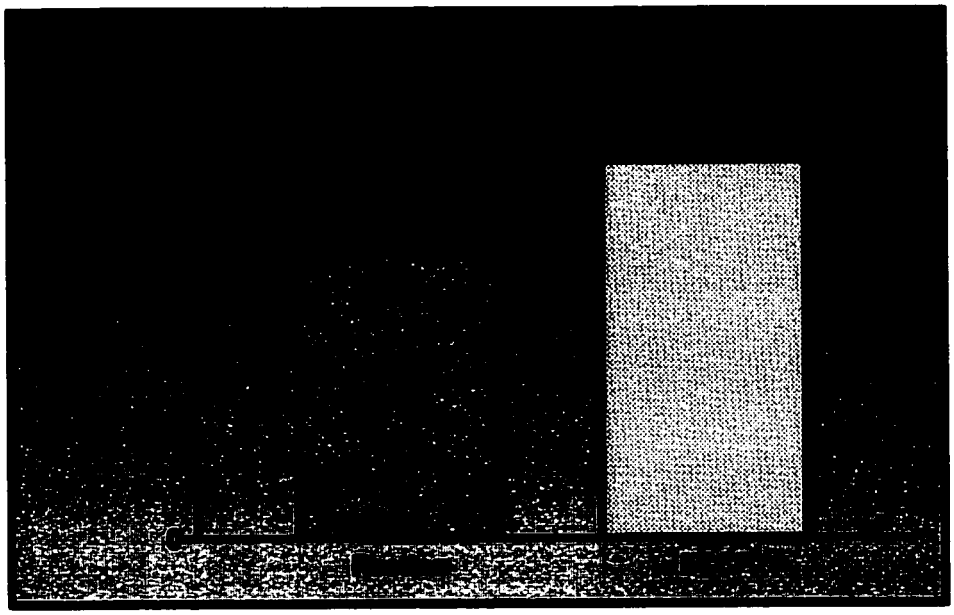

it was reasoned that one mechanism accounting for this could be through the activity of the recently characterized uncoupling protein 2 (Fleury, et al., 1997). The presence of UCP2 in both cell lines was measured using a polyclonal antibody specific for UCP2 in Western blot analysis (Figure 10). The results demonstrate that the drug resistant subline expresses higher levels of mitochondrial UCP2, a finding that was consistently observed with numerous mitochondrial fraction isolations. The detected mitochondrial protein has an approximate molecular weight of 33 kDa. In Figure 10 each cell line is represented by two distinct mitochondrial preparations.

Northern blot analysis confirmed expression of Ucp2 in both cell lines (Figure 11). RNA was isolated from both cell types and probed with a digoxigenin-labeled UCP2 probe. Lanes 3 and 4 contain RNA from the brown adipose tissue of a UCP1 knockout mouse and a UCP1 control mouse, respectively. As is shown in this figure, and has been described previously (Enerback, et al., 1997), there is an increased expression of UCP2 mRNA in the absence of UCP1. Surprising, however, is the higher amount of Ucp2 mRNA present in the L1210 cells compared to the L1210/DDP cells.

It has previously been shown that mitochondrial proteins can be found in extra-mitochondrial locations in the cell. There seems to exist a general assumption in protein localization that organellar proteins do not exit the compartment they are targeted to. However more and more mitochondrial proteins are being identified to function not only in mitochondria but also at unexpected, yet very specific extra-mitochondrial locations. They are identified as single protein products of single genes; in other words their location does not seem to be the result of mechanisms such as alternative splicing or translation initiation (Soltys and Gupta, 2000). A proposal put

Figure 10 Representative Western blot of protein isolated from purified mitochondrial fractions of L1210 and L1210/DDP cells. Mitochondria were isolated using differential centrifugation. Protein content was determined using the modified Lowry method. Lane 1: Molecular weight markers (Santa Cruz Biotechnology, Santa Cruz, CA). Lanes 2 and 3: L1210 mitochondrial protein (60 μg) from two distinct mitochondrial preparations. Lanes 4 and 5: L1210/DDP mitochondrial protein (60 μg) from two distinct mitochondrial preparations. The primary antibody was goat anti-human UCP2 (Santa Cruz Biotechnology, Santa Cruz, CA) used at a concentration of 1.5 μg/ml. The secondary antibody was donkey anti-goat IgG horseradish peroxidase conjugate (Santa Cruz Biotechnology, Santa Cruz, CA) used at a dilution of 1:5000. Detection was performed using an Enhanced chemiluminescence (ECL) kit (Amersham Pharmacia Biotech).

Western Blot

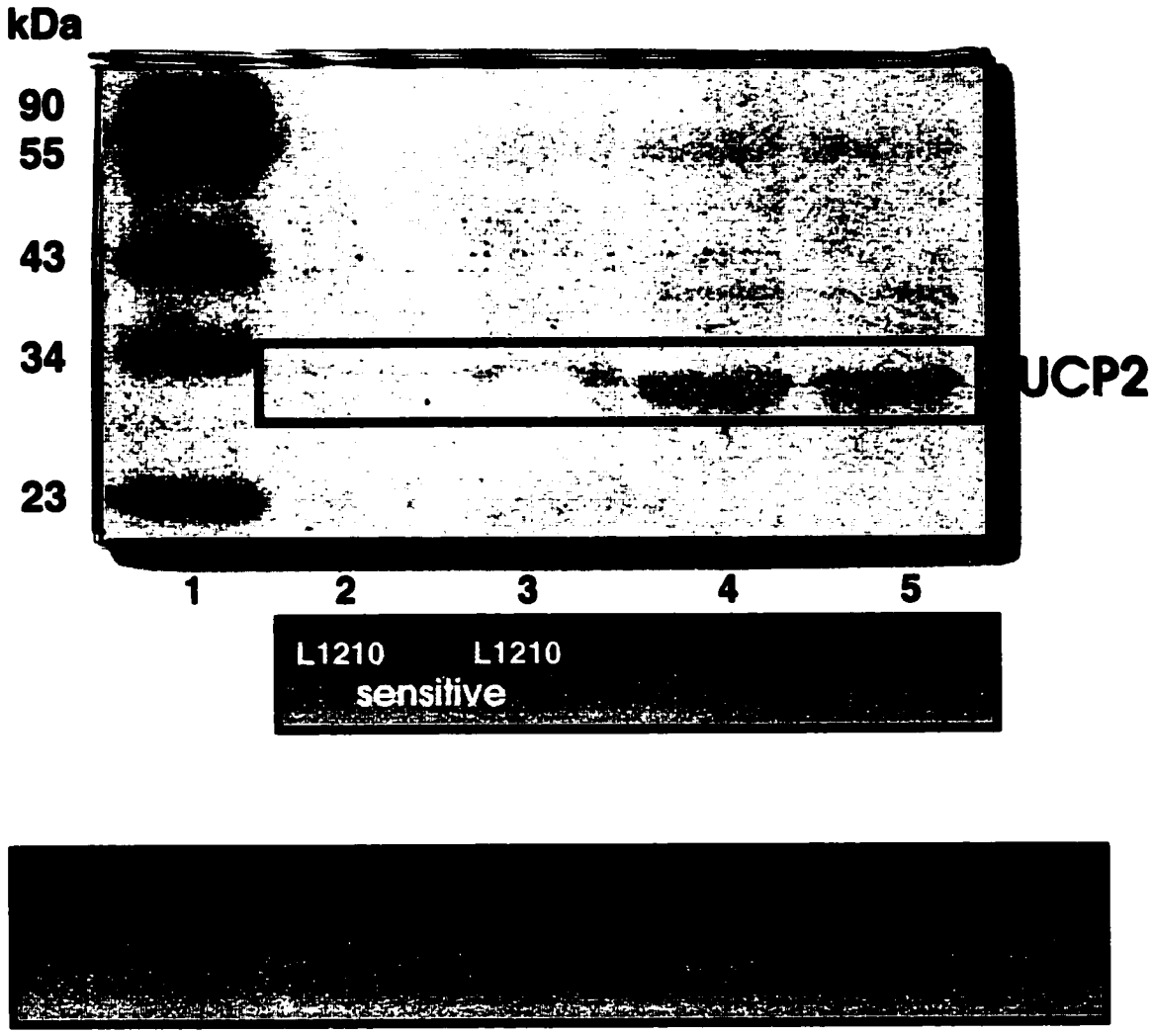

Figure 11 Northern blot analysis to evaluate the level of uncoupling protein 2 mRNA expression in L1210 and L1210/DDP cells. RNA was isolated as described in Methods and Materials. Electrophoresis was performed followed by transfer to a nylon membrane which was probed with a digoxigenin-labeled Ucp2 probe previously prepared in our laboratory. Lane 1: L1210/DDP RNA (20 μg). Lane 2: L1210 RNA (20 μg). Lane 3: Brown adipose tissue RNA (20 μg) from a UCP1 knockout mouse. Lane 4: Brown adipose tissue RNA (20 μg) from a UCP1 control mouse.

Northern Blot

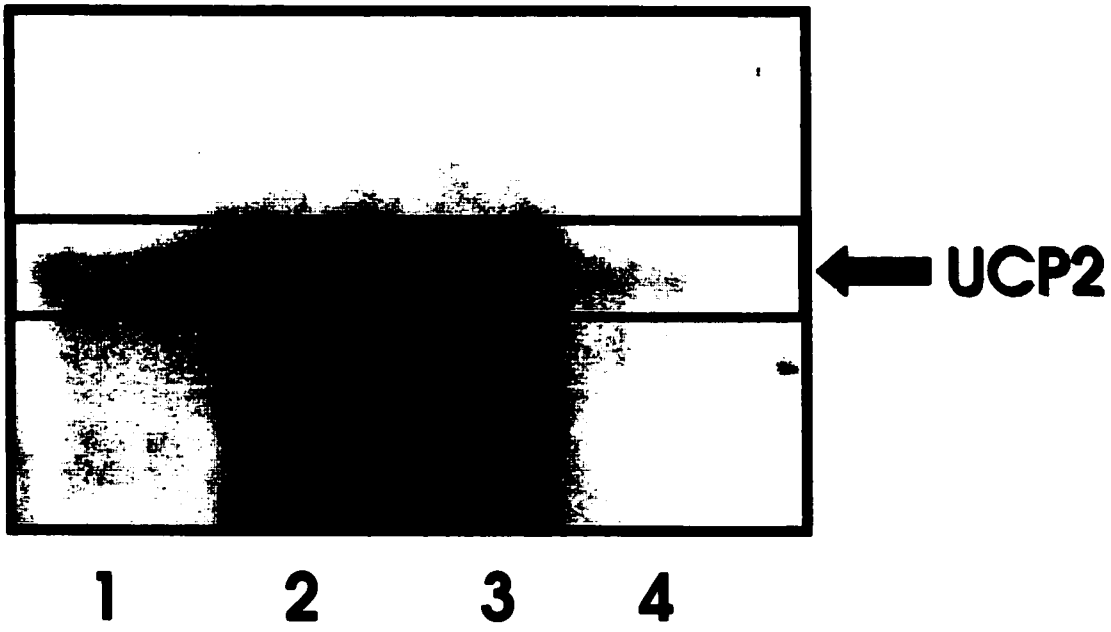

forward suggests that specific export mechanisms exist by which specific proteins can exit the mitochondrion, allowing these proteins to have additional functions at certain extra-mitochondrial sites (Soltys and Gupta, 2000). The cell surface as a potential site of relocation has received a large amount of interest. The protein that has received the most attention in these studies is Hsp60, a mitochondrial molecular chaperone that has also been found on the plasma membrane of a number of cell types (Soltys and Gupta, 2000). Another mitochondrial protein found on the cell surface is aspartate aminotransferase (Bradbury and Berk, 2000). Studies confirmed that its extra-mitochondrial location in 3T3-L1 fibroblasts is not due to alternative splicing. Other proteins found on the plasma membrane include mitochondrially transmitted factors (MTF), P32 protein, and Hsp70 (Soltys and Gupta, 1999). Cytochrome c has been found to localize in secretory granules in the pancreas and anterior pituitary (Soltys, et al., 2001).

With this in mind, the search for UCP2 in the L1210 and L1210/DDP cells was extended to the cell surface. Plasma membrane fractions were isolated using sucrose density gradient ultracentrifugation. The protocol applied is one that has been shown to produce minimal contamination by organellar components (Caldwell, et al., 1988). Western blot analysis (Figure 12) revealed the presence of UCP2 in these fractions, with higher amounts being observed in the L1210 cells, coincident with the higher mRNA expression (described above). These findings were repeated with several other plasma membrane isolations. Each cell line in Figure 12 is represented by two distinct plasma membrane preparations. In Lane 6 the UCP2 standard is conjugated to a small protein and the expected molecular weight is 39 kDa. The supplier of the standard explained

Figure 12 Representative Western blot of protein isolated from purified plasma membrane fractions of L1210 and L1210/DDP cells. Plasma membrane fractions were isolated using sucrose density gradient ultracentrifugation. Protein content was determined using the modified Lowry method. Lanes 1 and 7: Molecular weight markers (Santa Cruz Biotechnology, Santa Cruz, CA). Lanes 2 and 3: L1210 plasma membrane protein (60 μg) from two distinct membrane preparations. Lanes 4 and 5: L1210/DDP plasma membrane protein (60 μg) from two distinct membrane preparations. Lane 6: uncoupling protein 2 standard (15 ng; Stratagene, La Jolla, CA). The standard is conjugated to a small protein and the expected molecular weight is 39 kDa. The primary antibody was goat anti-human UCP2 (Santa Cruz Biotechnology, Santa Cruz, CA) used at a concentration of 1.5 μg/ml. The secondary antibody was donkey anti-goat IgG horseradish peroxidase conjugate (Santa Cruz Biotechnology, Santa Cruz, CA) used at a dilution of 1:5000. Detection was performed using an Enhanced chemiluminescence (ECL) kit (Amersham Pharmacia Biotech).

Western Blot

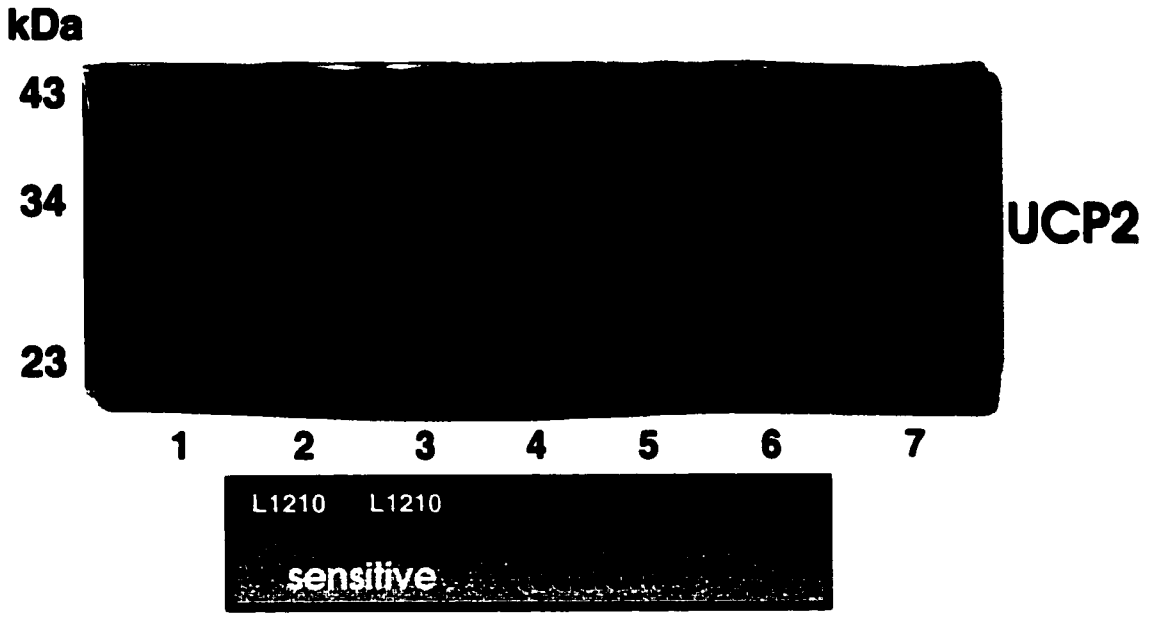

the lower of the two bands in this lane as an unknown breakdown product.

E) Plasma Membrane Potential

Uncertain as to the function of UCP2 on the cell surface, the plasma membrane potential ($\Delta\Psi_p$) of the two cell types was measured to gain some insight (Figure 13). Under resting conditions $\Delta\Psi_p$ was significantly lower ($p < 0.05$) in the L1210 cells. Values were 20.60 ± 1.90 mV (n=4) and 35.90 ± 5.20 mV (n=5) for L1210 and L1210/DDP cells, respectively. GDP, a known inhibitor of UCP1 and proposed inhibitor of UCP2 (Negre-Salvayre, et al., 1997), was added to the cells. No difference is $\Delta\Psi_p$ was observed in the L1210/DDP cells, which express very little cell surface UCP2, but there was a significant increase ($p < 0.05$) in $\Delta\Psi_p$ in the L1210 cells which have higher amounts of UCP2 in the plasma membrane. The $\Delta\Psi_p$ increased to 33.65 ± 4.70 mV (n=4), very similar to the value for the resistant cells. These results suggest that UCP2 may function as a transporter of protons (and perhaps other ions) on the cell surface and its activity can be inhibited by GDP. But GDP is known to act on many cell surface proteins, and there may exist other differences between the two cell types that would account for this change in $\Delta\Psi_p$. Therefore these results are preliminary and require further investigation.

F) Cytochrome Oxidase Activity

Activity of cytochrome oxidase is accepted as an indicator of cellular mitochondrial content. In Figure 14A, results are presented as a function of total cellular protein content with no significant difference observed between the two cell types. Values were 152.9 ± 26.9 (n=3) and 191.8 ± 19.2 (n=3) nmol cytochrome c

Figure 13 Plasma membrane potential ($\Delta\Psi_p$) of L1210 and L1210/DDP cells under normal conditions and in the presence of GDP. Cells were incubated at 37 °C in a shaking water bath at a concentration of 10 million cells per ml of incubation medium in glass vials. The gas phase above each suspension was 95% air and 5% CO_2 to allow the medium to equilibrate to a pH of 7.4. The cells were preincubated in the water bath for 10 minutes to allow the cells to reestablish steady state ion gradients after being stored on ice. Cells were then incubated a further 20 minutes in the presence of ^3H_2O and $^{36}Cl^-$. To examine the effects of GDP on plasma membrane potential, 1 mM GDP was added after the preincubation period. Values are presented as the mean ± SEM of 4 determinations for L1210 cells under normal conditions and in the presence of GDP, and 5 determinations for L1210/DDP cells under normal conditions and in the presence of GDP. Assessments were performed in triplicate for each determination.

Plasma Membrane Potential

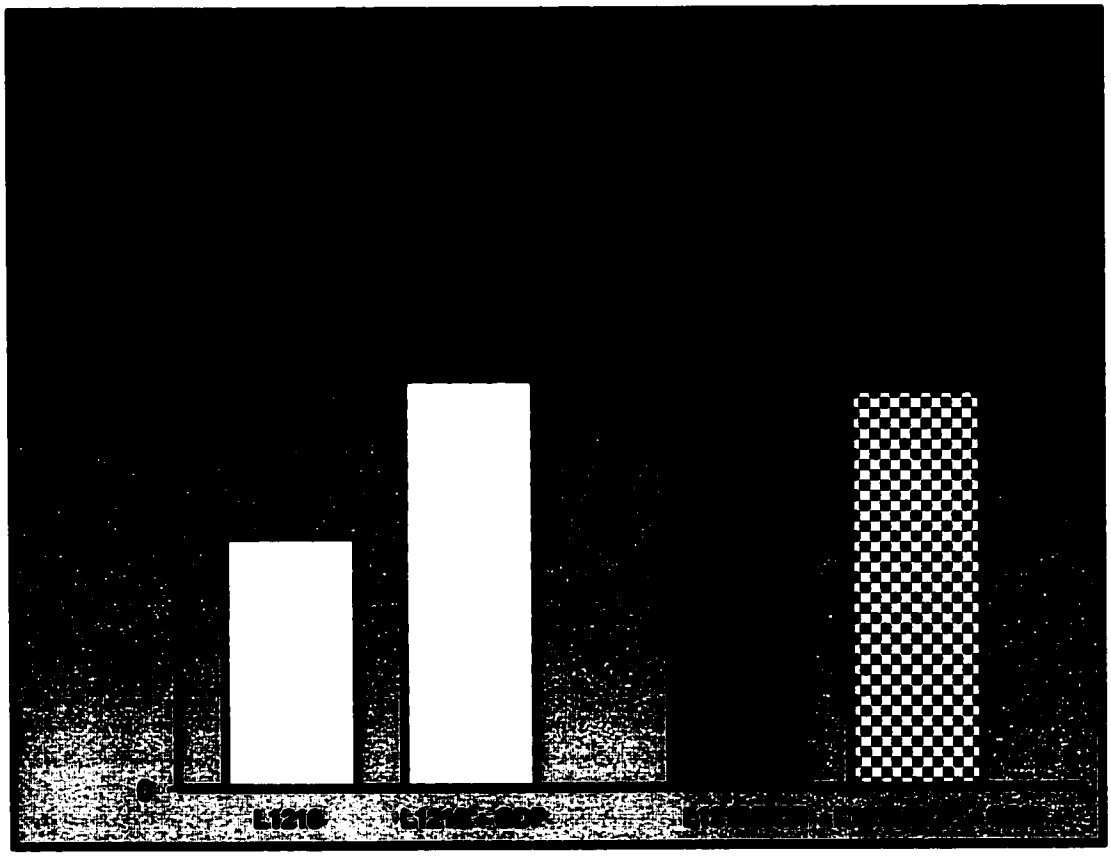

Figure 14 Cytochrome oxidase activity of L1210 and L1210/DDP cells. A spectrophotometric assay was used to determine the rate at which cytochrome oxidase can oxidize its substrate cytochrome c by measuring the rate of disappearance of reduced cytochrome c which absorbs light at 550 nm. Activity of cytochrome oxidase is used as an indicator of cellular mitochondrial content. In (A), values are expressed as a function of total cellular protein content. In (B), values are expressed on a per cell basis to take into account the size of the cells. Values are presented as the mean ± SEM of 3 determinations. Assessments were performed in triplicate for each determination.

Cytochrome Oxidase

A

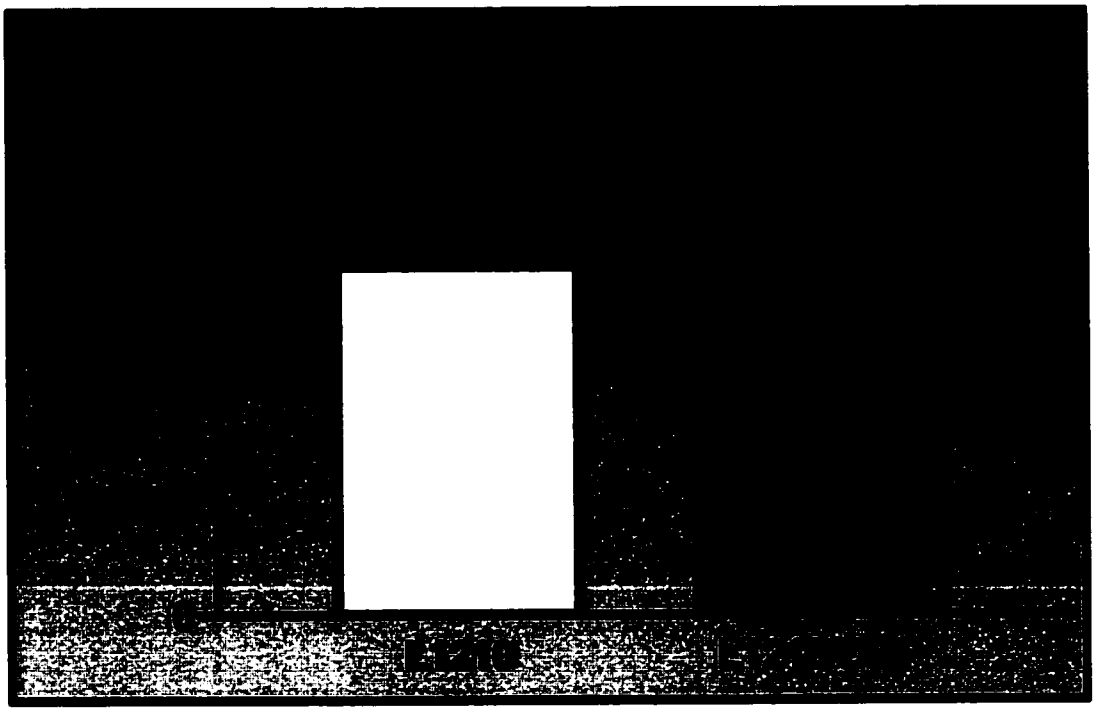

B

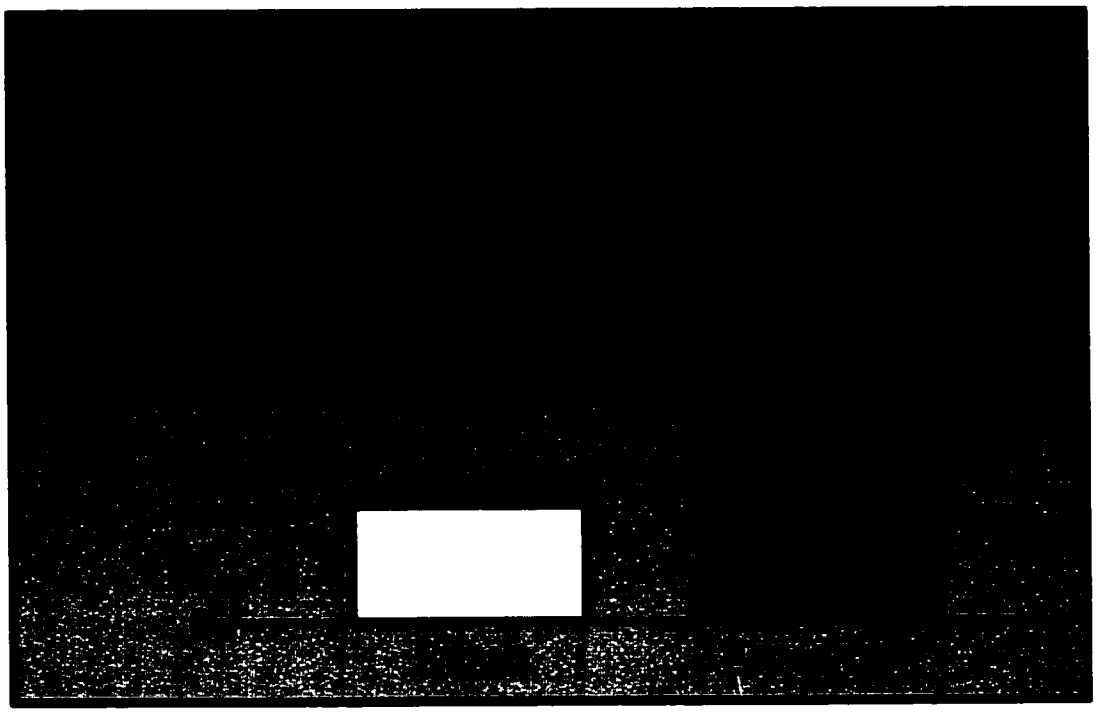

oxidized x min^{-1} x μg cellular $protein^{-1}$ for L1210 and L1210/DDP cells, respectively. In other words, per unit cellular protein both cell types have similar amounts of mitochondria. However, by examining the cells under a microscope and by performing a total cellular protein determination (Table 1), it was evident that the L1210/DDP are much larger and contained higher amounts of protein than the L1210 cells.

TABLE 1

Cell Type	Mass of Protein per Cell (ng)
L1210	0.14 ± 0.03
L1210/DDP	0.43 ± 0.05

Cellular Protein Content of L1210 and L1210/DDP cells. Total cell homogenates were used to determine protein concentrations using the modified Lowry method (described in Methods and Materials). Values are presented as the mean ± SEM of 5 determinations for each cell type. Assessments were performed in duplicate for each determination.

When cytochrome oxidase values are expressed to take into account cell size (Figure 14B), the resistant L1210/DDP cells appear to have a greater mitochondrial content. Values were 21.3 ± 3.7 (n=3) and 82.1 ± 8.2 (n=3) nmol cytochrome c oxidized x min^{-1} x 10^3 $cells^{-1}$ for L1210 and L1210/DDP cells, respectively.

If oxygen consumption is normalized for total cytochrome oxidase activity, the oxygen consumption of the resistant cells becomes very low. To illustrate this, in Figure 15 the overall kinetics of mitochondrial proton leak first described in Figure 7 are shown

Figure 15 Relationship between mitochondrial membrane potential ($\Delta\Psi_m$) and leak-dependent respiration (corrected for mitochondrial content) in L1210 and L1210/DDP cells. The kinetic response of the proton leak subsystem to $\Delta\Psi_m$ was determined by titrating the substrate oxidation reactions with increasing amounts of antimycin (50 nM, 250 nM, 5 μM) in the presence of a saturating concentration of oligomycin (100 nM). State 4 respiration is defined as maximal non-phosphorylating respiration and is achieved with the saturating concentration of oligomycin. Oxygen consumption is expressed in this figure to take into account differences in mitochondrial content. Values are presented as the mean ± SEM of 6 determinations. Assessments were performed in duplicate for oxygen consumption and triplicate for mitochondrial membrane potential.

Proton Leak Kinetic Curves

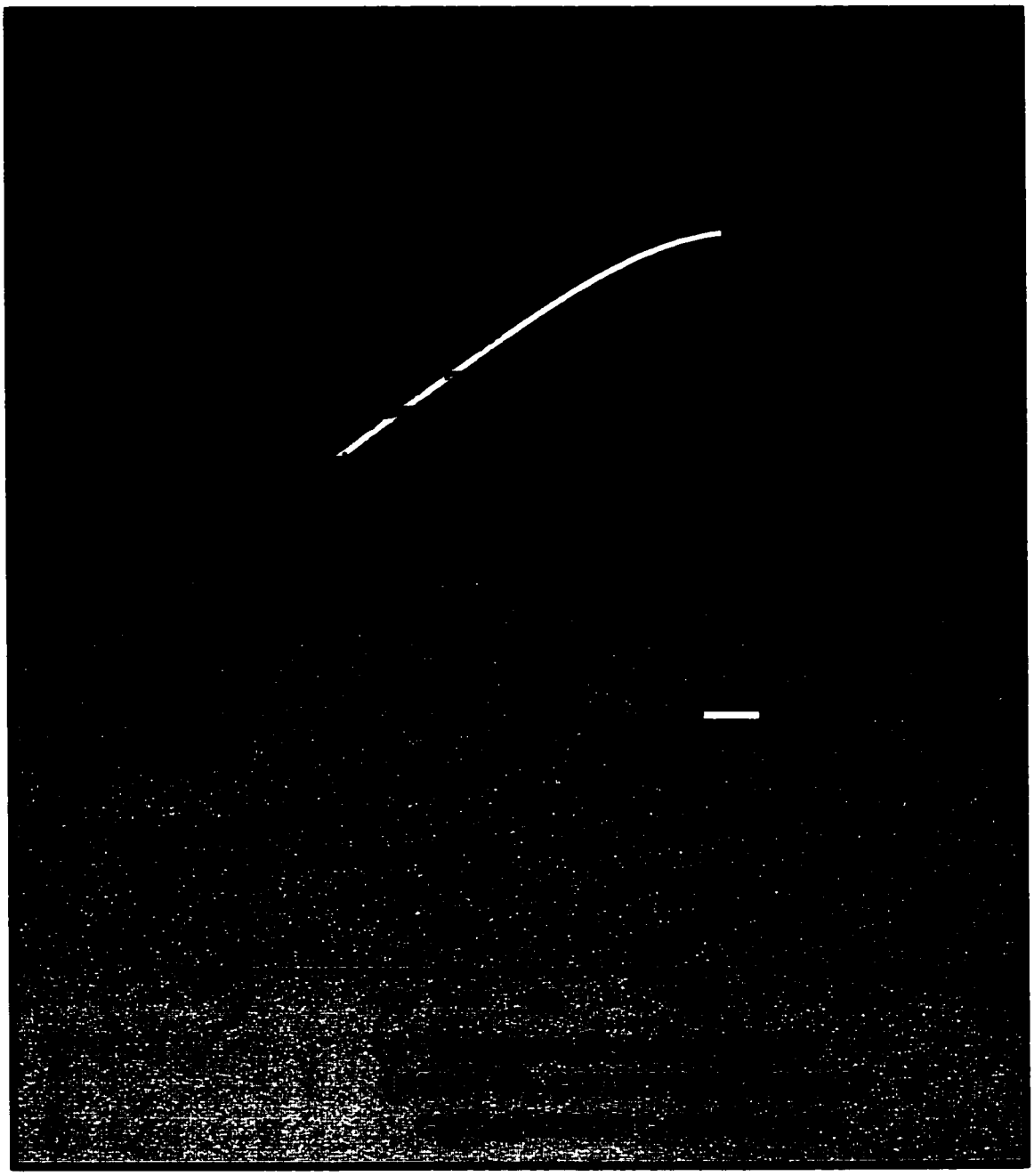

with oxygen consumption expressed to reflect the estimated mitochondrial content. $\Delta\Psi_m$ is not affected by these changes, but oxygen consumption in the resistant L1210/DDP cells is no longer indicative of increased proton leak. Because the assay measures maximal activity of the cytochrome oxidase, it is not possible to compare the actual *in vivo* activities of the enzyme between the cell types. This is further discussed below.

G) Cellular ATP Content

Because mitochondrial oxidative phosphorylation appears to be uncoupled in resistant cells, and because uncoupling lowers mitochondrial ATP synthesis, levels of ATP were compared between sensitive and resistant cells. When ATP was assayed on a per cell basis (Figure 16A), the results showed a higher amount in the L1210/DDP cells ($p < 0.01$). Values were 63.0 ± 3.5 (n=3) and 108.0 ± 7.0 (n=4) pmol ATP/50000 cells for L1210 and L1210/DDP cells, respectively. Initially the lower amount in the sensitive cells was thought to be due to their higher turnover rate. But when corrections were made for differences in total protein content (Figure 16B), the results showed a lower amount in the L1210/DDP cells ($p < 0.001$). Values were 9.1 ± 0.5 (n=3) and 5.1 ± 0.3 (n=4) pmol ATP/μg cellular protein for L1210 and L1210/DDP cells, respectively. This was thought to be due to increased uncoupling or the possibility of inactive mitochondria in resistant cells (discussed below).

Figure 16 Cellular ATP content of L1210 and L1210/DDP cells. ATP was extracted from the cells and quantified using a Luciferase-luciferin assay (Sigma®). In (A), values are expressed on a per cell basis. In (B), values are expressed to reflect total cellular protein content. Values are presented as the mean ± SEM for 3 independent experiments for L1210 cells and 4 independent experiments for L1210/DDP cells. Each experiment consisted of 4 individual determinations of ATP content.

Cellular ATP Content

A

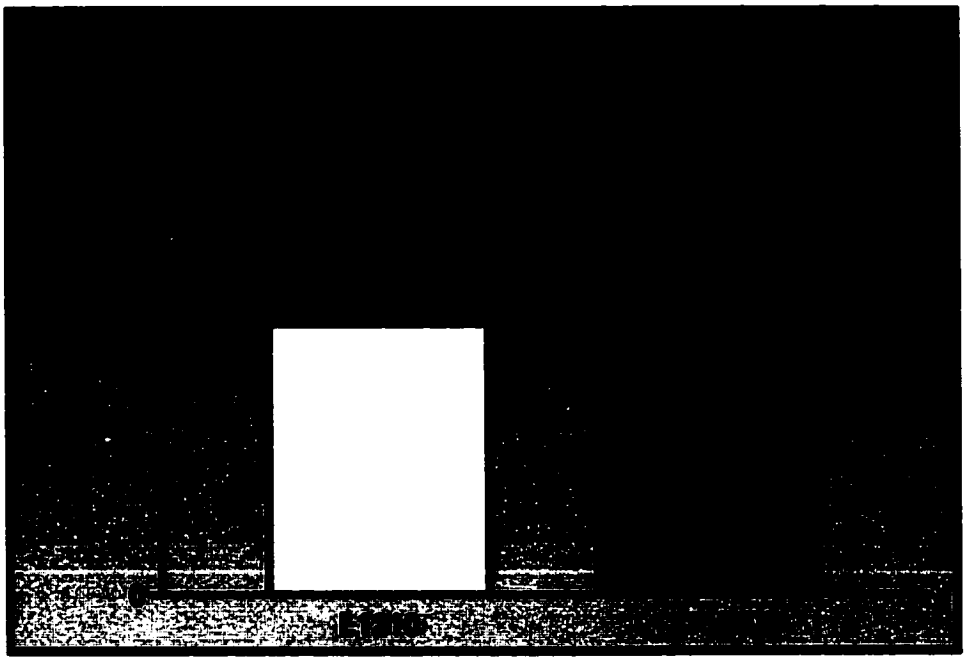

B

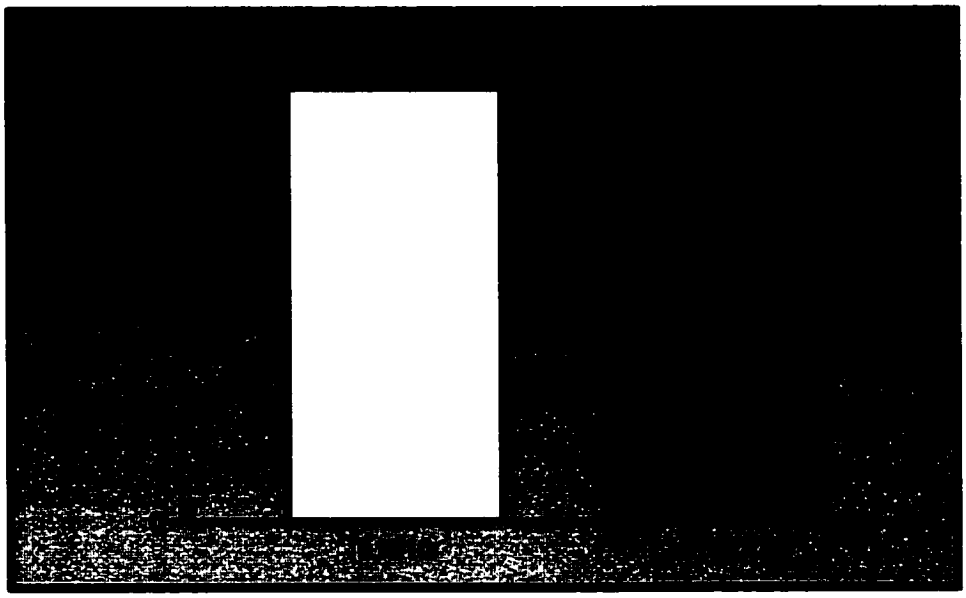

H) Confocal Microscopy Analysis

In an attempt to obtain more information on the cellular localization of UCP2, L1210 and L1210/DDP cells were transfected with a UCP2-pIRES2-EGFP construct. Upon successful incorporation into the cell, once translated the protein will appear green when examined under fluorescence. To provide a visual account of mitochondrial membrane potential, cells were simultaneously treated with the mitochondrion-selective dye Mitotracker® Red, which stains mitochondria with an intensity that is proportional to $\Delta\Psi_m$. Figure 17 shows several micrographs of L1210 cells. Cellular localization proved difficult to interpret, however, because the very large nuclei of the cells forces the contents of the cytosol against the plasma membrane, making it difficult to distinguish between mitochondria and cell surface. In the bottom left corner of each panel there is a cell which is dying, as evidenced by the lower $\Delta\Psi_m$ and the lack of UCP2-EGFP expression. In the bottom right panel the orange colour created by the overlap of green and red fluorescence indicates that UCP2 is expressed in mitochondria. Similarly in Figure 18 the large nuclei of the L1210/DDP cells is evident, as is the significant amount of overlap between mitochondria and UCP2 (bottom right panel). However if one looks closely there is still a fair amount of green fluorescence, indicating that perhaps UCP2 is found in other parts of the cell as well. In Figure 19 a comparison is made between the two cell types. Note the difference in cell size as well as the lower $\Delta\Psi_m$ in the L1210/DDP cells, indicated by the weaker red fluorescence. This weaker fluorescence was consistently observed when comparing the cell lines at equal magnification, but for the purpose of presentation the L1210 cells are shown at a greater magnification.

Figure 17 Confocal micrographs of L1210 cells. Cells were transfected with a UCP2-pIRES2-EGFP construct followed by treatment with the mitochondrion-selective dye Mitotracker® Red, as described in Methods and Materials. Cells were then fixed and visualized by confocal microscopy. Upper left panel: non-fluorescence micrograph. Upper right panel: visualization of Mitotracker® Red staining. Bottom left panel: visualization of UCP2-pIRES2-EGFP localization. Bottom right panel: fluorescence overlap of Mitotracker® Red and EGFP. Magnification: 1000x.

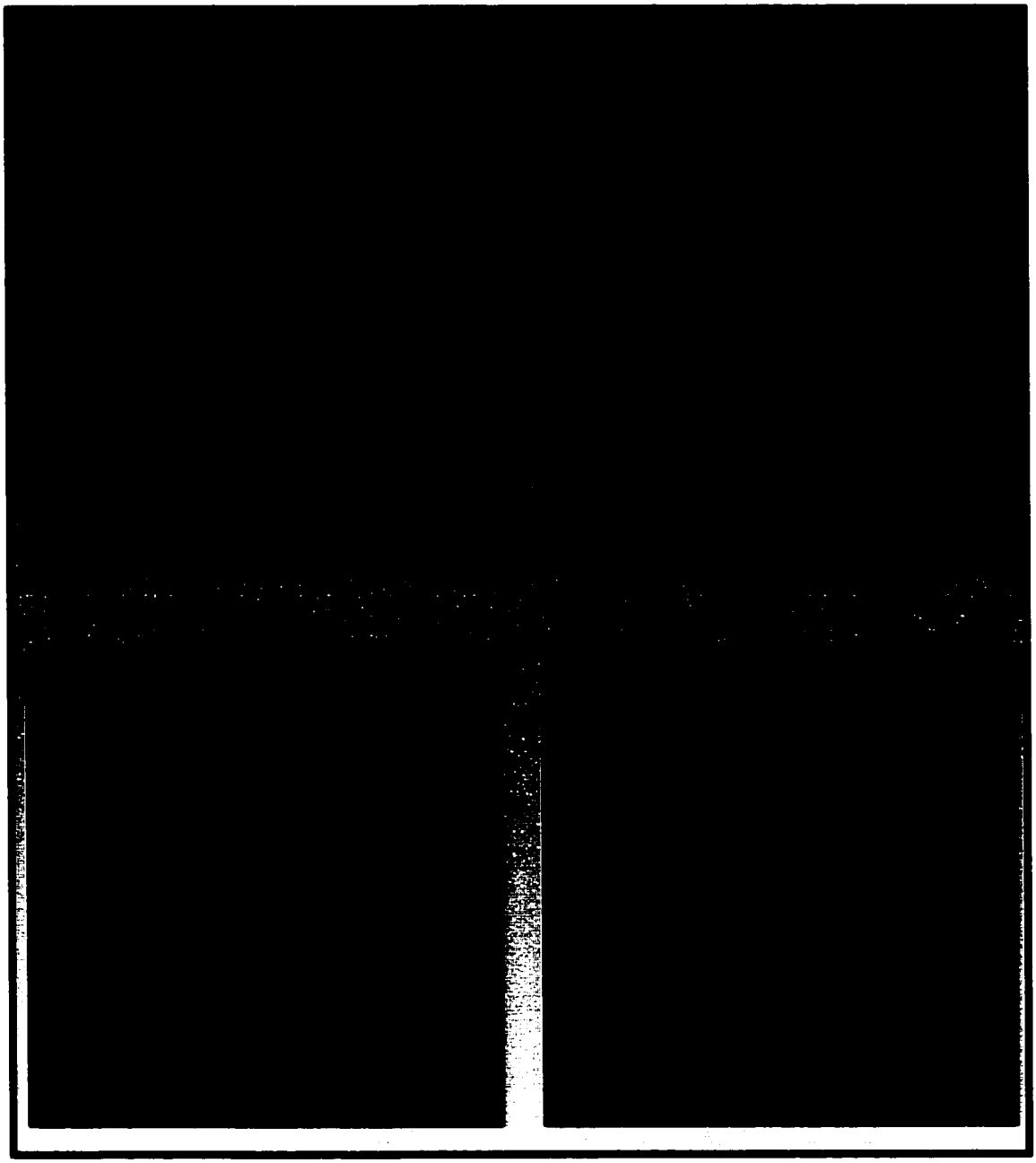

Figure 18 Confocal micrographs of L1210/DDP cells. Cells were transfected with a UCP2-pIRES2-EGFP construct followed by treatment with the mitochondrion-selective dye Mitotracker® Red, as described in Methods and Materials. Cells were then fixed and visualized by confocal microscopy. Upper left panel: non-fluorescence micrograph. Upper right panel: visualization of Mitotracker® Red staining. Bottom left panel: visualization of UCP2-pIRES2-EGFP localization. Bottom right panel: fluorescence overlap of Mitotracker® Red and EGFP. Magnification: 400x.

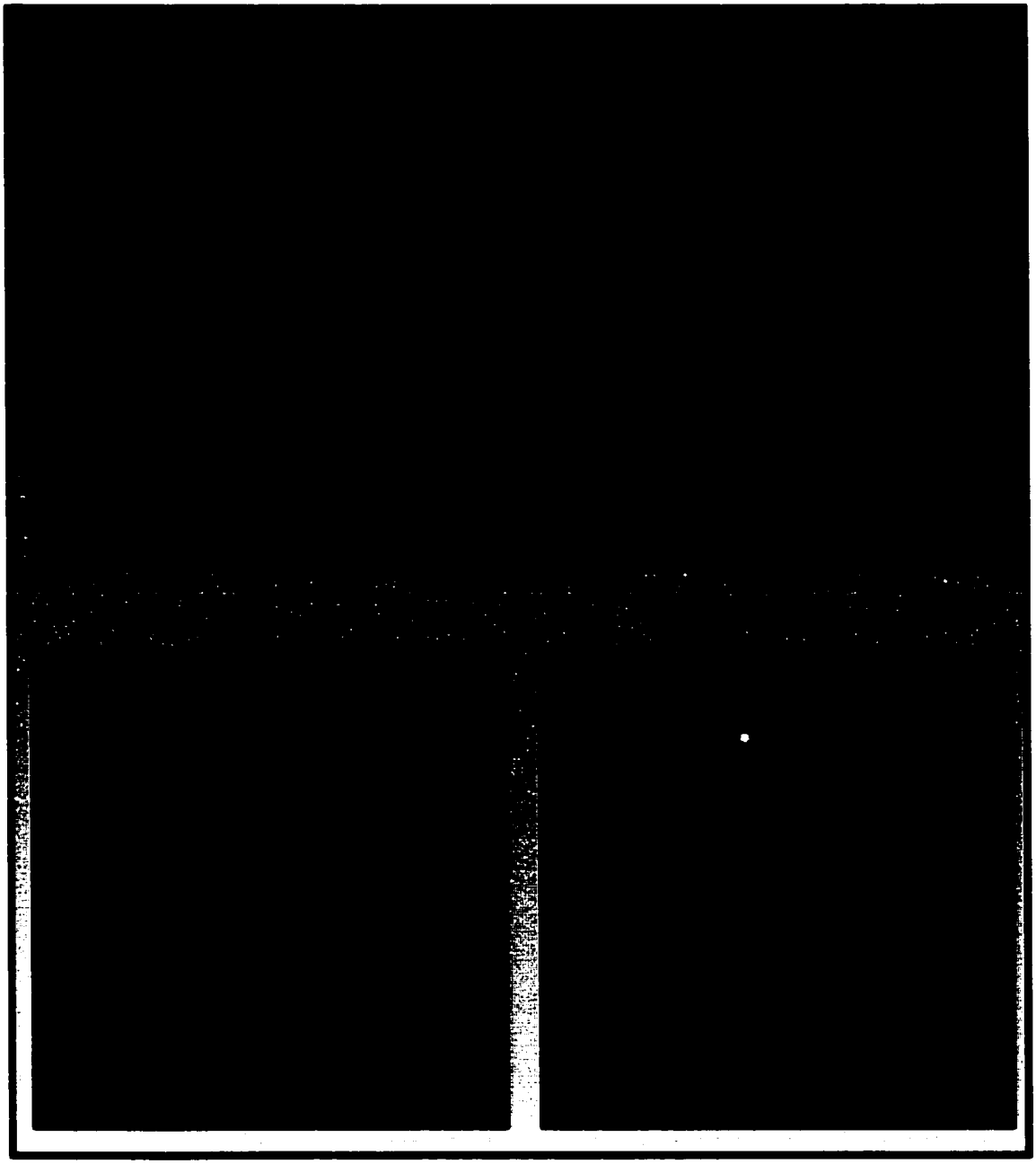

Figure 19 Confocal micrograph comparison of L1210 and L1210/DDP cells. Cells were transfected with a UCP2-pIRES2-EGFP construct followed by treatment with the mitochondrion-selective dye Mitotracker® Red, as described in Methods and Materials. Cells were then fixed and visualized by confocal microscopy. Upper left panel: visualization of Mitotracker® Red staining in L1210 cells. Upper right panel: visualization of UCP2-pIRES2-EGFP localization in L1210 cells. Bottom left panel: visualization of Mitotracker® Red staining in L1210/DDP cells. Bottom right panel: visualization of UCP2-pIRES2-EGFP localization in L1210/DDP cells. Magnification: 1000x (L1210), 400x (L1210/DDP).

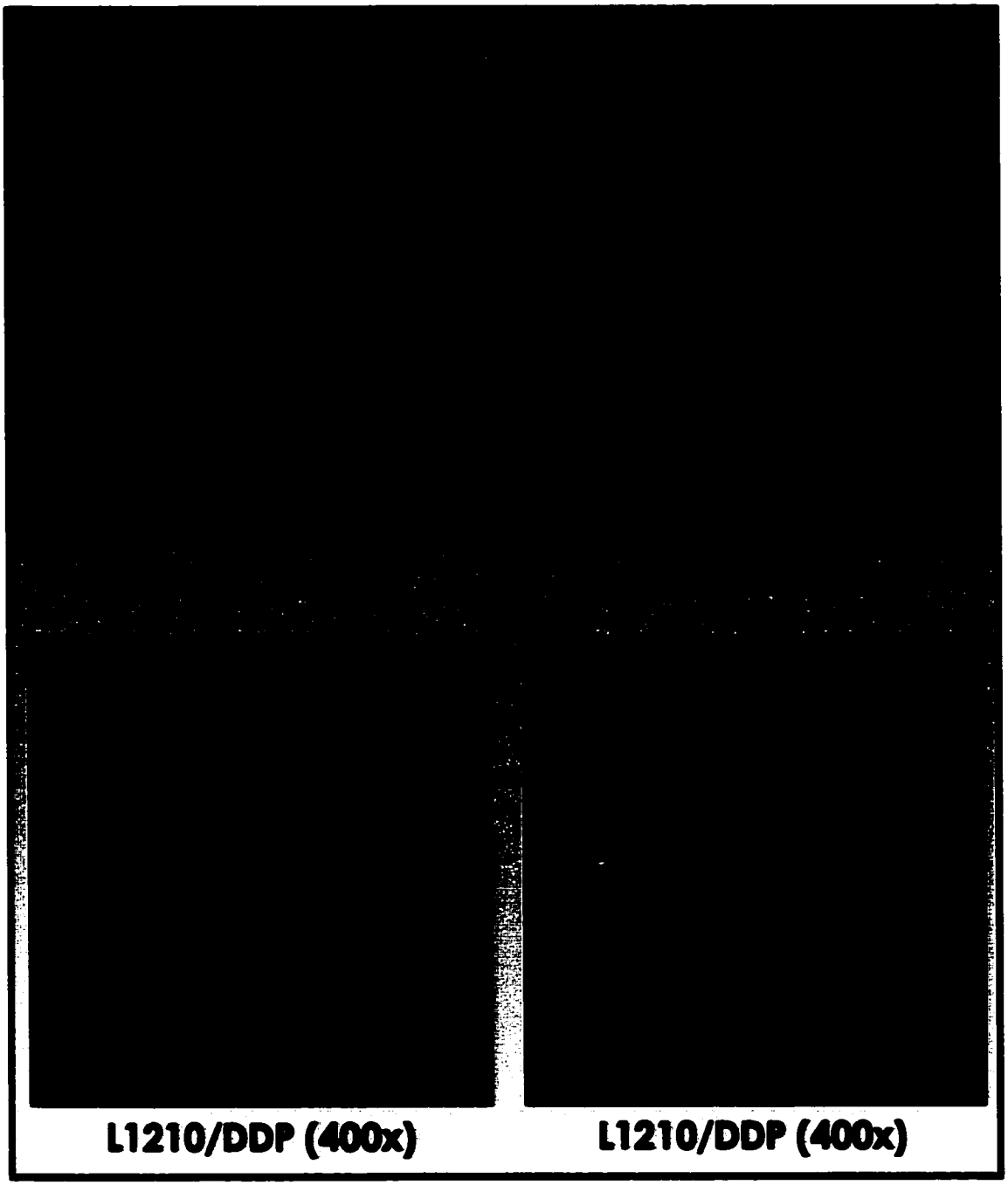
L1210/DDP (400x)
L1210/DDP (400x)

2. Analysis of HL60 and HL60/MDR Cells

In addition to providing a second set of results that would support the findings in the L1210 and L1210/DDP cells, switching to a human leukemic cell line pair of sensitive and resistant cells also allows for an analysis of mitochondrial bioenergetics in a different species.

A) Resting and State 4 Conditions

In assessing resting and state 4 oxygen consumption, the resistant HL60/MDR cells exhibited significantly higher rates ($p < 0.05$) under both conditions (Figure 20A and 20B). Values for resting oxygen consumption were 23.71 ± 2.42 (n=6) and 34.74 ± 3.73 (n=6) nmol $O_2 \times 10^7$ cells^{-1} × min^{-1} for the HL60 cells and HL60/MDR cells, respectively. Under state 4 conditions, oxygen consumption was 9.00 ± 1.74 (n=6) nmol $O_2 \times 10^7$ cells^{-1} × min^{-1} for the HL60 cells and 15.75 ± 1.10 (n=6) nmol $O_2 \times 10^7$ cells^{-1} × min^{-1} for the HL60/MDR cells. Within each cell type, there is a significant inhibition of respiration ($p < 0.001$) upon addition of oligomycin to achieve state 4 conditions.

Both resting and state 4 $\Delta\Psi_m$ were significantly lower ($p < 0.005$) in the HL60/MDR cells compared to the HL60 cells (Figure 20C and 20D). The $\Delta\Psi_m$ for resting conditions was 170.6 ± 2.9 (n=6) and 148.3 ± 6.8 (n=6) mV for the HL60 and HL60/MDR cells, respectively. Values for state 4 $\Delta\Psi_m$ were 166.3 ± 1.9 mV (n=6) for the HL60 cells and 153.8 ± 8.0 mV (n=6) for the resistant HL60/MDR cells.

As evidenced with the resistant L1210/DDP cells, higher oxygen consumption and lower $\Delta\Psi_m$ in the drug resistant HL60/MDR cells suggest that mitochondrial proton leak is increased compared to the sensitive HL60 cells.

Figure 20 Oxygen consumption and mitochondrial membrane potential of HL60 and HL60/MDR cells. Cells were incubated at 37 °C in a shaking water bath at a concentration of 10 million cells per ml of incubation medium in glass vials. The gas phase above each suspension was 95% air and 5% CO_2 to allow the medium to equilibrate to a pH of 7.4. The cells were preincubated in the water bath for 10 minutes to allow the cells to reestablish steady state ion gradients after being stored on ice. Cells were then incubated a further 20 minutes in the presence of any inhibitors and isotopes before aliquots were taken for the measurement of oxygen consumption and mitochondrial membrane potential. Panels A and B: Oxygen consumption of HL60 and HL60/MDR cells under (A) 'resting' (absence of inhibitors) and (B) 'state 4' (100 nM saturating concentration of the specific inhibitor of ATP synthase oligomycin) conditions. Values for both panels are presented as the mean ± SEM of 6 determinations (assessments performed in duplicate for each determination). Panels C and D: Mitochondrial membrane potential of HL60 and HL60/MDR cells under (C) 'resting' and (D) 'state 4' conditions. Values for both panels are presented as the mean ± SEM of 6 determinations (assessments performed in triplicate for each determination).

Oxygen Consumption

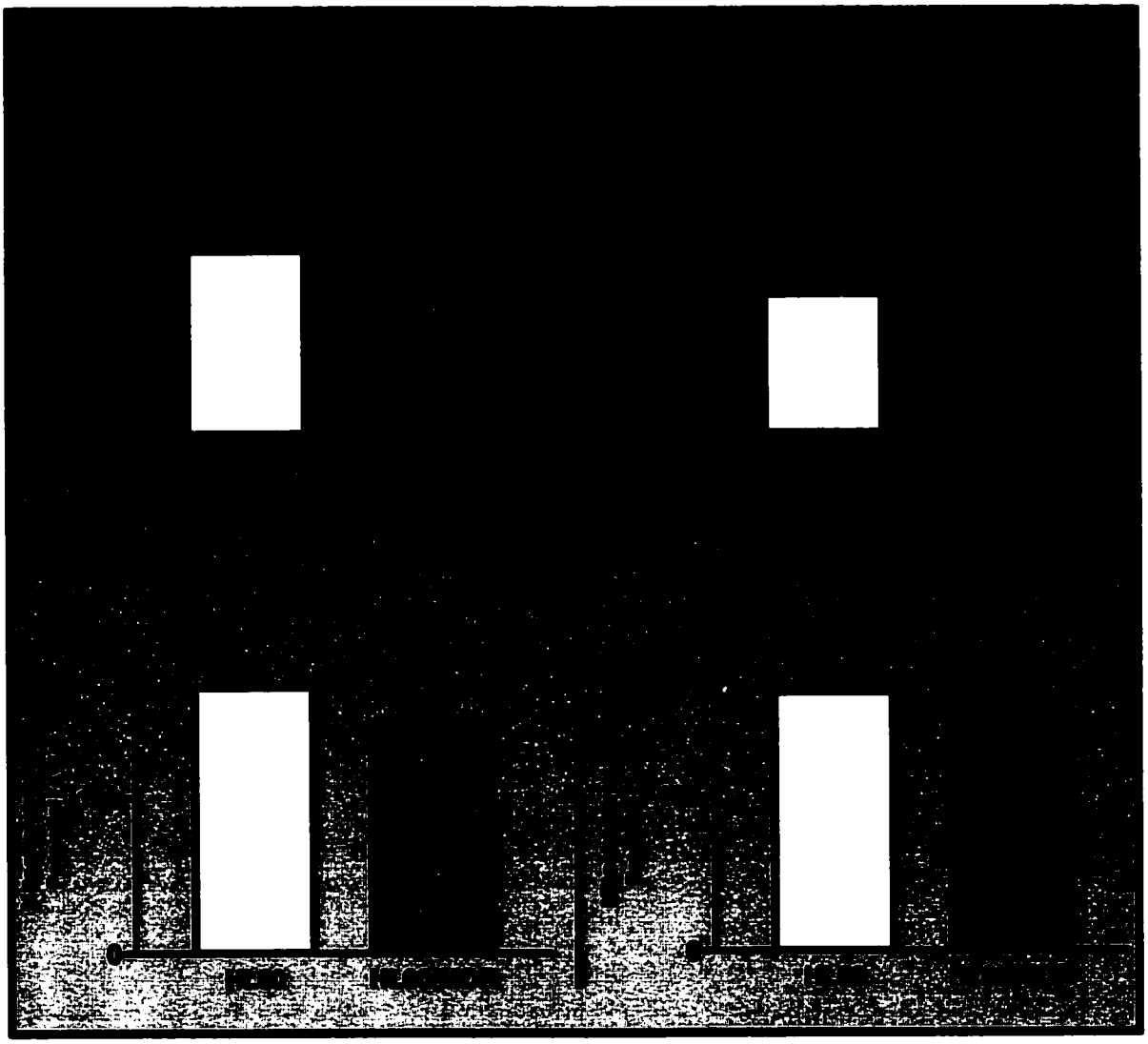

Mitochondrial Membrane Potential

B) Kinetics of Mitochondrial Proton Leak

Extending to the left of state 4 values in Figure 21 are the curves that represent mitochondrial proton leak kinetics. Each point on the curve for the resistant HL60/MDR cells has a higher oxygen consumption and lower $\Delta\Psi_m$ than the corresponding point on the curve for the sensitive HL60 cells. Again, more oxygen is required by the resistant cells in order to maintain the same level of $\Delta\Psi_m$ as in the sensitive cells. Thus leak is increased in the resistant cells.

C) Cellular Respiratory Capacity

Figure 22 shows the acute effects of FCCP on the resting respiration rates of the two cell lines. There was a significant increase ($p < 0.05$) in oxygen consumption in the presence of FCCP for both cell lines. Values for HL60 cells were 20.85 ± 1.40 (n=6) and 29.52± 2.05 (n=6) nmol $O_2 \times 10^7$ cells^{-1} × min^{-1} for resting and FCCP-stimulated, respectively. For the HL60/MDR cells, values were 30.74 ± 1.95 (n=6) and 39.50 ± 2.35 (n=6) nmol $O_2 \times 10^7$ cells^{-1} × min^{-1} for resting and FCCP-stimulated, respectively. Thus the resistant cells have a higher ($p < 0.01$) maximum respiratory capacity.

D) Uncoupling Protein 2 Expression

To determine if increased mitochondrial proton leak in the HL60/MDR cells is correlated to differences in mitochondrial UCP2 content, mitochondrial fractions were isolated and analyzed by Western blot analysis (Figure 23). The results demonstrate that the drug resistant cells express higher levels of mitochondrial UCP2.

Based on the results of the Northern blot analyses performed on the L1210 and

Figure 21 Relationship between mitochondrial membrane potential ($\Delta\Psi_m$) and leak-dependent respiration (per cell) in HL60 and HL60/MDR cells. The kinetic response of the proton leak subsystem to $\Delta\Psi_m$ was determined by titrating the substrate oxidation reactions with increasing amounts of antimycin (50 nM, 250 nM, 5 μM) in the presence of a saturating concentration of oligomycin (100 nM). State 4 respiration is defined as maximal non-phosphorylating respiration and is achieved with the saturating concentration of oligomycin. Oxygen consumption is defined in this figure on a per cell basis. Values are presented as the mean ± SEM of 6 determinations. Assessments were performed in duplicate for oxygen consumption and triplicate for mitochondrial membrane potential.

Proton Leak Kinetic Curves

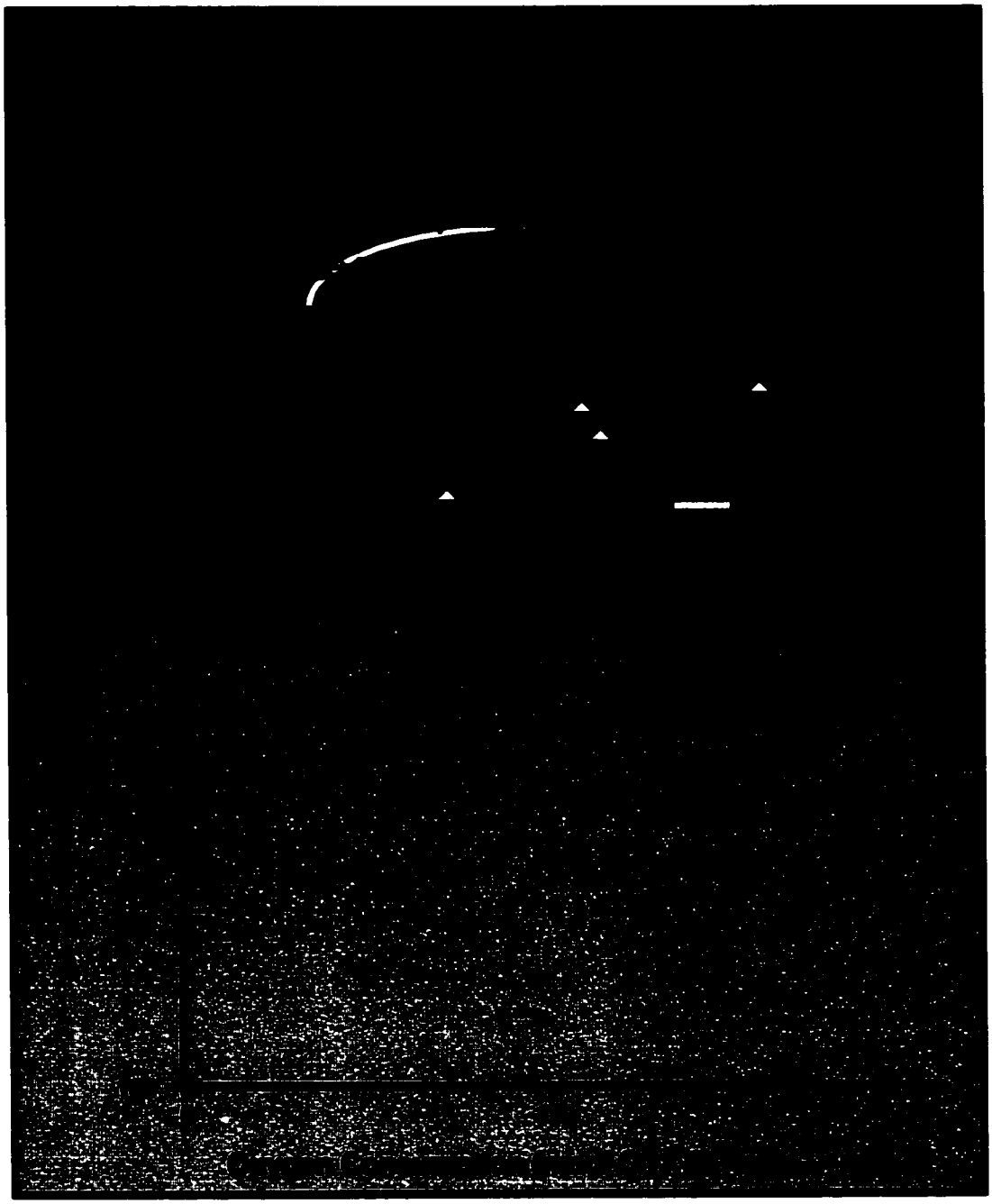

Figure 22 Acute effect of FCCP on the resting respiration rates in (A) HL60 and (B) HL60/MDR cells. To determine the maximum respiratory capacity of the cells, 10 μM of the artificial uncoupler carbonyl cyanide p-trifluoromethoxyphenylhydrazone (FCCP) was added to cells in the resting state and measured for approximately 5 minutes. FCCP is a protonphore that catalyzes the net electrical uniport of protons and increases the proton conductance of the mitochondrial inner membrane. For both graphs, values are presented as the mean ± SEM of 6 determinations (assessments performed in duplicate for each determination).

HL60

A

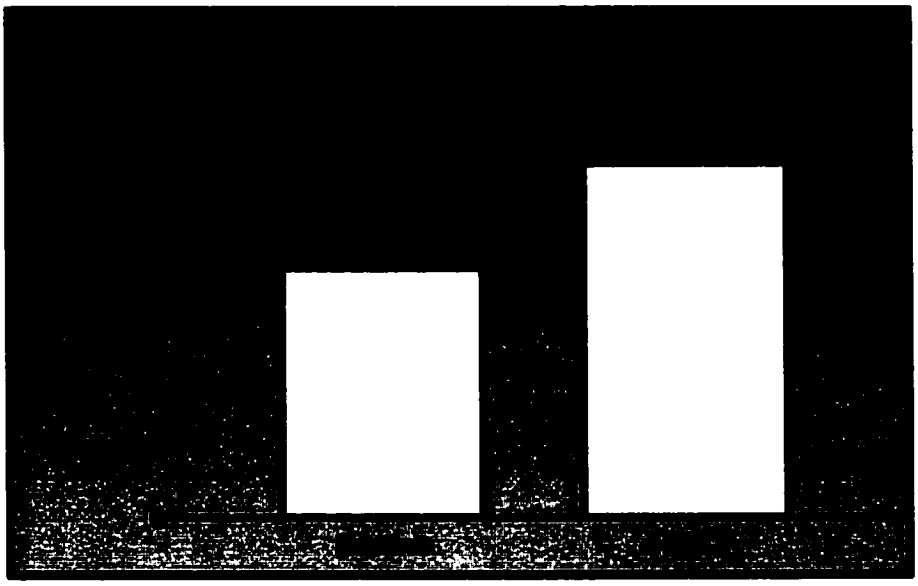

HL60/MDR

B

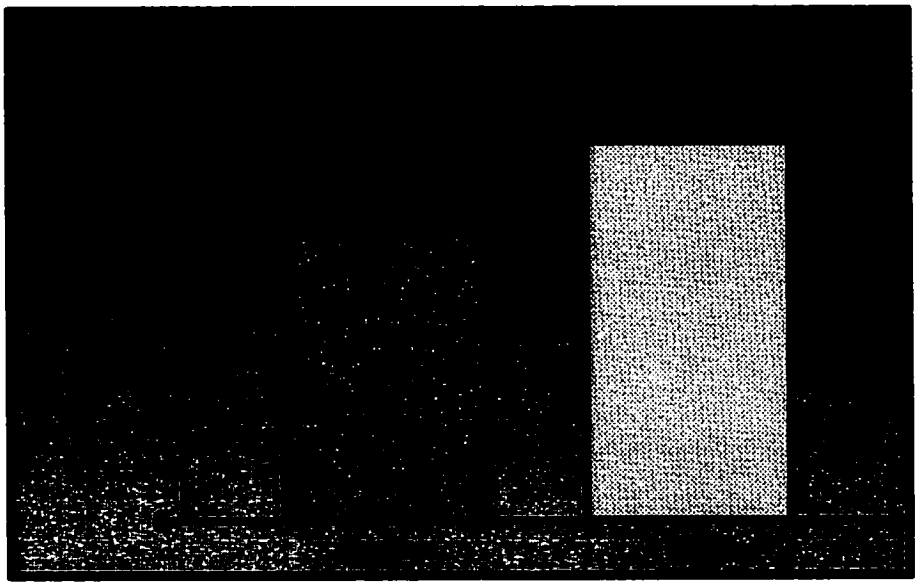

Figure 23 Representative Western blot of protein isolated from purified mitochondrial fractions of HL60 and HL60/MDR cells. Mitochondria were isolated using differential centrifugation. Protein content was determined using the modified Lowry method. Lane 1: Molecular weight markers (Santa Cruz Biotechnology, Santa Cruz, CA). Lanes 2 and 3: HL60 mitochondrial protein (60 μg) from two distinct mitochondrial preparations. Lanes 4 and 5: HL60/MDR mitochondrial protein (60 μg) from two distinct mitochondrial preparations. The primary antibody was goat anti-human UCP2 (Santa Cruz Biotechnology, Santa Cruz, CA) used at a concentration of 1.5 μg/ml. The secondary antibody was donkey anti-goat IgG horseradish peroxidase conjugate (Santa Cruz Biotechnology, Santa Cruz, CA) used at a dilution of 1:5000. Detection was performed using an Enhanced chemiluminescence (ECL) kit (Amersham Pharmacia Biotech).

Western Blot

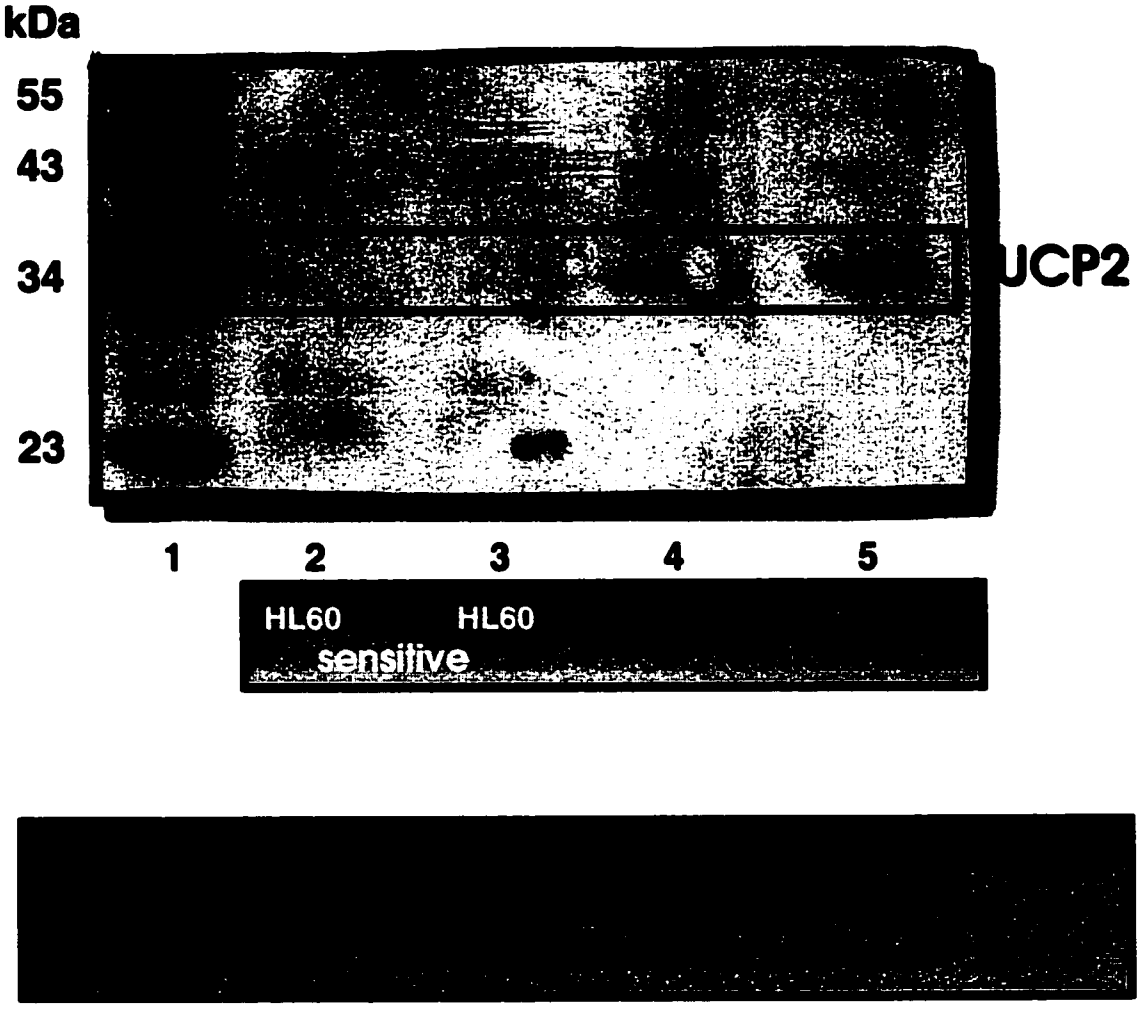

L1210/DDP cells (Figure 11), plasma membrane fractions were isolated from both HL60 and HL60/MDR cell lines to look for the presence of UCP2 on the cell surface. Similar to previous results with the mouse cell lines, UCP2 levels were found to be higher in the drug sensitive HL60 cells (Figure 24). These findings support the notion that UCP2, like some other mitochondrial proteins, can be found in other parts of the cell, particularly the cell surface.

E) Plasma Membrane Potential

The $\Delta\Psi_p$ of the two cell types was measured in an attempt to determine the possible role of UCP2 on the plasma membrane (Figure 25). Under resting conditions $\Delta\Psi_p$ was significantly lower ($p < 0.01$) in the HL60 cells. Values were 22.40 ± 5.10 mV (n=5) and 34.00 ± 5.57 mV (n=5) for HL60 and HL60/MDR cells, respectively. Unlike the results reported in the L1210 and L1210/DDP cells, no significant difference in $\Delta\Psi_p$ was observed in either cell line when GDP was added. Differences in resting conditions, however, provide an important start in determining the function of a mitochondrial protein like UCP2 on the cell surface.

F) Cytochrome Oxidase Activity

In examining cellular mitochondrial content, similar results were obtained in the human leukemic cells as in the mouse cell lines. When results are presented as a function of total cellular protein content (Figure 26A), there is no difference observed between the HL60 and HL60/MDR cells. Values were 101.1 ± 34.7 (n=3) and 125.3 ± 30.0 (n=3) nmol cytochrome c oxidized × min^{-1} × μg cellular $protein^{-1}$ for sensitive and resistant cells, respectively. After determining differences in cell size using a total

Figure 24 Representative Western blot of protein isolated from purified plasma membrane fractions of HL60 and HL60/MDR cells. Plasma membrane fractions were isolated using sucrose density gradient ultracentrifugation. Protein content was determined using the modified Lowry method. Lanes 1 and 7: Molecular weight markers (Santa Cruz Biotechnology, Santa Cruz, CA). Lanes 2 and 3: HL60 plasma membrane protein (60 μg) from two distinct membrane preparations. Lanes 4 and 5: HL60/MDR plasma membrane protein (60 μg) from two distinct membrane preparations. Lane 6: uncoupling protein 2 standard (15 ng; Stratagene). The standard is conjugated to a small protein and the expected molecular weight is 39 kDa. The primary antibody was goat anti-human UCP2 (Santa Cruz Biotechnology, Santa Cruz, CA) used at a concentration of 1.5 μg/ml. The secondary antibody was donkey anti-goat IgG horseradish peroxidase conjugate (Santa Cruz Biotechnology, Santa Cruz, CA) used at a dilution of 1:5000. Detection was performed using an Enhanced chemiluminescence (ECL) kit (Amersham Pharmacia Biotech).

Western Blot

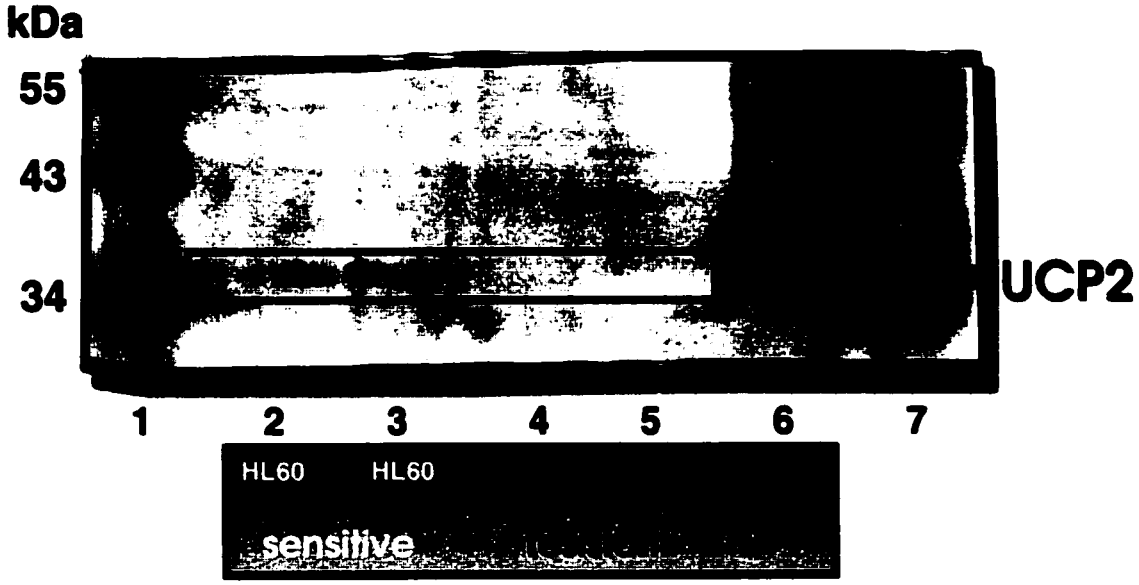

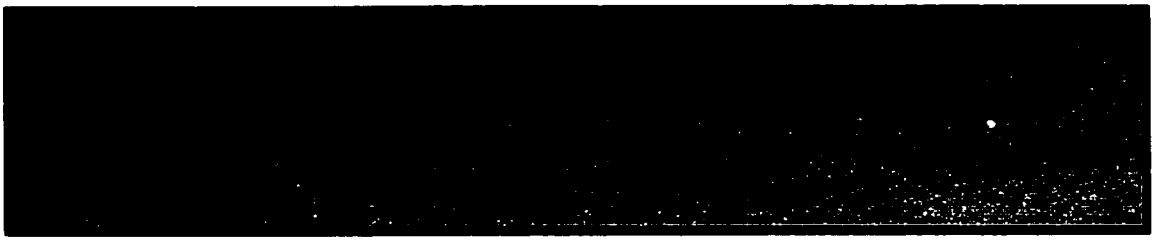

Figure 25 Plasma membrane potential ($\Delta\Psi_p$) of HL60 and HL60/MDR cells under normal conditions and in the presence of GDP. Cells were incubated at 37 °C in a shaking water bath at a concentration of 10 million cells per ml of incubation medium in glass vials. The gas phase above each suspension was 95% air and 5% CO_2 to allow the medium to equilibrate to a pH of 7.4. The cells were preincubated in the water bath for 10 minutes to allow the cells to reestablish steady state ion gradients after being stored on ice. Cells were then incubated a further 20 minutes in the presence of ^3H_2O and $^{36}Cl^-$. To examine the effects of GDP on plasma membrane potential, 1 mM GDP was added after the preincubation period. Values are presented as the mean ± SEM of 5 determinations for both cell types under normal conditions and in the presence of GDP. Assessments were performed in triplicate for each determination.

Plasma Membrane Potential

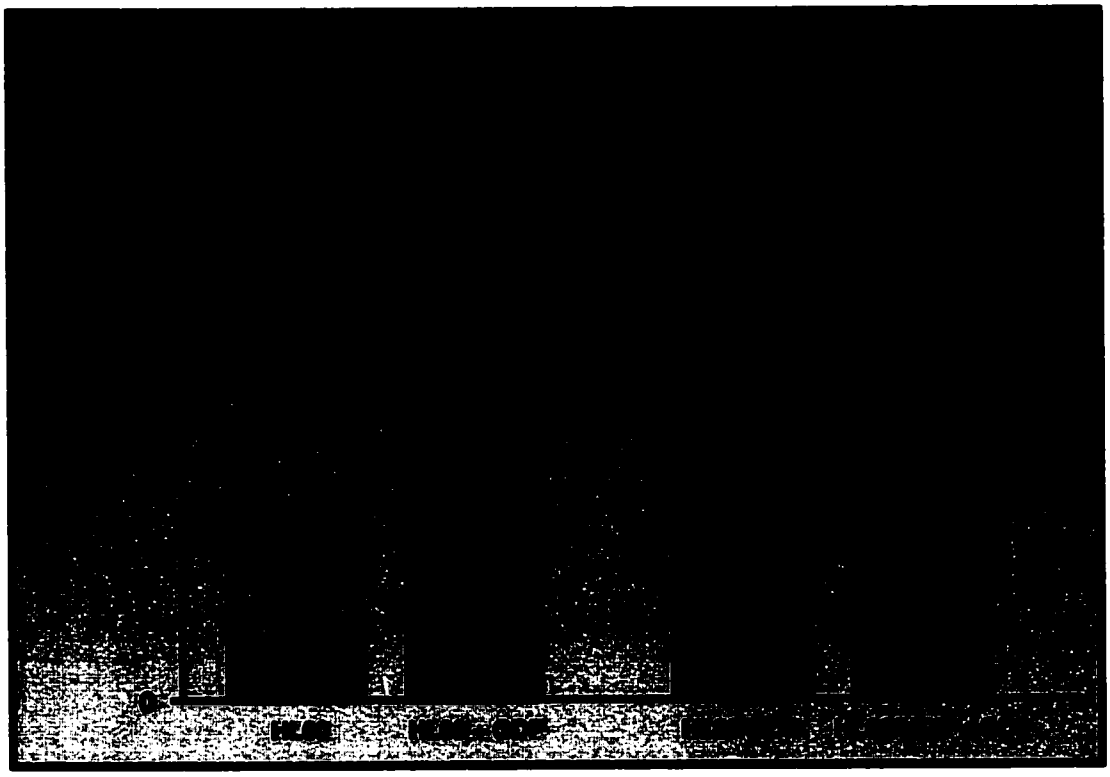

Figure 26 Cytochrome oxidase activity of HL60 and HL60/MDR cells. A spectrophotometric assay was used to determine the rate at which cytochrome oxidase can oxidize its substrate cytochrome c by measuring the rate of disappearance of reduced cytochrome c which absorbs light at 550 nm. Activity of cytochrome oxidase is used as an indicator of cellular mitochondrial content. In (A), values are expressed as a function of total cellular protein. In (B), values are expressed on a per cell basis to take into account the size of the cells. Values are presented as the mean ± SEM of 3 determinations. Assessments were performed in triplicate for each determination.

Cytochrome Oxidase

A

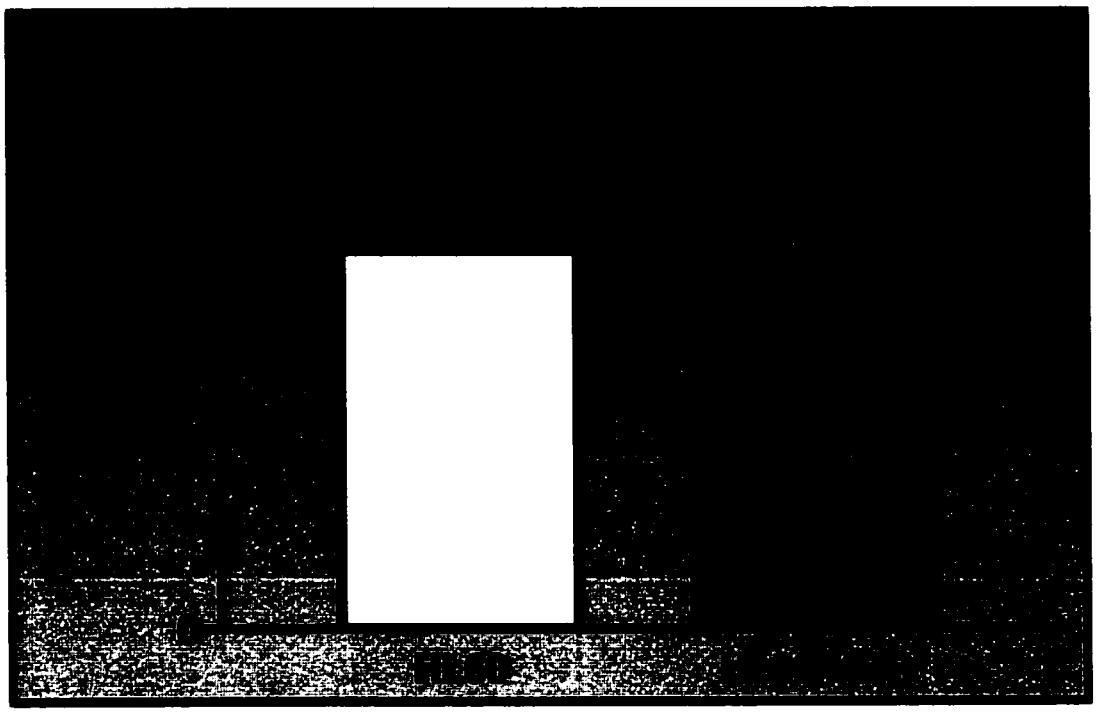

B

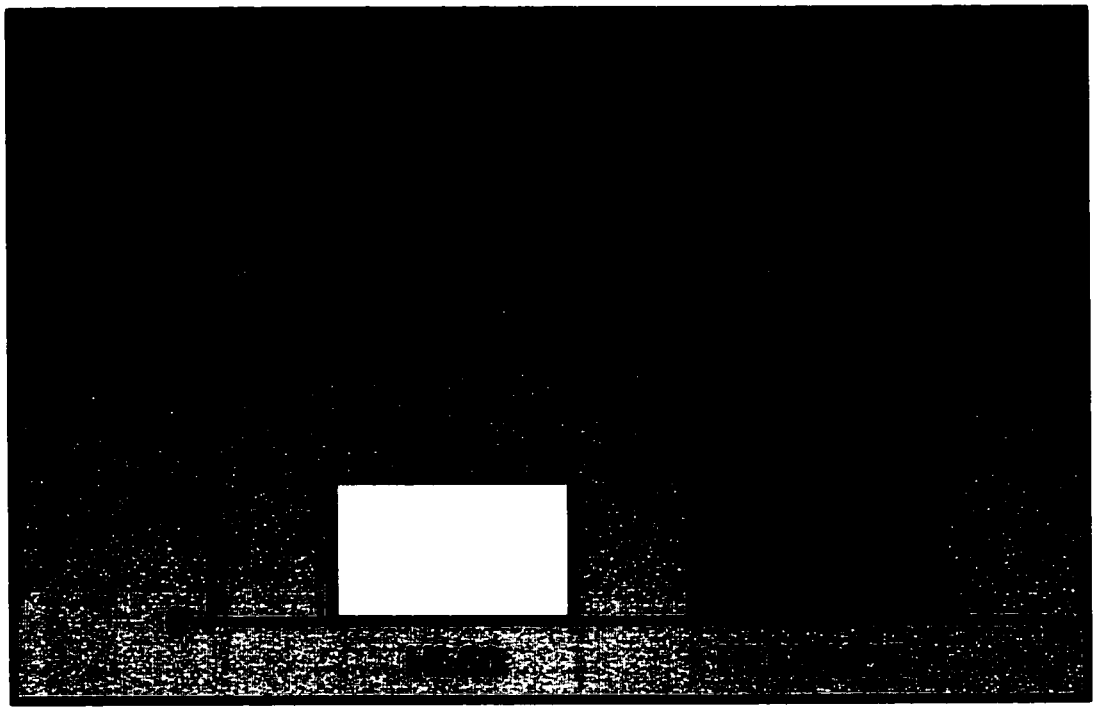

cellular protein determination (Table 2), results were expressed to reflect this.

TABLE 2

Cell Type	Mass of Protein per Cell (ng)
HL60	0.12 ± 0.04
HL60/MDR	0.30 ± 0.04

Cellular Protein Content of HL60 and HL60/MDR cells. Total cell homogenates were used to determine protein concentrations using the modified Lowry method (described in Methods and Materials). Values are presented as the mean ± SEM of 5 determinations for each cell type. Assessments were performed in duplicate for each determination.

Results presented in Figure 26B indicate that the HL60/MDR cells appear to have a greater mitochondrial content. Values were 12.5 ± 4.3 (n=3) and 38.0 ± 9.1 (n=3) nmol cytochrome c oxidized × min^{-1} × 10^3 $cells^{-1}$ for L1210 and L1210/DDP cells, respectively.

The overall kinetics of mitochondrial proton leak of these cells are shown in Figure 27 with oxygen consumption expressed to reflect the differences in estimated mitochondrial content between cell types. Again, $\Delta\Psi_m$ is not affected by these changes, but oxygen consumption in the HL60/MDR cells is no longer indicative of increased proton leak. An interpretation of these results along with those observed for the mouse leukemic cell lines is provided below in the Discussion section.

Figure 27 Relationship between mitochondrial membrane potential ($\Delta\Psi_m$) and leak-dependent respiration (corrected for mitochondrial content) in HL60 and HL60/MDR cells. The kinetic response of the proton leak subsystem to $\Delta\Psi_m$ was determined by titrating the substrate oxidation reactions with increasing amounts of antimycin (50 nM, 250 nM, 5 μM) in the presence of a saturating concentration of oligomycin (100 nM). State 4 respiration is defined as maximal non-phosphorylating respiration and is achieved with the saturating concentration of oligomycin. Oxygen consumption is expressed in this figure to take into account differences in cellular size and mitochondrial content. Values are presented as the mean ± SEM of 6 determinations. Assessments were performed in duplicate for oxygen consumption and triplicate for mitochondrial membrane potential.

Proton Leak Kinetic Curves

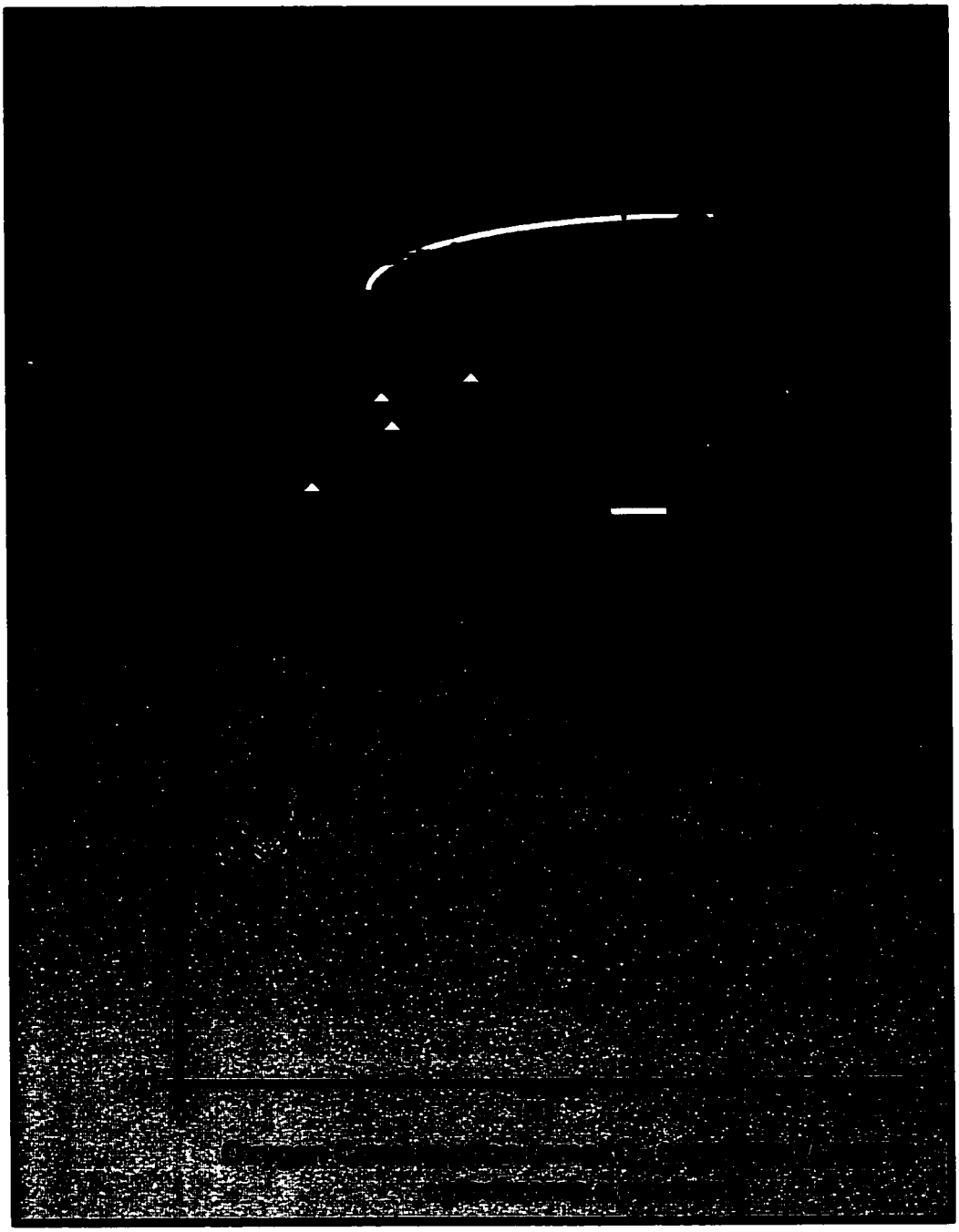

G) Confocal Microscopy Analysis

HL60 and HL60/MDR cells were also transfected with the UCP2-pIRES2-EGFP construct and treated with Mitotracker® Red to obtain visual information on UCP2 cellular localization and $\Delta\Psi_m$ is. Figure 28 shows micrographs of HL60 cells examined under the various fluorescence conditions. Again the large nuclei hindered attempts to decipher between mitochondrial and extra-mitochondrial localization. This is also the case for the HL60/MDR cells (Figure 29). A less intense red fluorescence for the resistant cells supports the previous findings of lower $\Delta\Psi_m$ determined with the lipophilic cation $TPMP^+$. The orange overlap produced as well as the traces of green areas in this overlapping panel (bottom right) are similar to the results described in the L1210 and L1210/DDP cells.

Figure 28 Confocal micrographs of HL60 cells. Cells were transfected with a UCP2-pIRES2-EGFP construct followed by treatment with the mitochondrion-selective dye Mitotracker® Red, as described in Methods and Materials. Cells were then fixed and visualized by confocal microscopy. Upper left panel: non-fluorescence micrograph. Upper right panel: visualization of Mitotracker® Red staining. Bottom left panel: visualization of UCP2-pIRES2-EGFP localization. Bottom right panel: fluorescence overlap of Mitotracker® Red and EGFP. Magnification: 1000x.

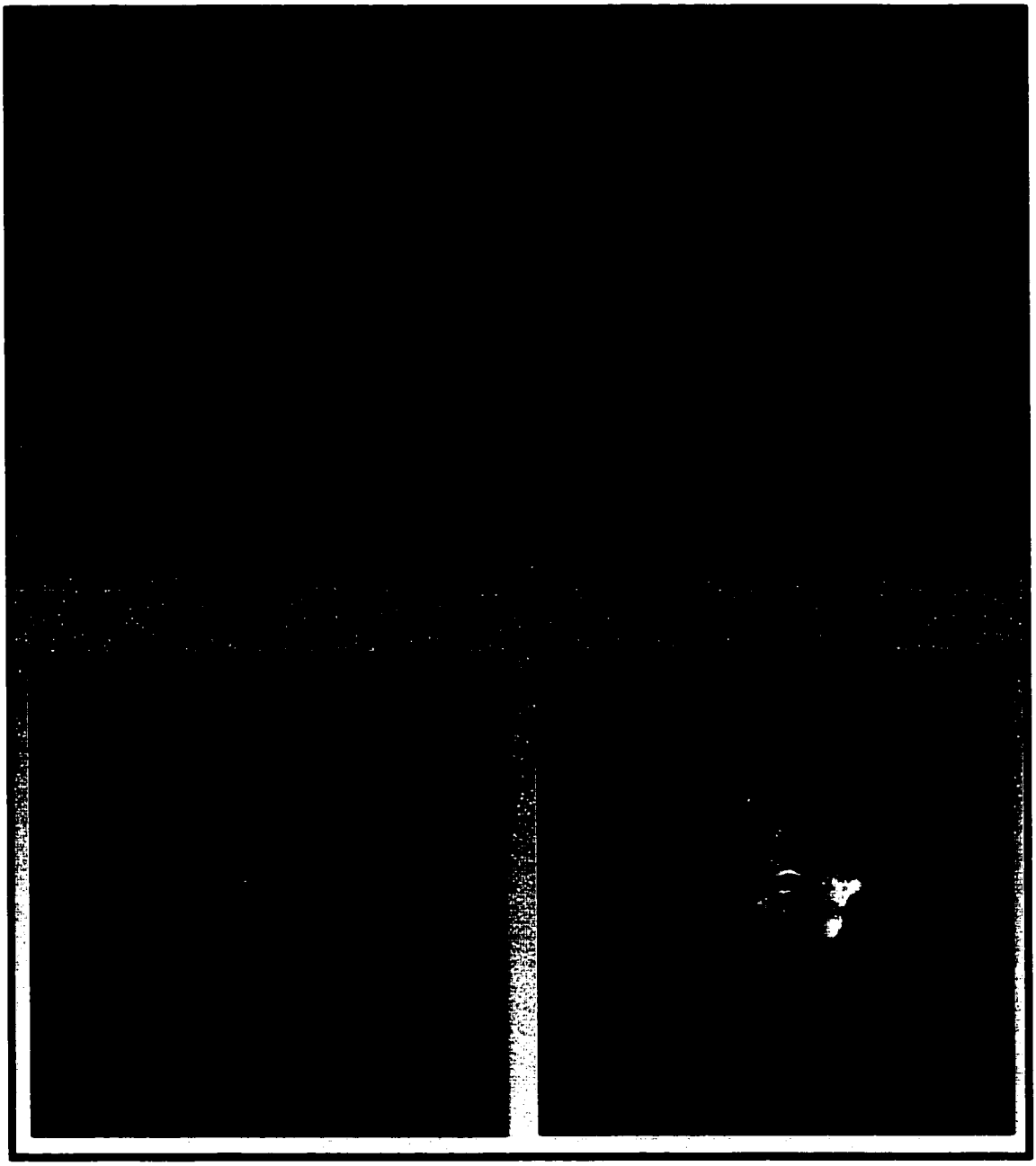

Figure 29 Confocal micrographs of HL60/MDR cells. Cells were transfected with a UCP2-pIRES2-EGFP construct followed by treatment with the mitochondrion-selective dye Mitotracker® Red, as described in Methods and Materials. Cells were then fixed and visualized by confocal microscopy. Upper panel: visualization of Mitotracker® Red staining. Bottom left panel: visualization of UCP2-pIRES2-EGFP localization. Bottom right panel: fluorescence overlap of Mitotracker® Red and EGFP. Magnification: 1000x.

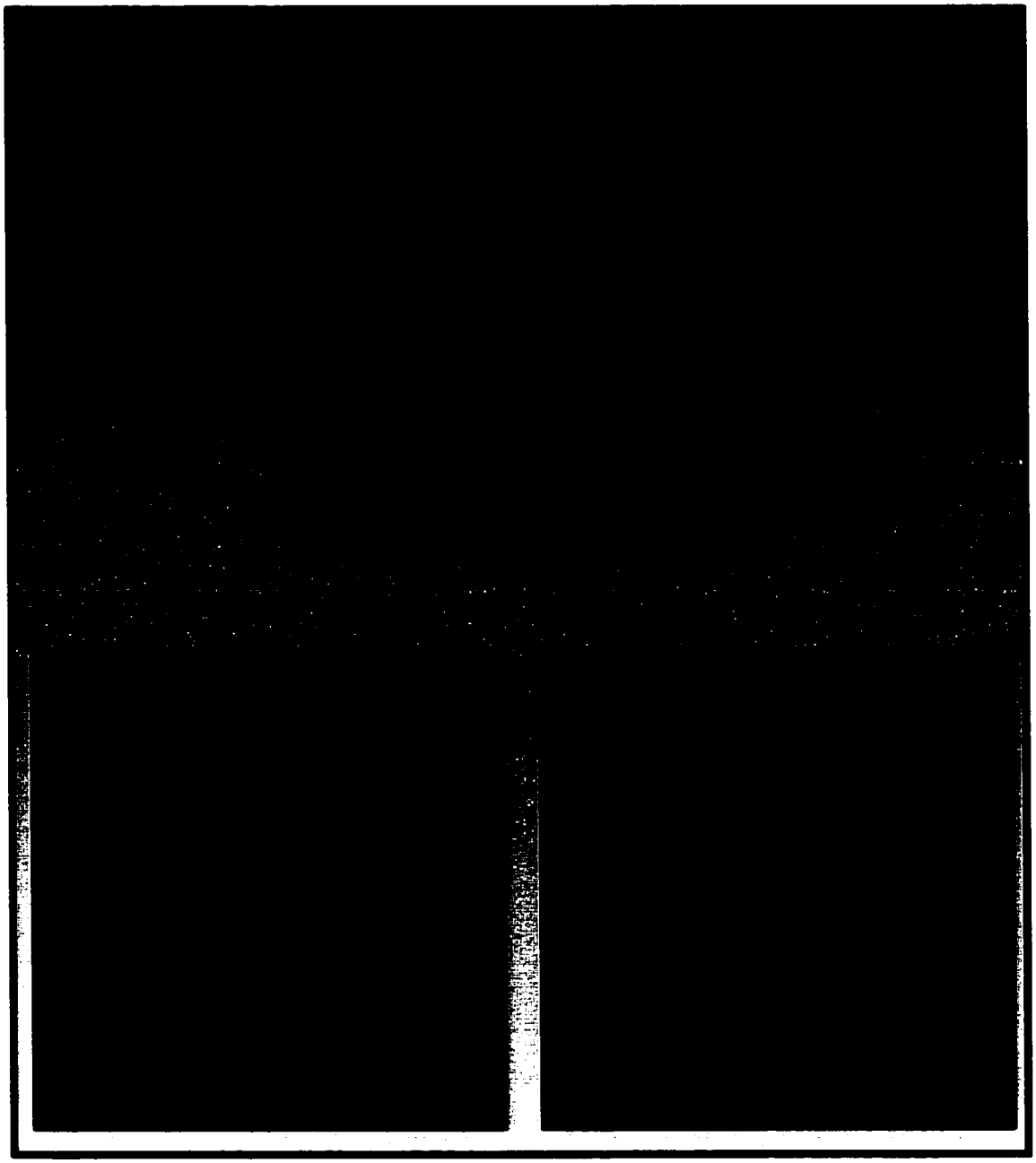

Discussion

Consistent with the proposal put forward at the beginning of this research, the results of this thesis demonstrate that drug sensitive and drug resistant leukemic cells differ in many of aspects of mitochondrial bioenergetics. Because the uncoupling of energy substrate oxidation from ADP phosphorylation is known to result in decreased mitochondrial membrane potential, accompanied by increased rates of substrate oxidation, electron transport, and oxygen consumption, the results show that drug resistant leukemic cells use a metabolic strategy in which mitochondrial oxidative phosphorylation is less coupled compared to the sensitive cells. This work is consistent with experiments performed by Harper and colleagues (Harper, Antoniou, Villalobos-Menuey et al., submitted), as well as the findings of others, that implicate uncoupling proteins in the regulation of reactive oxygen species production and their possible role in protection of tumor cells from cytotoxic therapies.

Under both resting and state 4 conditions, drug resistant cells consistently exhibited higher rates of cellular oxygen consumption and lower $\Delta\Psi_m$ compared to leukemic cells that are sensitive to apoptosis induced by chemotherapeutic agents and radiation (Figures 6 and 20). An investigation into the overall kinetics of mitochondrial proton leak revealed that, over a range of mitochondrial membrane potentials, leak-dependent oxygen consumption is much higher in the resistant cells (Figures 7 and 21). Due to the increased amount of proton leak in the drug resistant cells, more oxygen is being consumed in an attempt to re-establish the protonmotive

force across the mitochondrial inner membrane (MIM). The higher respiratory capacity of the resistant cells (Figures 9 and 22) may be due to the need for increased oxygen consumption when leak is increased in these cells.

Differences were also shown to exist in the substrate oxidation and phosphorylation reactions between the L1210 and L1210/DDP cells (Figure 8). In the resistant cells, increased activity of the substrate oxidation reactions may be a direct result of the increased proton leak in an effort to restore protonmotive force to normal values. It is difficult to speculate as to the specific mechanisms responsible for the differences seen in the kinetic responses of the phosphorylation subsystem to $\Delta\Psi_m$ in the L1210 and L1210/DDP cells. As described in Figure 5, the phosphorylation branch of the oxidative phosphorylation system includes ATP synthesis and all cellular ATP-consuming reactions, such as those involved in protein, DNA, and RNA synthetic reactions. These two branches of the three branch system were only briefly looked at, however, and should be examined further to provide more insight as to the exact mechanisms responsible for the differences seen.

A higher degree of mitochondrial proton leak in the resistant cells was supported by the Western blot analyses showing higher amounts of UCP2 in the mitochondria of resistant cells compared to sensitive cells (Figures 10 and 23). A major issue in the study of the new members of the uncoupling protein family is the absence of reliable antibodies to detect the proteins as well as to decipher between the different isoforms. In the case of UCP2, levels of expression also pose a problem. Mitochondria from spleen have a higher amount of UCP2 compared to other tissues, yet Pecqueur *et al.* (Pecqueur, et al., 2001) showed that the level of expression is less

than 1% of the level of UCP1 in brown adipose tissue mitochondria. Nevertheless, bands were seen in the 33 kDa range of all Western blots probed with the N-terminal UCP2 antibody (Santa Cruz Biotechnology, Inc.) that has also been used by others (Yang, et al., 2000). This antibody was also able to recognize the UCP2 standard (Figures 12 and 24). Although most of the commercially available anti-UCP antibodies are said to cross react with other proteins, the amount of cross-reactivity observed for this antibody was very low in the mitochondrial preparations.

These results showing a greater amount of UCP2 in the mitochondria of resistant cells are in agreement with the proposal that the decrease of $\Delta\Psi_m$ by uncoupling proteins may provide a means by which cells can safely minimize ROS production, and in turn provide resistance against apoptosis induced by oxidative stress. It is well established that mitochondria are the main source of ROS in the cell, however the idea that uncoupling proteins are involved in their regulation is relatively new. These findings, however, are consistent with the concept (Skulachev, 1996) that a decrease in $\Delta\Psi_m$ would increase the transport of electrons through the electron transport chain, decreasing the period of interaction between these electrons and molecular oxygen, thus reducing the formation of ROS.

Looking beyond leukemic cells and apoptosis prevention, these observations in general broaden our view of uncoupling proteins and their possible roles throughout the body (Vidal-Puig, 2000). Shown to be expressed in macrophages, the levels of UCP2 could be regulated in order to increase ROS production during infection. Conversely, increased levels of UCP2 and also UCP3 in other tissues in response to food restriction or exercise may constitute a physiological response to prevent unwanted

oxidative stress.

In confirming the presence of UCP2 in these cells, Northern blot analysis revealed that the drug sensitive L1210 cells have higher amounts of Ucp2 mRNA compared to the resistant L1210/DDP cells (Figure 11). Previous reports have shown that the level of UCP2 mRNA does not correlate with the amount of UCP2 protein in lung and stomach mitochondria (Pecqueur, et al., 2001). Protein amounts were 4 and 10 times lower, respectively, than in spleen mitochondria; however mRNA levels were very similar in the three tissues. Therefore it is also possible that mRNA levels do not reflect protein content in the L1210 and L1210/DDP cells. It was decided to investigate this further, and the possibility that this protein may be found in other parts of the cell was examined. This was not a radical concept, as others have identified mitochondrial proteins that function in extra-mitochondrial sites throughout the cell (Bradbury and Berk, 2000, Soltys, et al., 2001, Soltys and Gupta, 2000, Soltys and Gupta, 1999). A prominent location is the cell surface, and isolation of the plasma membrane revealed the presence of UCP2, with higher amounts found in the sensitive cells of both the mouse and human cell lines (Figures 12 and 24). Interesting to note is the position of the bands found in the plasma membrane fractions of the HL60 cells. The bands are slightly higher than the 34 kDa molecular weight marker; this may be due to possible glycosylation or phosphorylation that is specific to extra-mitochondrial UCP2. Current work in our laboratory is investigating this possibility. Mitochondrial UCP2 in the human leukemic cells migrated to a position similar to the UCP2 of the mouse cell lines. Flow cytometric work of permeabilized and non-permeabilized cells by our collaborator, Dr. M. Karen Newell, also contributed to the notion that UCP2 may be found elsewhere in

the cell (unpublished data). Localization to other cellular locations is possible, and should be investigated further.

Since the true physiological function of the uncoupling protein homologues is unclear, the function of UCP2 on the cell surface is, at best, an educated guess. With the resources that are available in our laboratory, the plasma membrane potential of the cells was examined to gain some insight. Under normal conditions the $\Delta\Psi_p$ was significantly lower in the sensitive cells, which contain higher amounts of cell surface UCP2 compared to the resistant cells (Figures 13 and 25). An increase in the $\Delta\Psi_p$ of the L1210 cells was observed in the presence of GDP, a known inhibitor of UCP1 and a proposed inhibitor of UCP2 (Negre-Salvayre, et al., 1997), whereas no effect was seen in the L1210/DDP cells. GDP may be acting on other structures on the cell surface, however, and may be causing the change in $\Delta\Psi_p$ in a way that does not involve UCP2. This, and the results which show no effect of GDP on the human leukemic cell lines, demonstrates the need for a more precise and detailed look into the role of plasma membrane UCP2 as a potential transporter of ions.

When the analysis of cellular ATP content was first performed on the L1210 and L1210/DDP cells, the lower amount present in the sensitive cells was thought to be due to the need for greater use of energy for their higher rate of turnover (Figure 16A). When cellular protein content was determined, values were corrected and indicated significantly lower levels of ATP in the resistant L1210 cells as a function of total protein content (Figure 16B). This is thought to be due to either increased uncoupling or the possibility of inactive mitochondria in the resistant cells (discussed below). The experiments were conducted with cells under normal conditions. At the time of the

discovery concerning cell size and protein content it was not possible to repeat the analyses under different conditions to obtain a more definite answer as to the reasons for the difference in ATP levels. Perhaps this could be accomplished by incubating the cells with a saturating concentration of oligomycin to look at non-mitochondrial ATP production, then present values to reflect ATP synthesis by oxidative phosphorylation only. Also the cells could be placed in a quiescent, non-dividing state to investigate differences in cellular ATP-consuming reactions that do not include cell division.

Corrections for differences in cellular protein content between cell sublines also led to modifications in the interpretation of the cytochrome oxidase values first presented (Figures 14A and 26A). When corrected for total protein content, the results demonstrate higher total mitochondrial content in the drug resistant cells (Figures 14B and 26B). When cellular oxygen consumption rates are normalized for total cytochrome oxidase activity, oxygen consumption of the resistant cells is very low. Mitochondrial membrane potential is unaffected by this, but changes in oxygen consumption values do not reflect increased proton leak in the resistant cells (Figures 15 and 27). Because the assay measures the maximal activity of the cytochrome oxidase, it is not possible to compare the actual *in vivo* activities of the enzyme between cell types. Thus it was most appropriate to present cellular oxygen consumption on a per cell basis. It has been shown that mitochondria sorted for low $\Delta\Psi_m$ are in an ultracondensed shape whereas those in cells that have a normal $\Delta\Psi_m$ were not condensed (Dinsdale, et al., 1999). This change in structure may affect normal respiratory chain activity and thus provide an explanation as to the reasons for low oxygen consumption values when normalized for cytochrome oxidase activity.

Other studies have described ultracondensed mitochondria in leukemic cells and implicated them in the signaling of the apoptotic process (Jia, et al., 1997a, Jia, et al., 1997b). It may seem ideal to perform the analyses of oxygen consumption and $\Delta\Psi_m$ using isolated mitochondria instead of intact cells. This was attempted but never was successful due to a low mitochondrial yield, and more importantly, the inability to isolate fully functional, respiring mitochondria with which to conduct the experiments.

Confocal microscopy analysis provided images of $\Delta\Psi_m$ as well as expression of the GFP-tagged UCP2 in cells. The differences in $\Delta\Psi_m$ between sensitive and resistant cells under resting conditions were clear, however nuclear size and the reduced cytoplasmic volume made cellular localization of UCP2 difficult to interpret. The contents of the cytosol were shown to be pressed against the plasma membrane as a result of the large nucleus present in all the cell types studied. In the superimposed images of red and green fluorescence, some green is still seen amidst the dominant orange, but this was visible only in a few images.

Work by Dr. Newell has complemented the results obtained in this thesis by examining more closely the levels of H_2O_2 production by drug sensitive and drug resistant leukemic cells under various conditions. In spite of the increased rate of cellular oxygen consumption in the resistant cells, the basal levels of H_2O_2 as detected by a fluorescent probe were similar between sensitive and resistant cells (Harper, Antoniou, Villalobos-Menuey et al., submitted). Maximal levels of H_2O_2 were determined by irradiation, and DNA damage was measured in parallel. Both cell types exhibited increased levels of H_2O_2, but the increase was lower in the resistant cells, suggesting a mechanism of protection. DNA damage was also found to be less severe

compared to the sensitive cells. Addition of an artificial uncoupler of mitochondrial ATP synthesis reduced H_2O_2 levels in L1210 cells, but had no effect on the resistant L1210/DDP cells.

Among the potential roles of ROS in apoptosis, one is their effect on mitochondrial permeability transition (MPT). With the electron transport chain serving as the main source of ROS leading to MPT, and based on evidence that MPT can be inhibited by antioxidants (Kowaltowski, et al., 2001), it is plausible that decreased ROS production due to increased mitochondrial UCP2 expression could act as a protective mechanism against MPT and the apoptotic cascade that follows it.

The work on these sensitive and resistant leukemic cells serves as evidence for the proposal that uncoupling of mitochondrial ATP synthesis provides a mechanism for dual resistance to both chemotherapeutic agents that induce apoptosis and to radiation by decreasing the production of reactive oxygen species. That uncoupling proteins are involved in protection from reactive oxygen species damage has been described (Negre-Salvayre, et al., 1997, Nishikawa, et al., 2000). This work is also consistent with the recent report that the production of ROS and subsequent cellular damage induced by hyperglycemia in endothelial cells is prevented by transfection with UCP1 (Nishikawa, et al., 2000). Ucp2 mRNA has been reported to be expressed in drug resistant cells (Voehringer, et al., 2000). As well, in pancreatic β-cells, overexpression of UCP2 was accompanied by increased cell survival after H_2O_2-induced toxicity (Li, et al., 2001). Finally, reports demonstrating that mice without UCP2 have increased levels of ROS and revert from susceptibility to resistance to *Toxoplasma gondii* (Arsenijevic, et al., 2000), likely from availability of ROS, suggest that the

mechanism is important in many aspects of immunity. This research suggests that such a metabolic strategy may provide the basis for survival of inherently resistant or drug-selected resistant cells and accounts for the commonly recognized dual resistance to both drugs and irradiation. This discovery impacts both tumor therapeutics and potentially the therapeutic approach to other diseases where damage from reactive oxygen species is involved.

REFERENCES

Alnemri, E. S. Hidden powers of the mitochondria. *Nature Cell Biology* 1: E40-42., 1999.

Arceci, R. J. Can multidrug resistance mechanisms be modified? *British Journal of Haematology* 110: 285-291., 2000.

Arceci, R. J. Mechanisms of resistance to therapy and tumor cell survival. *Current Opinions in Hematology* 2: 268-274., 1995.

Arsenijevic, D., H. Onuma, C. Pecqueur, S. Raimbault, B. S. Manning, B. Miroux, E. Couplan, M. C. Alves-Guerra, M. Goubern, R. Surwit, F. Bouillaud, D. Richard, S. Collins, and D. Ricquier. Disruption of the uncoupling protein-2 gene in mice reveals a role in immunity and reactive oxygen species production. *Nature Genetics* 26: 435-439., 2000.

Ashkenazi, A., and V. M. Dixit. Death receptors: signaling and modulation. *Science* 281: 1305-1308., 1998.

Bernardi, P., L. Scorrano, R. Colonna, V. Petronilli, and F. Di Lisa. Mitochondria and cell death. Mechanistic aspects and methodological issues. *European Journal of Biochemistry* 264: 687-701., 1999.

Beutler, E. The treatment of acute leukemia: past, present, and future. *Leukemia* 15: 658-661., 2001.

Bhushan, A., M. P. Hacker, and T. R. Tritton. Collateral methotrexate resistance in cisplatin-selected murine leukemia cells. *Brazilian Journal of Medical and Biological Research* 32: 827-833., 1999.

Bhushan, A., J. L. Kupperman, J. E. Stone, P. J. Kimberly, N. S. Calman, M. P. Hacker, R. B. Birge, T. R. Tritton, and M. K. Newell. Drug resistance results in alterations in expression of immune recognition molecules and failure to express Fas (CD95). *Immunology and Cell Biology* 76: 350-356., 1998.

Biswas, S., M. Ray, S. Misra, D. P. Dutta, and S. Ray. Selective inhibition of mitochondrial respiration and glycolysis in human leukaemic leucocytes by methylglyoxal. *Biochemical Journal* 323: 343-348., 1997.

Boss, O., P. Muzzin, and J. P. Giacobino. The uncoupling proteins, a review. *European Journal of Endocrinology* 139: 1-9., 1998.

Boss, O., S. Samec, A. Paoloni-Giacobino, C. Rossier, A. Dulloo, J. Seydoux, P. Muzzin, and J. P. Giacobino. Uncoupling protein-3: a new member of the mitochondrial carrier family with tissue-specific expression. *FEBS Letters* 408: 39-42., 1997.

Bouillaud, F., E. Couplan, C. Pecqueur, and D. Ricquier. Homologues of the uncoupling protein from brown adipose tissue (UCP1): UCP2, UCP3, BMCP1 and UCP4. *Biochimica et Biophysica Acta* 1504: 107-119., 2001.

Bouillaud, F., D. Ricquier, J. Thibault, and J. Weissenbach. Molecular approach to thermogenesis in brown adipose tissue: cDNA cloning of the mitochondrial uncoupling protein. *Proceedings of the National Academy of Science USA* 82: 445-448., 1985.

Bradbury, M. W., and P. D. Berk. Mitochondrial aspartate aminotransferase: direction of a single protein with two distinct functions to two subcellular sites does not require alternative splicing of the mRNA. *Biochemical Journal* 345 Pt 3: 423-427., 2000.

Bradshaw, D. M., and R. J. Arceci. Clinical relevance of transmembrane drug efflux as a mechanism of multidrug resistance. *Journal of Clinical Oncology* 16: 3674-3690., 1998.

Brand, M. D. The contribution of the leak of protons across the mitochondrial inner membrane to standard metabolic rate. *Journal of Theoretical Biology* 145: 267-286., 1990.

Brand, M. D. The proton leak across the mitochondrial inner membrane. *Biochimica et Biophysica Acta* 1018: 128-133., 1990.

Brand, M. D., L. F. Chien, E. K. Ainscow, D. F. Rolfe, and R. K. Porter. The causes and functions of mitochondrial proton leak. *Biochimica et Biophysica Acta* 1187: 132-139., 1994.

Brand, M. D., P. Couture, P. L. Else, K. W. Withers, and A. J. Hulbert. Evolution of energy metabolism. Proton permeability of the inner membrane of liver mitochondria is greater in a mammal than in a reptile. *Biochemical Journal* 275: 81-86., 1991.

Brookes, P. S., J. A. Buckingham, A. M. Tenreiro, A. J. Hulbert, and M. D. Brand. The proton permeability of the inner membrane of liver mitochondria from ectothermic and endothermic vertebrates and from obese rats: correlations with standard metabolic rate and phospholipid fatty acid composition. *Comparative Biochemistry and Physiology Part B Biochemistry and Molecular Biology* 119: 325-334., 1998.

Brookes, P. S., D. F. Rolfe, and M. D. Brand. The proton permeability of liposomes made from mitochondrial inner membrane phospholipids: comparison with isolated mitochondria. *Journal of Membrane Biology* 155: 167-174., 1997.

Brown, G. C. The leaks and slips of bioenergetic membranes. *Faseb Journal* 6: 2961-2965., 1992.

Brown, G. C., and M. D. Brand. Changes in permeability to protons and other cations at high proton motive force in rat liver mitochondria. *Biochemical Journal* 234: 75-81., 1986.

Brown, G. C., R. P. Hafner, and M. D. Brand. A 'top-down' approach to the determination of control coefficients in metabolic control theory. *European Journal of Biochemistry* 188: 321-325., 1990.

Buttgereit, F., M. D. Brand, and M. Muller. ConA induced changes in energy metabolism of rat thymocytes. *Bioscience Reports* 12: 109-114., 1992.

Buttgereit, F., A. Grant, M. Muller, and M. D. Brand. The effects of methylprednisolone on oxidative phosphorylation in Concanavalin-A-stimulated thymocytes. Top-down elasticity analysis and control analysis. *European Journal of Biochemistry* 223: 513-519., 1994.

Buttgereit, F., M. Muller, and S. M. Rapoport. Quantification of ATP-producing and consuming processes in quiescent pig spleen lymphocytes. *Biochemistry International* 24: 59-67., 1991.

Caldwell, K. K., M. K. Newell, J. C. Cambier, K. N. Prasad, J. M. Masserano, W. Schlegel, and D. M. Cooper. Evaluation of methods for the isolation of plasma membranes displaying guanosine 5'-triphosphate-dependence for the regulation of adenylate cyclase activity: potential application to the study of other guanosine 5'-triphosphate-dependent transduction systems. *Analytical Biochemistry* 175: 177-190., 1988.

Castoldi, G. L., A. Cuneo, F. Lanza, and P. Tomasi. Diagnosis of leukemia: morphology. *Leukemia* 6 Suppl 4: 6-9., 1992.

Chan, H. S., T. M. Grogan, G. Haddad, G. DeBoer, and V. Ling. P-glycoprotein expression: critical determinant in the response to osteosarcoma chemotherapy. *Journal of the National Cancer Institute* 89: 1706-1715., 1997.

Chance, B., H. Sies, and A. Boveris. Hydroperoxide metabolism in mammalian organs. *Physiological Reviews* 59: 527-605., 1979.

Chomczynski, P., and N. Sacchi. Single-step method of RNA isolation by acid guanidinium thiocyanate- phenol-chloroform extraction. *Analytical Biochemistry* 162: 156-159., 1987.

Cohen, G. M. Caspases: the executioners of apoptosis. *Biochemical Journal* 326: 1-16., 1997.

DeBry, R. W., and M. F. Seldin. Human/mouse homology relationships. *Genomics* 33: 337-351., 1996.

Dinsdale, D., J. Zhuang, and G. M. Cohen. Redistribution of cytochrome c precedes the caspase-dependent formation of ultracondensed mitochondria, with a reduced inner membrane potential, in apoptotic monocytes. *American Journal of Pathology* 155: 607-618., 1999.

Echtay, K. S., E. Winkler, K. Frischmuth, and M. Klingenberg. Uncoupling proteins 2 and 3 are highly active H(+) transporters and highly nucleotide sensitive when activated by coenzyme Q (ubiquinone). *Proceedings of the National Academy of Science USA* 98: 1416-1421., 2001.

Enerback, S., A. Jacobsson, E. M. Simpson, C. Guerra, H. Yamashita, M. E. Harper, and L. P. Kozak. Mice lacking mitochondrial uncoupling protein are cold-sensitive but not obese. *Nature* 387: 90-94., 1997.

Erickson, L. C., L. A. Zwelling, J. M. Ducore, N. A. Sharkey, and K. W. Kohn. Differential cytotoxicity and DNA cross-linking in normal and transformed human fibroblasts treated with cis- diamminedichloroplatinum(II). *Cancer Research* 41: 2791-2794., 1981.

Estey, E. H. Prognostic factors in acute myelogenous leukemia. *Leukemia* 15: 670-672., 2001.

Finkel, E. The mitochondrion: is it central to apoptosis? *Science* 292: 624-626., 2001.

Fleury, C., M. Neverova, S. Collins, S. Raimbault, O. Champigny, C. Levi-Meyrueis, F. Bouillaud, M. F. Seldin, R. S. Surwit, D. Ricquier, and C. H. Warden. Uncoupling protein-2: a novel gene linked to obesity and hyperinsulinemia. *Nature Genetics* 15: 269-272., 1997.

Garland, J. M., and A. Halestrap. Energy metabolism during apoptosis. Bcl-2 promotes survival in hematopoietic cells induced to apoptose by growth factor withdrawal by stabilizing a form of metabolic arrest. *The Journal of Biological Chemistry* 272: 4680-4688., 1997.

Green, D. R., and J. C. Reed. Mitochondria and apoptosis. *Science* 281: 1309-1312., 1998.

Groen, A. K., R. J. Wanders, H. V. Westerhoff, R. van der Meer, and J. M. Tager. Quantification of the contribution of various steps to the control of mitochondrial respiration. *The Journal of Biological Chemistry* 257: 2754-2757., 1982.

Hafner, R. P., G. C. Brown, and M. D. Brand. Analysis of the control of respiration rate, phosphorylation rate, proton leak rate and protonmotive force in isolated mitochondria using the 'top-down' approach of metabolic control theory. *European Journal Biochemistry* 188: 313-319., 1990.

Halicka, H. D., B. Ardelt, X. Li, M. M. Melamed, and Z. Darzynkiewicz. 2-Deoxy-D-glucose enhances sensitivity of human histiocytic lymphoma U937 cells to apoptosis induced by tumor necrosis factor. *Cancer Research* 55: 444-449., 1995.

Halliwell, B. Oxidants and human disease: some new concepts. *Faseb Journal* 1: 358-364., 1987.

Hannun, Y. A. Apoptosis and the dilemma of cancer chemotherapy. *Blood* 89: 1845-1853., 1997.

Harper, M. E., and M. D. Brand. The quantitative contributions of mitochondrial proton leak and ATP turnover reactions to the changed respiration rates of hepatocytes from rats of different thyroid status. *The Journal of Biological Chemistry* 268: 14850-14860., 1993.

Harper, M.E., and M.D. Brand. The use of top-down elasticity analysis to identify sites of thyroid hormone thermogenesis. *Proceedings of the Society for Experimental Biology and Medicine* 208: 228-237.

Harper, M. E., S. Monemdjou, J. J. Ramsey, and R. Weindruch. Age-related increase in mitochondrial proton leak and decrease in ATP turnover reactions in mouse hepatocytes. *American Journal of Physiology* 275: E197-206., 1998.

Heinrich, R., and T. A. Rapoport. A linear steady-state treatment of enzymatic chains. General properties, control and effector strength. *European Journal of Biochemistry* 42: 89-95., 1974.

Himms-Hagen, J. Brown adipose tissue thermogenesis: Role in thermoregulation, energy regulation and obesity. In: *Thermoregulation: Physiology and Biochemistry*, edited by E. Schonbaum and P. Lomax. New York: Pergamon Press Inc., 1990, p. 327-414.

Jacobson, M. D. Reactive oxygen species and programmed cell death. *Trends in Biochemical Sciences* 21: 83-86., 1996.

Jia, L., R. R. Dourmashkin, P. D. Allen, A. B. Gray, A. C. Newland, and S. M. Kelsey. Inhibition of autophagy abrogates tumour necrosis factor alpha induced apoptosis in human T-lymphoblastic leukaemic cells. *British Journal of Haematology* 98: 673-685., 1997a.

Jia, L., R. R. Dourmashkin, A. C. Newland, and S. M. Kelsey. Mitochondrial ultracondensation, but not swelling, is involved in TNF alpha-induced apoptosis in human T-lymphoblastic leukaemic cells. *Leukemia Research* 21: 973-983., 1997b.

Johns, D. R. Seminars in medicine of the Beth Israel Hospital, Boston. Mitochondrial DNA and disease. *The New England Journal of Medicine* 333: 638-644., 1995.

Kacser, H., and J. A. Burns. The control of flux. *Symposia of the Society for Experimental Biology* 27: 65-104, 1973.

Kleinsmith, L. J., and V. M. Kish. *Principles of Cell and Molecular Biology*. New York, NY: HarperCollins College Publishers, 1995.

Klingenberg, M., and S. G. Huang. Structure and function of the uncoupling protein from brown adipose tissue. *Biochimica et Biophysica Acta* 1415: 271-296., 1999.

Korshunov, S. S., V. P. Skulachev, and A. A. Starkov. High protonic potential actuates a mechanism of production of reactive oxygen species in mitochondria. *FEBS Letters* 416: 15-18., 1997.

Kowaltowski, A. J., R. F. Castilho, and A. E. Vercesi. Mitochondrial permeability transition and oxidative stress. *FEBS Letters* 24750: 1-4, 2001.

Krebs, H. A. Body size and tissue respiration. *Biochimica et Biophysica Acta* 4: 249-269, 1950.

Krishnamoorthy, G., and P. C. Hinkle. Non-ohmic proton conductance of mitochondria and liposomes. *Biochemistry* 23: 1640-1645., 1984.

Kroemer, G., P. Petit, N. Zamzami, J. L. Vayssiere, and B. Mignotte. The biochemistry of programmed cell death. *Faseb Journal* 9: 1277-1287., 1995.

Kunz, W. S. Control of oxidative phosphorylation in skeletal muscle. *Biochimica et Biophysica Acta* 1504: 12-19., 2001.

Leith, C. Multidrug resistance in leukemia. *Current Opinions in Hematology* 5: 287-291., 1998.

Leith, C. P., K. J. Kopecky, I. M. Chen, L. Eijdems, M. L. Slovak, T. S. McConnell, D. R. Head, J. Weick, M. R. Grever, F. R. Appelbaum, and C. L. Willman. Frequency and clinical significance of the expression of the multidrug resistance proteins MDR1/P-glycoprotein, MRP1, and LRP in acute myeloid leukemia: a Southwest Oncology Group Study. *Blood* 94: 1086-1099., 1999.

Lenaz, G. Role of mitochondria in oxidative stress and ageing. *Biochimica et Biophysica Acta* 1366: 53-67., 1998.

Li, L.-X., F. Skorpen, K. Egeberg, I. H. Jørgensen, and V. Grill. Uncoupling Protein-2 Participates in Cellular Defense against Oxidative Stress in Clonal β-Cells. *Biochemical and Biophysical Research Communications* 282: 273-277, 2001.

Lowry, O. H., N. J. Rosebrough, A. L. Farr, and R. J. Randal. Protein measurement with the Folin phenol reagent. *The Journal of Biological Chemistry* 193: 265-275, 1951.

Mao, W., X. X. Yu, A. Zhong, W. Li, J. Brush, S. W. Sherwood, S. H. Adams, and G. Pan. UCP4, a novel brain-specific mitochondrial protein that reduces membrane potential in mammalian cells. *FEBS Letters* 443: 326-330., 1999.

Marks, D. C., G. M. Su, R. A. Davey, and M. W. Davey. Extended multidrug resistance in haemopoietic cells. *British Journal of Haematology* 95: 587-595., 1996.

Mitchell, P., and J. Moyle. Acid-base titration across the membrane system of rat-liver mitochondria. Catalysis by uncouplers. *Biochemical Journal* 104: 588-600., 1967.

Murphy, M. P. How understanding the control of energy metabolism can help investigation of mitochondrial dysfunction, regulation and pharmacology. *Biochimica et Biophysica Acta* 1504: 1-11., 2001.

Negre-Salvayre, A., C. Hirtz, G. Carrera, R. Cazenave, M. Troly, R. Salvayre, L. Penicaud, and L. Casteilla. A role for uncoupling protein-2 as a regulator of mitochondrial hydrogen peroxide generation. *Faseb Journal* 11: 809-815., 1997.

Nicholls, D. G. Brown adipose tissue mitochondria. *Biochimica et Biophysica Acta* 549: 1-29., 1979.

Nicholls, D. G. The influence of respiration and ATP hydrolysis on the proton-electrochemical gradient across the inner membrane of rat-liver mitochondria as determined by ion distribution. *European Journal of Biochemistry* 50: 305-315., 1974.

Nicholls, D. G., and E. Rial. A history of the first uncoupling protein, UCP1. *Journal of Bioenergetics and Biomembranes* 31: 399-406., 1999.

Nishikawa, T., D. Edelstein, X. L. Du, S. Yamagishi, T. Matsumura, Y. Kaneda, M. A. Yorek, D. Beebe, P. J. Oates, H. P. Hammes, I. Giardino, and M. Brownlee. Normalizing mitochondrial superoxide production blocks three pathways of hyperglycaemic damage. *Nature* 404: 787-790., 2000.

Nobes, C. D., G. C. Brown, P. N. Olive, and M. D. Brand. Non-ohmic proton conductance of the mitochondrial inner membrane in hepatocytes. *The Journal of Biological Chemistry* 265: 12903-12909., 1990.

Oudard, S., E. Boitier, L. Miccoli, S. Rousset, B. Dutrillaux, and M. F. Poupon. Gliomas are driven by glycolysis: putative roles of hexokinase, oxidative phosphorylation and mitochondrial ultrastructure. *Anticancer Research* 17: 1903-1911., 1997.

Pecqueur, C., M.-C. Alves-Guerra, C. Gelly, C. Lévi-Meyrueis, E. Couplan, S. Collins, D. Ricquier, F. Bouillaud, and B. Miroux. Uncoupling Protein 2, in Vivo Distribution, Induction upon Oxidative Stress, and Evidence for Translational Regulation. *The Journal of Biological Chemistry* 276: 8705-8712, 2001.

Porter, R. K. Mitochondrial proton leak: a role for uncoupling proteins 2 and 3? *Biochimica et Biophysica Acta* 1504: 120-127, 2001.

Porter, R. K., and M. D. Brand. Body mass dependence of H+ leak in mitochondria and its relevance to metabolic rate. *Nature* 362: 628-630., 1993.

Price, E. M., M. Ratnam, K. M. Rodeman, and J. H. Freisheim. Characterization of the methotrexate transport pathway in murine L1210 leukemia cells: involvement of a membrane receptor and a cytosolic protein. *Biochemistry* 27: 7853-7858., 1988.

Reinhart, P. H., W. M. Taylor, and F. L. Bygrave. A procedure for the rapid preparation of mitochondria from rat liver. *Biochemical Journal* 204: 731-735., 1982.

Richon, V. M., N. Schulte, and A. Eastman. Multiple mechanisms of resistance to cis-diamminedichloroplatinum(II) in murine leukemia L1210 cells. *Cancer Research* 47: 2056-2061., 1987.

Richter, C. Do mitochondrial DNA fragments promote cancer and aging? *FEBS Letters* 241: 1-5., 1988.

Richter, C., V. Gogvadze, R. Laffranchi, R. Schlapbach, M. Schweizer, M. Suter, P. Walter, and M. Yaffee. Oxidants in mitochondria: from physiology to diseases. *Biochimica et Biophysica Acta* 1271: 67-74., 1995.

Richter, C., J. W. Park, and B. N. Ames. Normal oxidative damage to mitochondrial and nuclear DNA is extensive. *Proceedings of the National Academy of Science USA* 85: 6465-6467., 1988.

Rolfe, D. F., and M. D. Brand. Contribution of mitochondrial proton leak to skeletal muscle respiration and to standard metabolic rate. *American Journal of Physiology* 271: C1380-1389., 1996.

Rolfe, D. F., and G. C. Brown. Cellular energy utilization and molecular origin of standard metabolic rate in mammals. *Physiological Review* 77: 731-758., 1997.

Rolfe, D. F., J. M. Newman, J. A. Buckingham, M. G. Clark, and M. D. Brand. Contribution of mitochondrial proton leak to respiration rate in working skeletal muscle and liver and to SMR. *American Journal of Physiology* 276: C692-699., 1999.

Rosenberg, B. Anticancer activity of cis-dichlorodiammineplatinum(II) and some relevant chemistry. *Cancer Treatment Reports* 63: 1433-1438., 1979.

Sanchis, D., C. Fleury, N. Chomiki, M. Goubern, Q. Huang, M. Neverova, F. Gregoire, J. Easlick, S. Raimbault, C. Levi-Meyrueis, B. Miroux, S. Collins, M. Seldin, D. Richard, C. Warden, F. Bouillaud, and D. Ricquier. BMCP1, a novel mitochondrial carrier with high expression in the central nervous system of humans and rodents, and respiration uncoupling activity in recombinant yeast. *The Journal of Biological Chemistry* 273: 34611-34615., 1998.

Schabel, F. M., Jr., H. E. Skipper, M. W. Trader, W. R. Laster, Jr., D. P. Griswold, Jr., and T. H. Corbett. Establishment of cross-resistance profiles for new agents. *Cancer Treatment Reports* 67: 905-922., 1983.

Sen, C. K., and L. Packer. Antioxidant and redox regulation of gene transcription. *Faseb Journal* 10: 709-720., 1996.

Skulachev, V. P. Membrane-linked systems preventing superoxide formation. *Bioscience Reports* 17: 347-366., 1997.

Skulachev, V. P. Role of uncoupled and non-coupled oxidations in maintenance of safely low levels of oxygen and its one-electron reductants. *Quarterly Reviews of Biophysics* 29: 169-202., 1996.

Sohal, R. S., and B. H. Sohal. Hydrogen peroxide release by mitochondria increases during aging. *Mechanisms of Ageing and Development* 57: 187-202., 1991.

Solanes, G., A. Vidal-Puig, D. Grujic, J. S. Flier, and B. B. Lowell. The human uncoupling protein-3 gene. Genomic structure, chromosomal localization, and genetic basis for short and long form transcripts. *The Journal of Biological Chemistry* 272: 25433-25436., 1997.

Soltys, B. J., D. W. Andrews, R. Jemmerson, and R. S. Gupta. Cytochrome-c localizes in secretory granules in pancreas and anterior pituitary. *Cell Biology International* 25: 331-338, 2001.

Soltys, B. J., and R. S. Gupta. Mitochondrial proteins at unexpected cellular locations: export of proteins from mitochondria from an evolutionary perspective. *International Review of Cytology* 194: 133-196, 2000.

Soltys, B. J., and R. S. Gupta. Mitochondrial-matrix proteins at unexpected locations: are they exported? *Trends in Biochemical Sciences* 24: 174-177., 1999.

Stuart, J. A., S. Cadenas, M. B. Jekabsons, D. Roussel, and M. D. Brand. Mitochondrial proton leak and the uncoupling protein 1 homologues. *Biochimica et Biophysica Acta* 1504: 144-158., 2001.

Su, G. M., M. W. Davey, R. A. Davey, and A. D. Kidman. Development of extended multidrug resistance in HL60 promyelocytic leukaemia cells. *British Journal of Haematology* 88: 566-574., 1994.

Susin, S. A., N. Zamzami, and G. Kroemer. Mitochondria as regulators of apoptosis: doubt no more. *Biochimica et Biophysica Acta* 1366: 151-165, 1998.

Taylor, I. W., and M. H. Tattersall. Methotrexate cytotoxicity in cultured human leukemic cells studied by flow cytometry. *Cancer Research* 41: 1549-1558., 1981.

Teicher, B. A., C. A. Cucchi, J. B. Lee, J. L. Flatow, A. Rosowsky, and E. Frei, 3rd. Alkylating agents: in vitro studies of cross-resistance patterns in human cell lines. *Cancer Research* 46: 4379-4383., 1986.

Vidal-Puig, A., G. Solanes, D. Grujic, J. S. Flier, and B. B. Lowell. UCP3: an uncoupling protein homologue expressed preferentially and abundantly in skeletal muscle and brown adipose tissue. *Biochemical and Biophysical Research Communications* 235: 79-82., 1997.

Vidal-Puig, A. J. Uncoupling expectations. *Nature Genetics* 26: 387-388., 2000.

Vidal-Puig, A. J., D. Grujic, C. Y. Zhang, T. Hagen, O. Boss, Y. Ido, A. Szczepanik, J. Wade, V. Mootha, R. Cortright, D. M. Muoio, and B. B. Lowell. Energy metabolism in uncoupling protein 3 gene knockout mice. *The Journal of Biological Chemistry* 275: 16258-16266., 2000.

Voehringer, D. W., D. L. Hirschberg, J. Xiao, Q. Lu, M. Roederer, C. B. Lock, L. A. Herzenberg, and L. Steinman. Gene microarray identification of redox and mitochondrial elements that control resistance or sensitivity to apoptosis. *Proceedings of the National Academy of Science U S A* 97: 2680-2685., 2000.

Warden, C. H., J. S. Fisler, S. M. Shoemaker, P. Z. Wen, K. L. Svenson, M. J. Pace, and A. J. Lusis. Identification of four chromosomal loci determining obesity in a multifactorial mouse model. *Journal of Clinical Investigation* 95: 1545-1552., 1995.

Weber, G. Enzymology of cancer cells. *The New England Journal of Medicine* 296: 486-492., 1977.

Yang, S., H. Zhu, Y. Li, H. Lin, K. Gabrielson, M. A. Trush, and A. M. Diehl. Mitochondrial adaptations to obesity-related oxidant stress. *Archives of Biochemistry and Biophysics* 378: 259-268., 2000.

Yonetani, T., and G. S. Ray. Studies on cytochrome c oxidase. I. Purification and some properties. *The Journal of Biological Chemistry* 240: 4503-4508., 1965.

ANDREAS ANTONIOU

2285 Shanegal Crescent
Gloucester, ON K1V 9P3
Tel: (613) 521-5316
Fax: (613) 562-5440
Mobile: (613) 769-3830
email: andreas@uottawa.ca

FORMAL EDUCATION

M.Sc. (Biochemistry)	University of Ottawa, Faculty of Medicine (2001) Title of Thesis: '*Uncoupling Protein 2 and Mitochondrial Biooenergetics in Drug Sensitive and Drug Resistant Leukemic Cells*'
B.Sc.	University of Ottawa, Faculty of Medicine (1999) Honours Biochemistry, Graduated *Summa Cum Laude* Title of Thesis: '*Mitochondrial Uncoupling and Susceptibility to Drug Induced Apoptosis in the L1210 and L1210/DDP Tumor Cell Lines*'
O.S.S.D.	Brookfield High School, Ottawa, Ontario (1995)

EMPLOYMENT HISTORY

1999 - 2001	**Master's Student** Department of Biochemistry, Microbiology, and Immunology University of Ottawa Supervisor: Dr. Mary-Ellen Harper
1999 - 2001	**Teaching Assistant/Laboratory Demonstrator** For third year undergraduate biochemistry laboratories Department of Biochemistry, Microbiology, and Immunology University of Ottawa
1999	**Summer Research Student** Department of Biochemistry, Microbiology, and Immunology University of Ottawa Supervisor: Dr. Mary-Ellen Harper Project: Investigated the proposal that mitochondrial energy metabolism plays a crucial role in the resistance of tumor cells to cytotoxic therapies, and that uncoupling proteins are involved in this protection.

1998	**Summer Research Student** Department of Biochemistry, Microbiology, and Immunology University of Ottawa Supervisor: Dr. Mary-Ellen Harper Project: examined the effects of troglitazone, a thiazolidinedione, on skeletal muscle mitochondria using mice as models.
1996, 1997	**Host/Waiter** Seal Rock Restaurant, San Francisco California
1993 - 1995	**Pro Shop Employee** Ottawa Hunt and Golf Club, Ottawa, Ontario

ACADEMIC AWARDS

2000	**United Mitochondrial Disease Foundation Fellow** Value: Fee waiver for the 3rd Albany Conference on Frontiers of Mitochondrial Research (U.S. $525)
2000	**University of Ottawa Excellence Scholarship** Value: Full Tuition Waiver (approximately $5,000)
2000	**Natural Sciences and Engineering Research Council (NSERC) Postgraduate Scholarship** Value: $17,300
2000	**Ontario Graduate Scholarship (Declined)** Value: approximately $12,000
2000	**Ontario Graduate Scholarship in Science and Technology** Value: $15,000
1999	**Strategic Areas of Development Scholarship** Value: $15,000
1999	**University of Ottawa Graduate School Admission Scholarship** Value: Full Tuition Waiver (approximately $5,000)
1999	**NSERC Undergraduate Student Research Award** Value: $4,000
1999	**Hellenic-Canadian Federation of Ontario Educational Scholarship** Value: $500
1998	**Renewal of University of Ottawa Admission Scholarship*** Value: $1,800
1997	**Renewal of University of Ottawa Admission Scholarship*** Value: $1,800

1996 **Renewal of University of Ottawa Admission Scholarship***
Value: $1,800

1995 **University of Ottawa Admission Scholarship**
Value: $1,800

* renewal of scholarship based on maintaining an annual Grade Point Average of 9.0 or more

PUBLICATIONS

Harper M-E., **Antoniou A.**, Bevilacqua L., Bezaire V., and Monemdjou S. (2001) Cellular energy expenditure and the importance of uncoupling. Submitted as a requested review to the *Journal of Animal Science*, August 2001.

Harper M-E., **Antoniou A.**, Villalobos-Menuey E., Russo A., Trauger R., Vendemelio M., Shaikh A., Kupperman J., Newell E.W., Rim J.S., Bespalov, I.A., Wallace S.S., Liu Y., Rogers J., Gibbs G.L., Berry-Lowe S., Leahy J.L., Kozak L.P., Melamede R., and Newell M.K. (2001) A mechanism of resistance to apoptosis-inducing stimuli involving low mitochondrial membrane potential in tumor cells. Provisionally accepted by *The FASEB Journal*, July 2001.

Harper M-E., Dent R.M., Bezaire V., **Antoniou A.**, Gauthier A., Monemdjou S., and McPherson R. (2001) UCP3 and its putative function. Consistencies and controversies. *Biochemical Society Transactions* (in press).

PUBLISHED ABSTRACTS

Antoniou A., Newell M.K., and Harper M-E. (2000) Mitochondrial UCP2 is associated with uncoupled respiration and low radiation-induced hydrogen peroxide levels in drug resistant leukemic cells. *3rd Albany Conference on Frontiers of Mitochondrial Research.* Rensselaerville, N.Y., U.S.A.; September 2000.

Antoniou A., Newell M.K., and Harper M-E. (2000) Uncoupling of oxidative phosphorylation in leukemic cell lines confers resistance to cytotoxic therapies. *43rd Annual Meeting of the Canadian Federation of Biological Societies.* Ottawa, Ontario, Canada; June 2000.

Antoniou A., Chan A., and Harper M-E. (2000) Mitochondrial uncoupling and susceptibility to drug-induced apoptosis in L1210 and L1210/DDP tumor cell lines. *Third Annual Interdisciplinary Conference*, sponsored by the Medical Research Council of Canada (MRC), the Natural Sciences and Engineering Research Council of Canada (NSERC), and the University of Ottawa. Ottawa, Ontario, Canada; February 2000.

VOLUNTEER EXPERIENCE

2000	**7th Canadian Conference on International Health: Health as a Bridge for World Peace** November 12 - 15, Hull, Quebec
2000 - 2001	**Canadian Society for International Health** Ottawa, Ontario
1999 - 2001	**University of Ottawa Biochemistry Graduate Students' Association** Vice-President
1992-1993, 1998	**Hellenic Community Festival of Ottawa**
1991 - 1995	**Altar Boy** Greek Orthodox Church, Ottawa, Ontario

SKILLS

- Experience in the use of various software in the areas of word processing (Microsoft Word, Corel WordPerfect), spreadsheets (Microsoft Excel, Corel Quattro Pro), data analysis (Graph Pad Prism), and presentations (Microsoft PowerPoint)
- Excellent organizational, leadership, and teamwork skills
- Exceptional written and verbal communication capabilities

LANGUAGES

- English, Intermediate French, Greek

INTERESTS

- Golf
- Photography
- Films